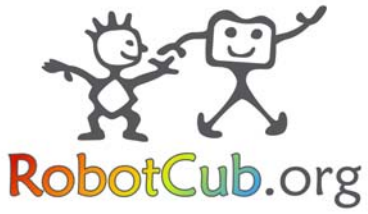

ROBotic Open-architectureTechnology for Cognition, Understanding and Behavior

Project no. 004370

RobotCub: Development of a cognitive humanoid cub

Instrument: Integrated Project
Thematic Priority: IST – Cognitive Systems

D3.1 Sensorimotor Integration

Due Date: 28/02/2007
Submission date: 2/10/2007

Start date of project: **01/09/2004** Duration: **60 months**

Organisation name of lead contractor for this deliverable: UNIFE

Responsible Person: Prof. Luciano Fadiga

Revision: **1.5**

Project co-funded by the European Commission within the Sixth Framework Programme (2002-2006)		
Dissemination Level		
PU	Public	**PU**
PP	Restricted to other programme participants (including the Commission Service)	
RE	Restricted to a group specified by the consortium (including the Commission Service)	
CO	Confidential, only for members of the consortium (including the Commission Service)	

Table of Contents

1 Introduction

This Deliverable deals with sensorimotor integration, a fundamental process linking the perceptual side of the brain with the motor one. Neuroscience of the last twenty years progressively became aware of the fact that the traditional idea of a unidirectional flow of information – from perception to action – is not true. Conversely, cortico-cortical connections are bidirectional and several evidence shows that motor planning potently modify, and sometimes filters, the incoming sensory information.

Some of the experiments here described have been carried out not only at UNIFE and UNIUP (the more neuroscience-related teams of the RobotCub community) but also at EPFL, SSSA, UGDIST, UNIHER, UNISAL, UNIZH, IST, all teams whose pedigree is essentially robotics. This is, in our view, the best demonstration in favour of the efficacy of the multidisciplinary nature of RobotCub Integrated Project.

1.1 The theoretical framework

Several lines of evidence point to a significant involvement of the motor system in supporting processes traditionally considered as `high level' or cognitive, such as action understanding, mental imagery of actions, objects perception and discrimination. The "biologically compatibility" constraint guiding the RobotCub project forces us to study these processes not only because of their scientific interest but also because our aim is to setup the artefact in a way that will allow this bi-directional information flow.

A typical example of how sensorimotor integration is used by the brain in practical tasks is provided by a population of neurons in the monkey ventral premotor cortex (mirror neurons) that discharge both when the monkey performs a grasping action and when it observes the same action performed by other individuals [Gallese et al. 1996]. Mirror neurons could provide the neurophysiological basis for the capacity of primates to recognize different actions made by other individuals: the same motor pattern which characterizes the observed action is evoked in the observer and activates its own motor repertoire. This matching mechanism, which can be framed within the motor theories of perception, offers the great advantage of using a repertoire of coded actions in two ways at the same time: at the output side to act, and at the input side, to analyse the visual percept. This matching system has also been demonstrated in humans. Transcranial Magnetic Stimulation (TMS) of the motor cortex of subjects observing hand actions made by the experimenter determined an enhancement of motor evoked potentials (MEPs) in the same muscular groups that were used by the experimenter in executing those actions [Fadiga et al. 1995]. This means that when we observe an action we utilize, as monkeys do, the same repertoire of motor representations used to produce the same action.

A further example of the involvement of the motor system in cognitive functions is given by motor imagery. Imagining a grasping action is a cognitive task that requires a conscious, detailed representation of the movement. Several brain imaging studies have shown that during motor imagery of grasping actions, premotor and inferior parietal areas are strongly activated [Decety et al. 1994, Grafton et al. 1996]. Furthermore, Parsons et al. [1995]

demonstrated by PET that implicit motor imagery (used to discriminate the orientation of visually presented hands) activates premotor and posterior parietal cortex. Moreover, Sirigu et al. [1996] showed that patients with lesions restricted to the posterior parietal cortex were selectively impaired at estimating, through mental imagery, the time necessary to perform differentiated finger movements. Taken together, all these results seem to contradict a sharp distinction between an `acting brain' and a `knowing brain'.

Among the processes traditionally considered to be `high level' or cognitive, selective attention is one of the most important. The term 'selective attention' refers to the capability of selecting a particular stimulus according to its physical properties, way of presentation, or previous contingencies and instructions. After selection, the stimulus is processed and, if convenient for the individual, acted on. A problem to solve is to understand how the sensitivity of different sectors of space can be increased in processing visual stimuli, in order to select some of them and discard others. The traditional view is that selective attention is controlled by a supramodal system `anatomically separate from the data processing systems' ([Posner and Petersen, 1990], p. 26). Like the sensory and motor systems, this `attention system' performs operations on specific inputs. It interacts with other centers of the brain but maintains its own identity [Posner and Petersen, 1990]. On the basis of data obtained from brain imaging experiments [Corbetta et al. 1990, Corbetta et al. 1991, Posner et al. 1988], it has been suggested that the attention system is not unitary but consists of at least two independent systems: a posterior one subserving spatial attention and an anterior one devoted to attention recruitment and control of brain areas involved in complex cognitive tasks [Posner and Dehaene 1994].

An alternative view of selective attention (that we favour) is that it derives from mechanisms that are intrinsic to the circuits underlying perception and action. Attention is modular, and there is no need to postulate control mechanisms anatomically separate from the sensorimotor circuits. This account for selective attention was originally formulated for visuospatial attention (premotor theory of attention; Rizzolatti and Camarda 1987, Rizzolatti et al. 1987) and it is deeply rooted in the idea that space is coded in a series of parieto-frontal circuits working in parallel and that the coordinate frame in which space is coded depends on the motor requirements of the effectors that a given circuit controls (see Rizzolatti et al. 1994). Given this strict link between space coding and action programming, the premotor theory of attention postulates that spatial attention is a consequence of the activation of those same cortical circuits and subcortical centers that are involved in the transformation of spatial information into actions. Its main assumption is that the motor programs for acting in space, once prepared, are not immediately executed. The condition in which action is ready but its execution is delayed corresponds to what is introspectively called spatial attention. In this condition, two events occur: (a) There is an increase in motor readiness to act in the direction of the space region toward which a motor program was prepared, and (b) the processing of stimuli coming from that same space sector is facilitated. There is no need, therefore, to postulate an independent control system because attention derives from the same mechanisms that generate action. Although, in principle, all the circuits responsible for spatially directed action can influence spatial attention, there is no doubt that, in humans, the central role in spatial attention is played by the circuits that code space for programming eye movements. Experiments in which the relations between attention and eye movements were either indirectly or directly tested, showed that the two mechanisms interact: Any time attention is directed to a

target, an oculomotor program toward that target is prepared. Particularly significant in this respect are experiments in which the relations between attention and eye movements were directly tested [Sheliga et al. 1995a, Sheliga et al. 1995b. Sheliga and coworkers instructed normal participants to pay attention to a given spatial location and to perform a predetermined vertical or horizontal ocular saccade at the presentation of the imperative stimulus. The results showed that the trajectory of ocular saccades in response to visual or acoustic imperative stimuli deviates according to the location of attention. Moreover, the deviation increased as the attentional task became more difficult. In a recent experiment, the role of oculomotion in orienting of attention was investigated by dissociating perceptual from motor capabilities [Craighero et al. 1994]. If a causal relationship links oculomotion and orienting of attention, any constraint limiting eye movements should abolish, or at least reduce, attentional benefits in the region of the spatial field barely reachable by the eye. On the contrary, if attention is a purely cognitive process, then no effects are expected to arise from oculomotor constraints. Subjects were submitted to a spatial attention orienting task, performing it in monocular vision and having the head rotated in such a way that the eye was kept at an extreme position in the orbit. This position limited the execution of a saccade toward the temporal hemifield, whereas it allowed saccadic execution toward the nasal hemifield. Results showed that orienting of attention was normal in the nasal but not in the temporal hemifield, indicating that eyes and attention show a common limit stop.

Whereas in primates eye movements are certainly the most important mechanism for selecting stimuli, there are also circumstances (e.g., stimuli presented very close to the face or stimuli appearing in the visual periphery) in which eye movements are not crucial for selecting stimuli in space. In these circumstances, spatial attention should depend on circuits other than those related to eye movements. In the frame of premotor theory of attention, Craighero and colleagues [2004] assumed that allocation of attention to a graspable object is a consequence of preparing a grasping movement to that same object. The authors predicted that, when a specific grasping movement was activated, there would be both: (i) increase in the motor readiness to execute that movement and, (ii) facilitation in visually process graspable objects whose intrinsic properties are congruent with the prepared grasping. In an experiment designed to investigate this hypothesis, normal subjects were required to grasp a bar after the presentation of a visual stimulus whose orientation was either congruent or incongruent with that of the bar. Results supported the hypothesis. The detection of a visual object was facilitated by the preparation of a grasping movement congruent with the object's intrinsic properties. This finding strongly suggests that the premotor theory of attention is not limited to orienting attention to a spatial location but can be generalized to the orienting of attention to any object that can be acted upon.

1.2 The organization of the document

In this Deliverable we describe experiments investigating the development and the characteristics of the capability to plan, execute and recognize actions. Three are the main experimental approaches used for this purpose: monkey electrophysiological studies based on single neurons recordings; psychophysical studies in normals and patients (both adults and children); brain imaging and transcranial magnetic stimulation studies in normals. The

presentation will follow the schema originally proposed in the Technical annex revision we presented at month 12. Thus, three main stream of research will be presented: (1) Ontogenetic cues in sensorimotor coordination; (2) Phylogenetic cues in sensorimotor coordination and (3) Schemas in artefacts for sensorimotor coordination. The experiments described here represent only one part of the work in progress. The final version of this Deliverable (D3.1b, to be presented at month 30) will give a more exhaustive description of the global picture. Some final results coming from experiments on monkey and human electrophysiology and on brain imaging of gaze sharing will be presented as well.

2 Experimental part

2.1 Ontogenetic cues in sensorimotor coordination

The results of these experiments come from a strict collaboration between UNIFE and UNIUP. Together, we have identified three main different techniques to study the development of the motor system in children (to act and to recognize actions):

1) Mu rhythm desynchronization during action observation.

2) Near infrared spectroscopy (NIRS).

3) Gaze tracking during action observation and execution

Experiments concerning point (1) are in progress and will be presented in the final version of this Deliverable at month 30. As far as (2) is concerned, art UNIFE we are actively collaborating at the setup of a new NIRS machine together with the Department of Physics at the Politecnico di Milano (Italy). The final goal of the study is to use NIRS in infants, to investigate the neural correlates of motor development (both for action execution and understanding). Moreover, the results of some experiments on crawling carried out jointly by EPFL and UNIUP, together with modelling of crawling studied at EPFL will be presented at the end of this section.

2.1.1 Mapping cerebral hemodynamics of the human motor cortex by multi-channel time-resolved near-infrared spectroscopy (UNIFE).

Introduction

Brain imaging techniques (PET and fMRI) are not usable on infants because of their invasiveness and because their require subjects' immobility. In recent years NIRS has been developed to non-invasively measure regional blood flow in infants. It allows detecting the regional modifications of blood flow by spectroscopically measuring the absorbance of low-power infrared light by regional hemoglobin concentration. In order to investigate the

applicability of the NIRS technique in the study of cognitive functions and to verify which method is the most suitable, we have conducted preliminary experiments on adults in collaboration with a group of researchers from the Politecnico di Milano (Alessandro Torricelli, Antonio Pifferi, Lorenzo Spinelli, Davide Contini), leaded by Rinaldo Cubeddu.

The problem of mapping functional activation in the human brain by optical radiation is challenging. The diffusive nature of biological tissues prevents the discrimination of absorption and scattering contributions by simple continuous wave techniques. Time domain techniques, on the contrary, are able to discriminate between them and to derive absolute values for the hemodynamic parameters in a real heterogeneous medium like the human head [1]. Moreover, relevant studies have shown that in the time domain depth sensitivity can be improved by simply exploiting the temporal information [2-4].

Here, we investigated the spatial resolution of a dual wavelength (690 and 820 nm) multi-channel time-resolved system for functional NIRS in the study of the antero-posterior extension of hand-related motor activation, and of the medio-lateral somatotopy of hand and shoulder motor representations.

Methods

Two right handed normal subjects participated to the experiment. During a preliminary mapping session, right hand and shoulder motor representations were assessed by using transcranial magnetic stimulation (TMS) [5]. The experimental session was subdivided into two tasks. The first task was aiming at investigating the antero-posterior extension of the right hand motor representation as detected by NIRS. A specially designed probe (4 source fibers and 10 collecting bundles, source-collector relative distance [rho]=2.0 cm), was placed over the right hand motor representation of the left hemisphere, perpendicularly to the central sulcus. The protocol consisted of 20 s baseline, 20 s right hand motor activity (Luria's finger tapping), and 40 s recovery. The protocol was repeated 10 times in order to increase the signal-to-noise ratio by block averaging. The acquisition rate was 1 s.The second task was designed to test the somatotopic representation of hand and shoulder motor representations by using a protocol similar to that of the previous task. The probe was placed over the shoulder/hand motor representations of the left hemisphere, along the central sulcus. The protocol consisted of 15 s baseline, 15 s right hand finger tapping or right shoulder rotation (randomized and executed according to visual instructions), and 30 s recovery. The protocol for each type of movement was repeated 5 times. The acquisition rate was 1 s. The analysis was restricted to the superior part of the probe (indicated by the yellow circle in the figure) since it was our region of interest.

Results

TASK 1: Antero-posterior extension of the right hand motor representation

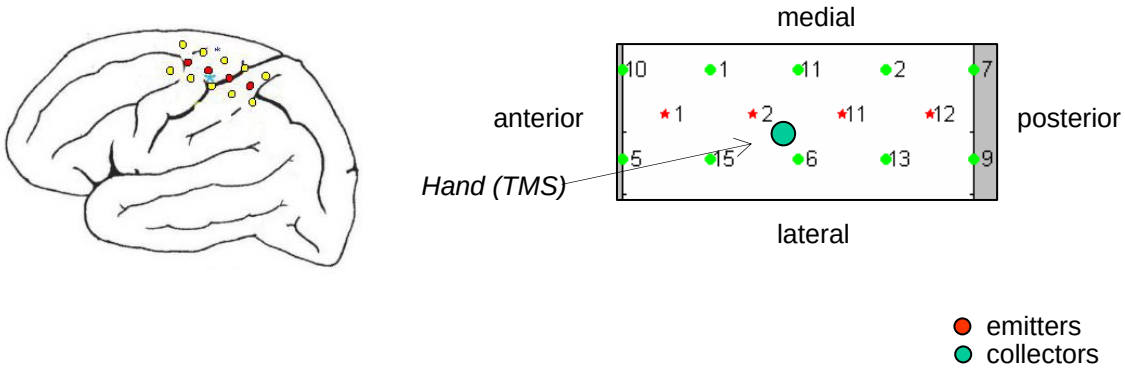

Figure 1. Blue asterisk indicates the right hand hot spot location (left hemisphere) as assessed by TMS in the subject according to the method described by Fadiga et al. (1995). On the right side, schema of the probe with the indication of the location of the hand hot spot.

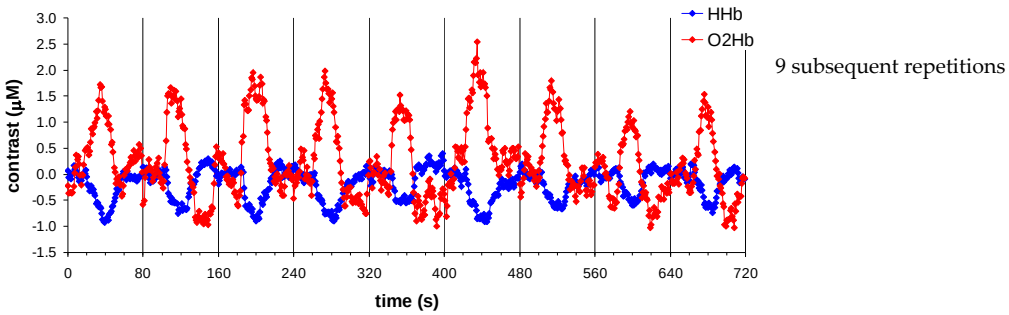

Figure 2. Deoxyhemoglobin (ΔHHb) and oxyhemoglobin (ΔO2Hb) during single trials (i.e. no block averaging) collected by a single couple of emitters-collectors during the finger tapping task.

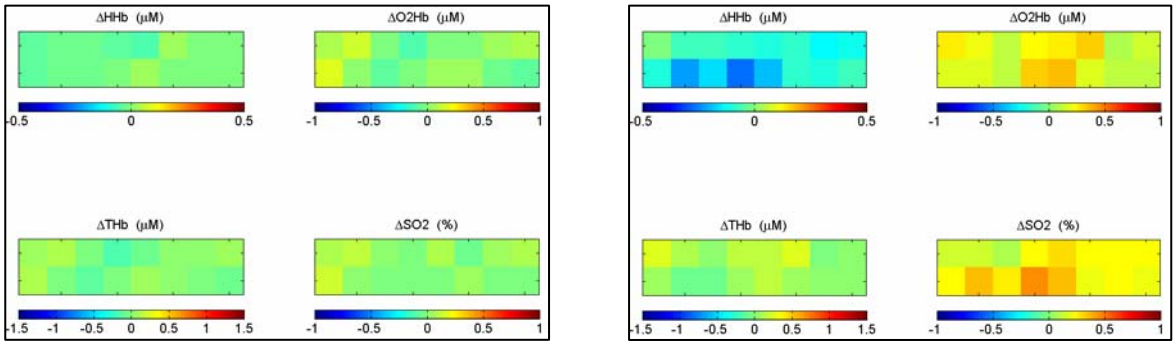

Figure 3. Spatial maps of HHb, O2Hb, THb, and SO2 concentration changes, separately presented for the baseline (left panel) and task (right panel) experimental phases (10 times block averaging).

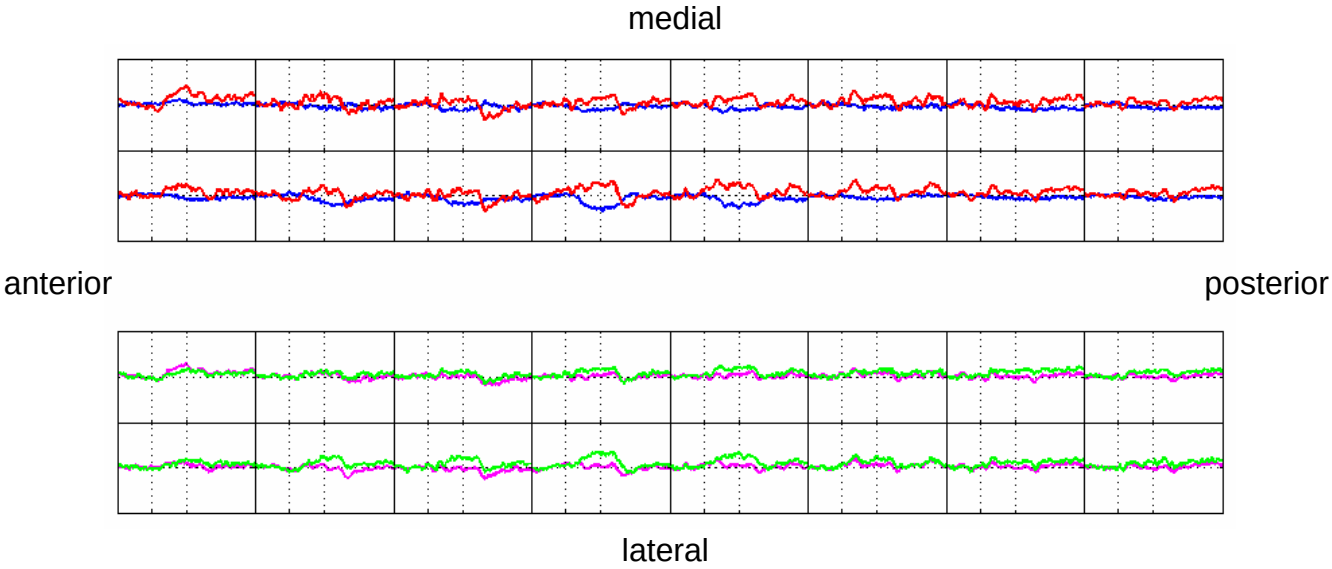

Figure 4. Average (10 trials) cerebral blood oxygenation changes in each of the 16 channels during the course of the experiment. The ordinates indicate the concentration changes of O2Hb (oxyhemoglobin, red line, ΔO2Hb -1.5 / +1.5 mM), HHb (deoxyhemoglobin, blue line, ΔHHb -1.0 / +1.0 mM), tHb (total hemoglobin, purple line, ΔtHb -2.5 / +2.5 mM), and SO2 (% of oxygen saturation, green line, ΔSO2 -1.5 / +1.5 mM). Dotted lines indicate the different phases of the experiment: 20 s baseline, 20 s task, and 40 s recovery, during time.

TASK 2: Somatotopic representation of hand and shoulder motor representations.

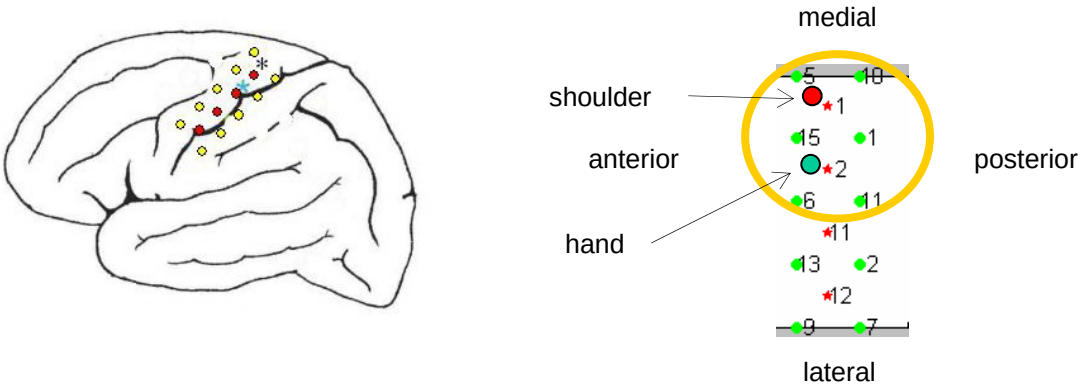

Figure 5. Blue and black asterisks indicate the right hand hot spot location (left hemisphere) and the right shoulder hot spot location, respectively, as assessed by TMS in the subject according to the method described by Fadiga et al. [5]. On the right side, schema of the probe with the indication of the location of the hand and shoulder hot spot.

TASK 3: Right shoulder rotation task

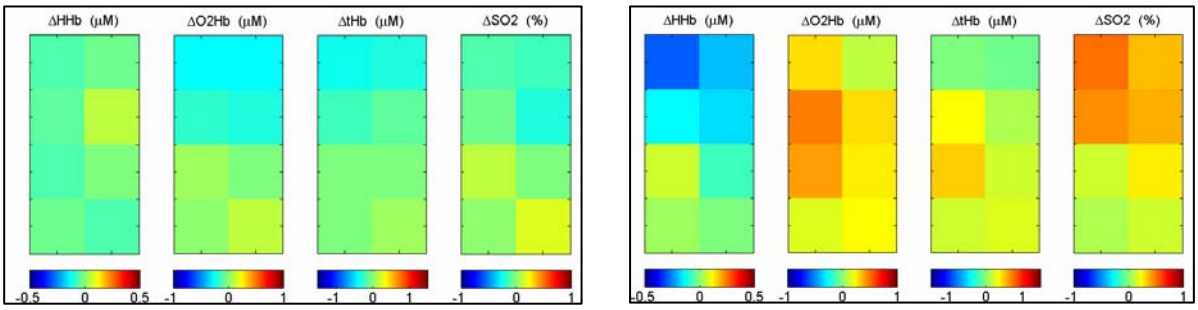

Figure 6. Spatial maps of HHb, O2Hb, THb, and SO2 concentration changes, separately presented for the baseline (left panel) and task (right panel) experimental phases (5 times block averaging).

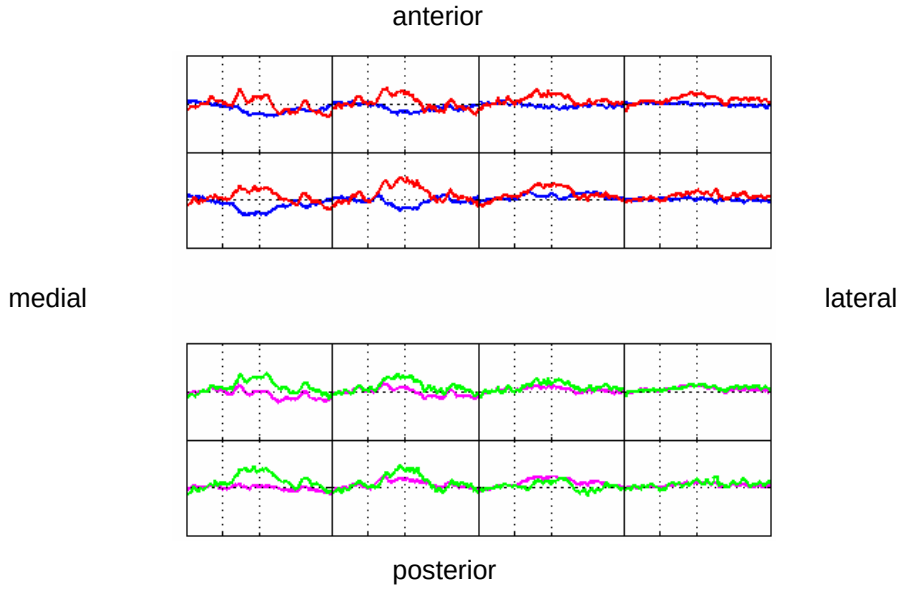

Figure 7. Average (5 trials) cerebral blood oxygenation changes in each of the 8 channels (superior part of the probe) during the course of the experiment. The ordinates indicate the concentration changes of O2Hb (oxyhemoglobin, red line, ΔO2Hb -1.5 / +1.5 mM), HHb (deoxyhemoglobin, blue line, ΔHHb -1.0 / +1.0 mM), tHb (total hemoglobin, purple line, ΔtHb -2.5 / +2.5 mM), and SO2 (% of oxygen saturation, green line, ΔSO2 -1.5 / +1.5 mM). Dotted lines indicate the different phases of the experiment: 15 s baseline, 15 s task, and 30 s recovery, during time.

Right hand finger tapping task

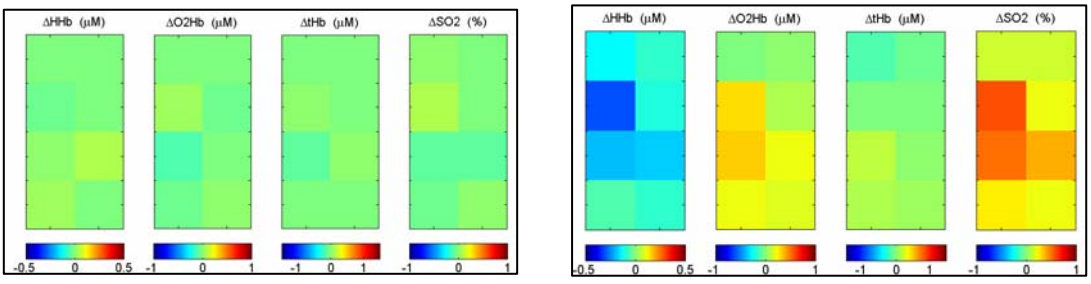

Figure 8. Spatial maps of HHb, O2Hb, THb, and SO2 concentration changes, separately presented for the baseline (left panel) and task (right panel) experimental phases (5 times block averaging).

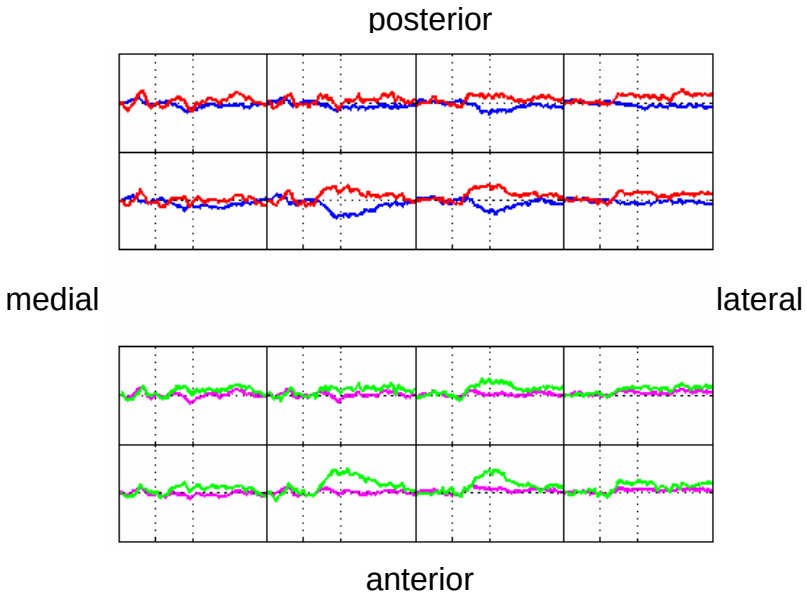

Figure 9. Average (5 trials) cerebral blood oxygenation changes in each of the 8 channels (superior part of the probe) during the course of the experiment. The ordinates indicate the concentration changes of O2Hb (oxyhemoglobin, red line, ΔO2Hb -1.5 / +1.5 mM), HHb (deoxyhemoglobin, blue line, ΔHHb -1.0 / +1.0 mM), tHb (total hemoglobin, purple line, ΔtHb -2.5 / +2.5 mM), and SO2 (% of oxygen saturation, green line, ΔSO2 -1.5 / +1.5 mM). Dotted lines indicate the different phases of the experiment: 15 s baseline, 15 s task, and 30 s recovery, during time.

Summary of Results

Results relative to the task aiming at investigating the antero-posterior extension of the right hand motor representation as detected by NIRS, demonstrated a focal increase of O2Hb and the corresponding decrease of HHb in the channels placed over the hand motor representation hot spot, determined by TMS, during the execution of a Luria's finger tapping with respect to a baseline acquisition. Results relative to the task designed to test the somatotopic representation of hand and shoulder motor representations, demonstrated a differential activation for finger and shoulder movements as detected by NIRS, when comparing right hand finger tapping and right shoulder rotation tasks.

Conclusions

In conclusion, a multi-channel time-resolved system for functional NIRS has been successfully employed to study hemodynamic response following motor activity in the adult brain. In addition, the system was able to discriminate the antero-posterior extension of hand-related motor activation and the somatotopy of hand and shoulder motor representations. Moreover, the system used in the present study is sensitive enough to significantly determine cortical motor activation in single trials. All these characteristics are strongly in favor of the possibility to use this technique in infants to study the ontogenetic development of the motor system in infants.

2.1.2 Gaze behaviour in normal and autistic children during observation of own and others' hand action (UNIFE+UNIUP).

The pattern of eye movements during action observation is the same as that recorded during action execution. In both cases, the eyes anticipate the hand and reach the target well before the arrival of the fingers. Thus, saccadic behaviour during action observation supports the direct matching hypothesis for action recognition. We decided to study the development of this predictive behaviour during action observation in developing infants (UNIUP) and in children affected by Autism Spectrum Disorders (ASD) (both UNIUP and UNIFE).

It is well known that autism spectrum disorders (ASD) are characterized by deficits in social and communicative skills. It has been proposed that the mirror-neuron system may play a critical role in higher order cognitive processes such as imitation, theory of mind, language, and empathy. Strikingly, these skills are among those mostly impaired in ASD individuals. Because of this correspondence, many have suggested that individuals with ASD may have mirror neuron system impairments, and some experimental evidence supports this interpretation. Therefore, we decided to investigate the gaze behavior of ASD children during execution of their own actions and during the observation of actions performed by others. We have tracked the gaze of 8 high-functioning autistic children while they were performing a modification of the Flanagan and Johansson paradigm, by using a version of the TOBII system that allows the recordings also during a real action (i.e. not presented by a video clip). Five normal children, matching patients for age and gender, have been tested as well as controls.

During action execution the agent's eyes never follow the acting effector, but the gaze is projected towards the end point of the action, anticipating it. More recently, it has been shown (Flanagan and Johansson, 2004) that this pro-active behaviour manifests itself not only during execution but also during the observation of action performed by others. Conversely, the presentation of moving objects, not held by hand, does not evoke the pro-active gaze behaviour. This evidence has been assumed to be a consequence of the involvement of the mirror-neuron system. Mirror neurons become however active only when observer and agent share a similar motor repertoire (see Rizzolatti and Craighero, 2004). It has been suggested that a fundamental deficit in autism could be the impairment of what has been called "the theory of mind" (i.e. the capacity to understand the intention behind the behaviour of others) (2). A full-fledged theory of mind is achieved, however, by children at about four years of age (3), while clinical signs of autism appear earlier, thus indicating that a more basic deficit should underlie the development of "theory of mind" (4). In recent years, it has been suggested that this deficit could depend on a poor development of mirror neuron system, which would be a neural precursor necessary for the development of the theory of mind. (5). Evidence coming form EEG , MEG, TMS and brain imaging data provided strong evidence that the mirror neuron system could be impaired in autistic children (6-7-8-9).

Methods

We applied four tasks to a neurologically healthy population of children, and to a group of "high-functioning" autistic children. A child with high-functioning autism fits the definition of autism but has much better cognitive and learning abilities. These children have initial difficulty in acquiring language but become then able to speak at a level appropriate for their

age. Autistic children were recruited in a centre of Paediatric Neuropsychiatry in the province of Empoli (Italy) "ASL 11". The diagnosis had been made by means of the Autism Diagnostic Observation Schedule (ADOS) (Lord et al. 1989). All subjects had an intelligence quotient (IQ) > 70, as calculated with the Wechsler Intelligence Scale for Children Revised (WISC-R). A group of 8 autistic children, 7 males and 1 female, aged 5.1 – 16.0 years (mean age: 7.1) participated to the experiment. The mean IQ of this group was of 98.7 ± 11.6 (SD). The group of neurologically healthy children that were used as a control, had IQ > 70 (WISC-R scale). A group of five children aging 5.2-11.9 years, (4 male and 1 females, mean age: 6.5) participated to the experiment. Their mean IQ was of 104.7 ± 7.7. All procedures were approved by the local ethical committee and the parents of children gave informed written consent.

Tasks: The experiment consisted in 4 conditions (see below) with 13 repetitions each (trials). Each trial started when the right hand of the participant was placed on the table in correspondence of the starting point. The four different task were:

1) To grasp with their right hand a toy placed on the table and to put it into a container, located on the table in front of them *(active condition, EXE)*

2) To observe the experimenter performing the same action with his right hand in front of them *(passive condition, Frontal Right Observation, FRO)*

3) To observe the experimenter performing the same action with his left hand in front of them ("specular" perspective-laterally reversed-) *(passive condition, Frontal Left Observation, FLO)*

4) To observe the experimenter performing the same action in lateral position: sideway to the children (the participants saw the hand of the experimenter according to their "egocentric perspective") *(passive condition, Lateral Observation, LO)*

The experimenter and the subject were sitting at a table, one in front of each other. In front of them there were a container and three objects-toys. During the "active-condition" the subject was instructed to grasp the objects, one at time, and to place them into the container. In the "passive-condition", the participants were requested to observe the same sequence of grasping-placing movements performed by the experimenter in front of them or in the lateral position. The four conditions were repeated in a pseudo-random order. All the participants performed a brief training session prior to recordings.

Experimental apparatus: During the experiment, the position of the subject's gaze was continuously recorded by using an eye-tracking device (Tobii, Sweden) and a video-camera. A transparent table with two different levels was used to run the experiment. In the lower level (behind the glass) we positioned the eye-tracking device, and in the upper plan we positioned a transparent and removable grid for the calibration. After the calibration was done, we removed the grid, so that the upper plan became the working space. Furthermore the hand/arm kinematics of the action performed by both, the subjects and the experimenter, was recorded during the whole experiment. This was done to measure the precise pattern and kinematics of goal-directed hand grasping. Indeed, autistic children might be affected in their capacity to efficiently plan goal-directed actions (see Mori et al. 2005). To this purpose, three infrared-reflecting markers were fixed to the wrist/hand of the experimenter and three on the wrist/hand

of the participants. Two markers (one on the tip of the index finger and one on the thumb) were used to measure fingers aperture during grasping. A third marker was positioned on subject's wrist to measure the transport component of the hand-reaching movements. Data were acquired by a high-speed optic tracking system (Qualysis, Sweden) which provided the contemporary 3D position of each infrared reflecting marker, at the temporal resolution up to 1 KHz.

Data pre-processing: The use of the eye-tracker to record the gaze, required a stable position of the head and a constant posture during the experimental session. We discarded part of the data, because of the difficulty to achieve this stability with young children and, particularly, with ASD children, typically presenting hyperactivity troubles, especially during the EXE condition. The object was initially positioned on a limited area of the desk and the box was not fixed on the table. Thus the trials were not performed on a standard space. In order to overcome this problem, we standardize the recordings according to a 0-1 ideal space.

Results.

In the preliminary data we present here, we restricted our analysis to the movement 'grasping the object-landing in the container' which is the most studied in the literature. After data pre-processing and cleaning, 296 valid movements were selected. The spatial distribution of wrist position in all four conditions was very similar between ASD and control subjects (movement duration and peak velocity were not significantly different between conditions). This let suppose that: 1) in FRO, FLO and LO conditions (observation) experimenter did perform similar movement in the two groups; 2) Autistics and control subjects performed similar movements (EXE condition). As a measure of pro-active gaze behaviour we determined for each trial the ratio of looking time in the goal area relative to total looking time (goal and trajectory areas) during object movement (GLT ratio). Goal area was defined as the space regions within .20 unit from the landing zone; while trajectory areas was defined as the space regions between .20 and .80 unit far from the landing zone. Therefore if subjects tracked the moving target (and hand movement is constant), the expected proportion of GLT is .20/(.60+.20)=.25. In other terms, more is the time the subject looks the target, more is her predictive behaviour.

By following this method, values of GLT exceeding significantly 25% ratio ($p<0.005$) defines a pro-active gaze behaviour. while values below it, indicate reactive gaze behaviour. Results are given in Table 2 and Figure 10.

Conditions	Normal	ASD
EXE	0.49 ± 0.08 *	0.47 ± 0.06 *
FRO	0.44 ± 0.09 *	0.34 ± 0.06
FLO	0.3 ± 0.08	0.33 ± 0.07
LO	0.33 ± 0.08	0.43 ± 0.07

Table 2. Average GLT ratio ± SEM. Asterisks indicate statistically significant pro-active gaze behaviour.

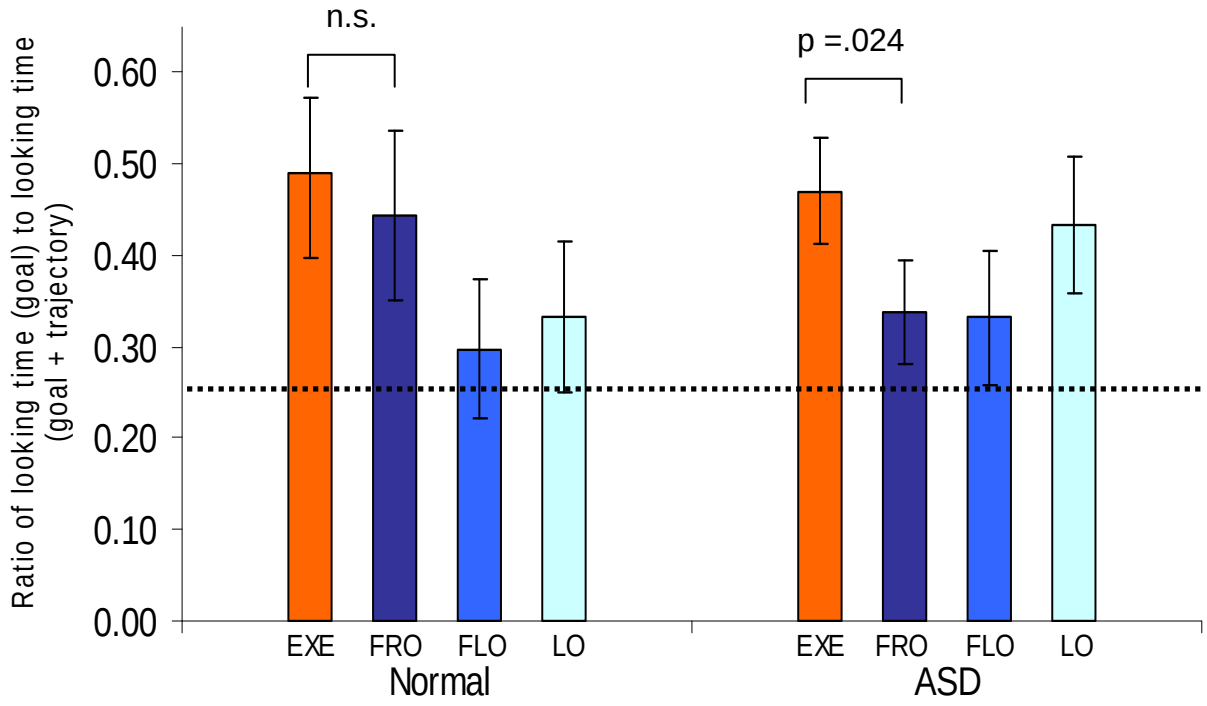

Figure 10. Gaze performance during observation of own (EXE) and other's (FRO, FLO, LO) actions. Statistics (means ± SEM) are based on all data points for controls (left) and ASD patients (right). Ratios of looking time at the goal area to total looking time in both goal are shown. The horizontal line at 0.25 shows the expected ratio if subjects were tracking the moving stimuli. Pro-active behaviour (one sample t-test for mean equal to 0.25, $p< .05$) is indicated with an asterisk the corresponding bars.

In execution (EXE condition), both normal controls and ASD patients show a pro-active gaze behaviour (*t*-test, p= 0.0238 and p=0.005 respectively). Conversely, during action observation (FRO, FLO and LO conditions), different gaze behaviours have been found. In this first phase of analysis we focus mainly on FRO condition because the higher average number of valid trials in each subject increases the stability of the single subject measurement (more trial we get for each subject, better estimate we get). In FRO condition, while data show a tendency in favour of pro-active gaze behaviour for normals (p=.052), ASD patients did not behave in a proactive way. Most importantly, while the direct comparison between EXE and FRO conditions in normals fail in reaching significance, the same comparison for ASD patients highlight a significant decrease in pro-active behaviour in FRO relative to EXE condition (paired t-test, p= 0.0241). Further interesting data comes from the comparison between EXE and LO. The statistical analysis show a tendency to the significance for normals, while ASD patient show no difference between the proactive behaviour during execution and that during observation of other's actions shown in egocentric perspective (see Figure 10).

In the present experiment, we have compared gaze and hand position during both grasping execution and grasping observation with different perspectives, in children affected or not by ASD. Preliminary analysis indicate that normal children show the same pro-active gaze behaviour both during execution (EXE) and during observation of grasping movement (FRO), while ASD patient show a pro-active gaze behaviour only during execution. This evidence is in favour of a failure of the mirror neuron system during other's action observation in ASD patients.

2.1.3 Ontogeny of locomotion: measuring and modelling crawling in infants (EPFL+UNIUP)

The neural mechanisms underlying locomotion control in humans are still not well-known. The main brain areas involved are the spinal cord, the brainstem, the cerebellum and the motor cortex. Recent studies show that like in other vertebrate animals, Central Pattern Generators (CPGs) in the spinal cord play an important role in generating and modulating the rhythmic signals underlying locomotion.

Our approach is to take inspiration from vertebrate locomotion at an abstract level and to model CPGs as systems of coupled nonlinear oscillators. This leads to the design of systems that can produce complex, coordinated, multidimensional rhythmic motor commands while being initiated and modulated by simple control signals (similarly to what has been demonstrated in decerebrated cats by Shik and colleagues in the 1960s). The CPGs produce desired trajectories (i.e. desired angles) to the PID controllers controlling the motor torques of the robot.

Our motivation is to take advantage of interesting properties of systems of coupled nonlinear oscillators and their limit cycle behaviour, namely asymptotic stability (the system returns to limit cycle after a transient perturbation), which is crucial for control the possibility to continuously modulate the periodic patterns by a few, non rhythmic, control signals, the produced trajectories remain smooth even if the control signals are abruptly changed, the system supports direct integration of feedback for modulating and synchronizing the trajectories according to sensory information (e.g. entrainment by proprioceptive signals from the body).

This CPG-based approach should make the locomotion controller easily usable by other control modules. Unless the crawling of the iCub requires specific limb placements, other modules only need to tune high-level commands determining speed and direction of crawling without having to worry about the multiple rhythmic signals that need to be sent to the actuators.

This work has 3 parts: programmable CPG, study of infant crawling kinematics, CPG-based crawling controller.

Programmable CPG

We developed a programmable CPG, i.e. a system able to automatically encode periodic signals into limit cycles. It allows control, modulation and robust integration of sensory feedback during locomotion control. We applied the system for biped locomotion control and modulation on a real robot. See our Physica D and ICRA 2006 papers, referenced below. Note that the first and main locomotion ability of the iCub will be crawling. We studied here biped walking because (1) we had biped walking trajectories available from Fujitsu for the HOAP 2 robot, and (2) because the HOAP 2 robot is not well-adapted for crawling. However, the programmable CPG offers a general method for encoding periodic trajectories into limit

cycles and can be directly applied of the control of crawling.

Study of infant crawling kinematics

There exists very few contributions on baby crawling and most of them do only qualitative analysis. We studied the kinematics of crawling babies, in collaboration with K. Rosander (Uppsala University).

Subjects: Eight infants, 9 to 11 months old have been studied. They were selected as crawlers practicing the "classic" style of locomotion using hands and knees. The parents were asked about approximate debut for crawling. Some infants were seen twice (Table 2).

Name	Birth (y/m/d)	Session 1 (y/m/d)	Body mass	Session 2(y/m/d)	Body mass 2	Start of crawling (approx.)	
Emil	050611	060324	9.5 kg	060509	10 kg	060309	
Alva	050718	060328	7kg	060510	7.5 kg	060228	
Jonathan	050613	060330	9kg			060130	
Vilmer	050614	060331	10kg			060310	
Matilda	050612	060412	11kg			060304	
Alvin	050719	060418	11kg	060516	12 kg	060328	
Elin	050623	060419	10,5kg			060216	
Oskar	050623	060508	10.5 kg			060208	
Milton	050903	060523	10 kg	060514			

Table 2. The subjects participating to the crawling experiment in Uppsala.

Procedure: When the parents came to the lab they were informed of the experiment and signed a consensus form that included permission for video recording. The parents undressed the infant and small markers were attached to the skin on places on or close to the joints (see Table 3). Three markers were put on the spine (neck, thoracic and lumbar). A hat with three markers (1 midsagittal, 2 coronal) was put on too. The complete list of the markers is the following: Head, R ear, L ear, Neck spine, Thoracic spine, Lumbar spine, R shoulder, R elbow, R

wrist, L shoulder, L elbow, L wrist, R hip, R knee, R ankle, L hip, L knee, L ankle. The markers on the wrists and knees were glued to a Velcro band. This gave stability to the critical parts that were close to the floor during locomotion. One disadvantage was that the knee markers were just above the joint. The remaining nine markers were attached with collars used for skin electrodes. When all 18 markers were properly attached the infant was encouraged to crawl on a rug (polypropylene, size 230 x 170 cm, "Arden blom" from IKEA, Sweden) on the floor. The parent and one experimenter were sitting on the floor on opposite sides of the rug using attractive toys to catch the infant´s attention. The second experimenter handled the measurements and was sitting close to the rug observing the infants behaviour.

Measurements: A motion capture system (Qualisys, Sweden) with passive markers (size 5 and 10 mm) was used in an external triggering mode. Data was collected at 240 Hz for 12 s periods. In close synchrony with the measurement sessions, a web camera monitored the infant during the trial. Before each experiment the system was calibrated. Five cameras were used, two were placed at a ceiling stand and three were placed on the floor so that the whole crawling area was covered (Figure 11). When the infant showed the intention to start crawling, the measurement was started by the second experimenter. Each trial was set to 12 seconds. Usually, 20-40 trials per infant were registered.

Data evaluation: The markers in each file (one session of 12 s) were transformed in the software and were identified. The identification was improved by comparing the web camera sessions with the movements of the markers. Short (<0.x s) intervals when one marker was hidden were interpolated using the software routines.

Results: The infants were interested and cooperative. During the trials, crawling and movements between crawling and sitting were recorded. Totally, 97 trials were selected for further analysis.

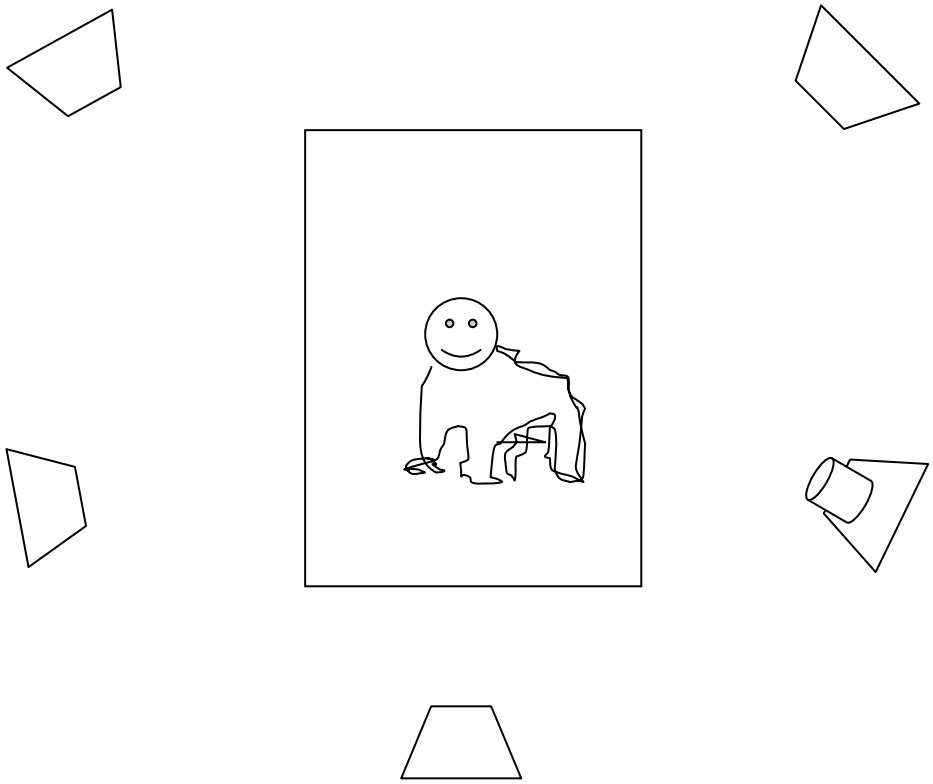

Figure 11. Schematic geometry of the experimental setup as seen from above.

The most common gait is a trot-like gait in terms of the temporal relations between the limbs. However the duration of the stance phase is much longer than the duration of the swing phase and it appears that during the swing phase of a limb, the opposite limb moves very little, which is very different from trot gait in most mammals.

CPG-based crawling controller

We developed a CPG able to reproduce the main features of crawling babies. To do so, we built an oscillator in which we can independently control the duration of the descending and ascending phases (i.e. the duration of the swing and stance phases), allowing us to shape the signal of the CPG using very simple control signals. Then we used insights from symmetric dynamical systems theory to design the CPG. We were able to reproduce the main features of real crawling and the CPG was used to control a physically realistic simulation of the iCub in Webots. Smooth modulation of the speed of the robot was also achieved. See our RSS06 paper for more details, reference below.

Note: Though we did not use the programmable CPG for crawling, the framework we developed with these two approaches is very similar and future work will show how to incorporate the properties of the programmable CPG into the crawling CPG.

Demos

We created a web page describing the crawling of the iCub and the collaboration with Uppsala (with movies), see http://birg.epfl.ch/page63115.html. See also the following page for our work and movies on biped locomotion control: http://birg.epfl.ch/page56604.html

2.2 Phylogenetic cues in sensorimotor coordination

In the framework of the phylogenetic cues in sensorimotor coordination, we are following two different lines of research:

1) Behavioural study of action observation in monkeys.

2) Single neurons recording study of grasping in monkey premotor and primary motor cortex.

3) Single neurons recording in rats.

2.2.1 Action observation behaviour in Macaque monkeys (UNIFE).

Some authors have proposed that one-year-old infants represent actions by relating relevant aspects of reality (action, goal-state and situational constraints) and assuming that actions function to realize goal-states by the most efficient means available. A series of experiments give support to this hypothesis. Indeed, the phylogeny of intentional action, namely the ability of non-human primates to interpret the other's action could be based on the attribution of a mental state, such as intention. In humans it is commonly held that the process of acquisition of mind reading unfolds during the first year of life and ends up with the ability of understanding false beliefs (i.e. to understand that other people can act by relying on beliefs that do not correspond to the state of reality). Gergely (1995) has shown that the attribution of a meaning to other people's actions can be independent from the ability to "mentalize". His experiments did show that even 12 months-old infants are able to successfully represent actions in connection with three aspects of reality (action, goal and obstacle). Such a teleological perspective (teleological stance) stems from the kernel principle of maximal efficiency, according to which actions are performed to achieve a planned final state as much effectively as possible. Uller (2003) has investigated the emergence of a teleological stance from a phylogenetic perspective by presenting chimpanzees with the experimental design that Gergley adopted with pre-verbal children. The results showed that the more evolved non-human primates are able to grasp the sense of a goal-oriented behaviour. In the present experiment we aim at verifying whether similar results can be obtained with non-human primates (macaca fascicularis and macaca nemestrina) at a lower level in the phylogeny scale. At difference with the children and chimps experiment, though, we employed as stimuli real hand actions performed by an experimenter in front of the monkey.

In order to verify the presence of action recognition in monkeys we applied a paradigm very similar to that used in infants. Gaze position in monkeys was tracked during observation of different types of actions performed by the experimenter in front of it. The experiment was subdivided into two different sessions: a “familiarization” session and a “test” session. During the familiarization session the experimenter overcame an obstacle with her arm in order to reach and grasp an object. During the test session the experimenter performed two different types of movements to grasp an object in the absence of the obstacle: “congruent” condition in

which the trajectory of the experimenter's arm is a normal one, and the "incongruent" condition in which the trajectory of the arm simulates the presence of the obstacle.

More in detail, the experimental setting was as follows: Six macaque monkeys have been properly trained to gaze different hand actions performed by an experimenter at about 50 cm from the animal. The direction of the monkey's gaze was mapped by means of an eye-tracker (Tobii, Sweden). The experimenter's actions was simultaneously videorecorded and digitized so that it was possible to superimpose on it the monkey fixation points. Six short hand grasping actions were performed by the experimenter in front of the monkey during an experimental and a control session, respectively; the two sessions took place at 4 weeks interval. For each session, a familiarization set was presented, consisting of a short sequence (repeated 10 times) in order to refrain the animal from perceiving the sequence as a novelty event. After the familiarization set, we presented 3 blocks of 4 action sequences each (situation test), in which the familiarization scene was slightly modified. In the familiarization block of the experimental session, the experimenter's hand was overstepping an obstacle when reaching a squeeking object. During the first block of Test actions (non-congruent condition) we displayed the same action with an identical (parabolic) trajectory, but in the absence of an obstacle. During the second block of Test actions (congruent condition) we displayed the grasping action in the absence of an obstacle being performed with a straight trajectory. The control actions presented a familiarization set in which the same action of grasping was performed with a parabolic trajectory, not required by the position of the obstacle (side-placed with respect of the background). The Test conditions was identical to those selected for the experimental session.

In the infants experiment results indicated that they looked significantly longer at the incongruent test display (old jumping approach) than at the congruent one (novel straight-line goal-approach). The authors interpret this result as an evidence of an inference on the correctness of action execution. From preliminary analysis, it appears that monkeys' behaviour is very similar to that of infants, indicating that also low-level non-human primates are able to recognize the correct way to execute an action according to the presence of situational constraints.

2.2.2 Single neuron study of visual feedback during grasping, in monkey premotor and primary motor cortex (UNIFE).

It is well known that the frontal cortex is strongly involved in action programming and motor control. In addition to the primary motor cortex (area F1) there are three pairs of areas: F3 (caudal, SMA proper) and F6 (rostral, pre-SMA) lay on the mesial wall of the frontal lobe; F2 (caudal) and F7 (rostral) form the dorsal premotor cortex and F4 (caudal) and F5 (rostral) form the ventral premotor cortex. Particularly interesting are the ventral premotor areas because of the strong visual input they receive from the inferior parietal lobule. These inputs subserve a series of visuomotor transformations for reaching (area F4, Fogassi et al., 1996) and grasping (area F5, Rizzolatti et al, 1988; Murata et al., 1997). In addition, area F5 contains neurons forming an observation/execution matching system, which maps observed actions on the observer's internal motor representations (mirror neurons). Electrical stimulation studies revealed that area F5 contains extensively overlapping representations of hand and mouth movements (Rizzolatti et al., 1988; Hepp-Reymond, et al., 1994). Single neurons studies have shown that most F5 neurons code specific actions, rather than the single movements that form them (Rizzolatti et al. 1988, Fadiga et al. 2000). It has been therefore proposed that, in area F5, a vocabulary of goals more than a set of individual movements, is stored. Several F5 neurons, in addition to their motor properties, respond also to visual stimuli. According to their visual responses, two classes of visuomotor neurons can be distinguished within area F5: canonical neurons and mirror neurons (Rizzolatti and Fadiga, 1998). Canonical neurons respond to visual presentation of three-dimensional objects (Murata et al., 1997). About one quarter of F5 neurons show object-related visual responses, which are, in the majority of cases, selective for objects of certain size, shape and orientation and congruent with the motor specificity of these neurons. They are thought to take part in a sensorimotor transformation process dedicated to select the goal-directed action, which most properly fits to the particular physical characteristics of the to-be-grasped object.

The mirror neurons form the second class of visuomotor neurons of area F5. This name was coined because of their property to "reflect" with their visual response an action executed by another individual, if the seen action is similar to that motorically coded by them (di Pellegrino, et al., 1992; Gallese et al., 1996; Rizzolatti et al., 1996). In contrast to the canonical neurons, mirror neurons do not respond to the mere presentation of objects. Thus, the vision of a real action, performed by a biological agent (the experimenter or another monkey) is essential for their activation. A mimed action, not interacting with an object, or an action executed by a tool (e.g. pliers) are ineffective in triggering most of F5 mirror neurons. Almost all mirror neurons show a certain degree of congruence between the effective observed and executed action. This congruence is very strict in about one third of F5 mirror neurons. Very recently, it has been reported that a fraction of mirror neurons, in addition to their visual response, become also active when the monkey listens to an action-related sound (e.g. breaking of a peanut) (Kohler et al., 2002). It is tempting therefore to conclude that mirror neurons may form a multimodal representation of goal directed actions, possibly involved in action recognition.

Aim.

The goal of monkey experiments was to investigate the nature of the visuomotor coupling at the basis of the "mirror" response. Our hypothesis was that mirror discharge could be initially generated by the observation of one's own acting effector, seen from different perspectives, performing repetitively the same action. We assumed that these different visual information could be associated by the brain as "common signals", having in common the same motor goal. Following this learning phase, the system could become therefore capable to extract motor invariance also during observation of actions made by others. Although the learning process described above should mainly occur during development, we postulated that also in adult animals some vestigial residuals of this visuomotor coupling could have resisted in F5 motor neurons (generally considered as devoid of any visual property). To investigate this hypothesis, we programmed a series of single neuron recordings in monkey premotor area F5 while the animal was executing a grasping movement with normal and manipulated visual information (e.g.: complete dark, brief flash of light during different phases of the movement). As a control, primary motor cortex neurons (area F1) have been recorded too.

Methods.

To standardize the grasping movement, a specially designed apparatus has been used. It consists of a box that was mounted at reaching distance (30 cm) in front of the monkey, with little pieces of food hidden inside (Figure 12).

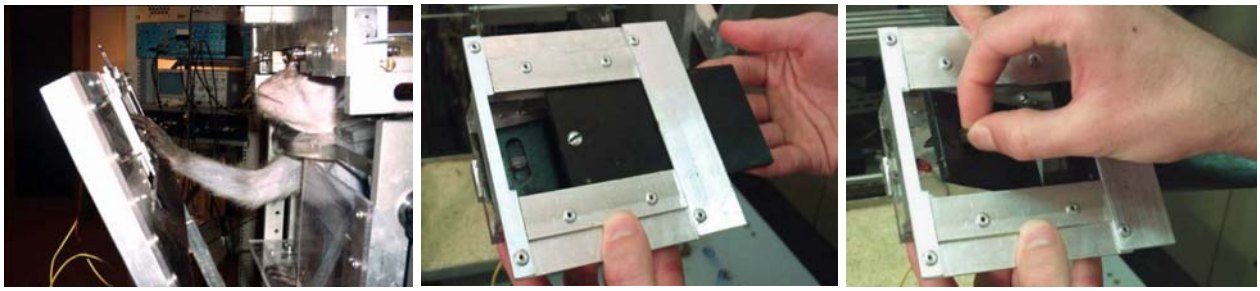

Figure 12. The experimental apparatus.

The box was covered by two doors. A more superficial one (see figure 12, center) whose opening at distance by the experimenter signaled to the monkey the beginning of the trial, and a second one (see figure 12, right), hosting a small plastic cube working as a handle. This plastic cube was translucent and back-illuminated from inside the box by a red LED in order to allow the monkey to fast reach it, also in the dark. The handle was buried inside a grove that forced the monkey to open the door by grasping the handle only by using a precision grip. When both thumb and index finger touched the handle, an electronic circuit (Schmitt's trigger) gave to the acquisition system the synchronization signal. Neuronal activity was recorded during the two seconds following handle grasping, with one second of pre-trigger acquisition.

In order to test the experimental hypothesis, recorded neurons were submitted to four conditions:
a. grasping in full vision
b. grasping in dark with no hand visual feedback
c. grasping in dark with instantaneous visual feedback before contact
d. grasping in dark with instantaneous visual feedback at object contact

In the last two conditions a very brief (20 microseconds) xenon flash illuminated the scene at two different phases of the grasping action: during hand approaching (as triggered by a pyroelectric infrared sensor) (c) and at the moment of handle touch (d).

Results.

We have now finished to collect data in monkey electrophysiological experiments aiming at investigating the role of visual feedback in hand action planning and execution, and we are now analysing those of the second animal. In the analysis we performed on the first animal, we were particularly interested in neurons showing a reduction of their activity in the dark condition with respect to the light one. While in area F1 only about 15% of neurons satisfy this criterion, in area F5 about 57% of the recorded neurons reduced their activity when the grasping hand was not visible. Moreover, neurons responses were subdivided into different epochs according to the phase of movement: Hand shaping epoch, from 250 ms before to the touch of the target handle with both thumb and index finger (precision grip); Touch/manipulation epoch, from handle grasping to 250 ms after (door opening). The statistical comparison between grasping with the hand fully visible (light condition) and grasping without hand vision (dark condition), in the two different epoch, showed that when the modulation is negative it mainly concerns the hand shaping epoch. A further aspect of our analysis was concerned with the effect on neuronal discharge of a brief flash of light, which caused a sudden appearance of the acting hand. Although the dimension of our sample does not allow drawing a conclusive picture on neurons' behavior during flash conditions, these two conditions were included to control for the presence of phasic modulation of activity due to own hand vision. Few cells (about 10% of the modulated ones), showed this very specific phase-dependent modulation.

Conclusions.

The results of monkey experiments presented in this deliverable are, in our view, of great interest. They firstly demonstrate that within a premotor area, involved in hand action programming and execution, there are motor neurons specifically modulated by the vision of monkey's own acting hand. The first important result achieved by these experiments is related to the direction of the modulation. In contrast with area F1, F5 motor neurons are negatively modulated by the absence of the visual hand. This reduction of the response could be, very likely, attributed to the lack of the hand-related visual input in this condition. The second result is that, when a negative modulation occurs, in general it involves the epoch preceding handle touching. If one consider that prediction is strongly embedded in feed-forward control systems, this anticipatory effect, specific for area F5, speaks in favor of a control role played by this area. In the final version of D3.1 (month 30) these results will be further expanded on the basis of the full dataset.

2.2.3 Single neuron study of rat premotor cortex: are there mirror neurons too? (UNIFE)

In the framework of WP3, at UNIFE we are exploring the possibility that a mirror-neuron system exist not only in primates but also in simpler animals such as rats, characterized by an intense social interaction. To this purpose, we projected and realized a multi-electrode amplifier (32 channels) and we started experiments of intracortical microstimulation and recording in rats, in collaboration with the University of Parma (Italy) and the University of Odessa (Ukraine).

Several lines of evidence demonstrate the existence in the primate's premotor cortex of a motor resonant system, the so called 'mirror-neuron system', firstly described in the rostral part of monkey ventral premotor cortex (area F5). Mirror neurons discharge both when the animal performs goal-directed hand actions and when it observes another individual performing the same or a similar action (Rizzolatti et al. 1999; Rizzolatti et al. 1996). More recently, in the same area, but more ventrally, mirror neurons responding to the observation of mouth actions have been found. Most of mouth mirror neurons become active during the execution and observation of mouth ingestive actions such as grasping, sucking or breaking food as well as of communicative mouth actions, such as lipsmacking (Ferrari et al. 2003). Mirror neurons are not limited to premotor cortex but have also been found in area PF of the inferior parietal lobule, which is bidirectionally connected with area F5 (Fogassi et al. 1998). Although at the present there are no studies in which single neurons have been recorded from the mirror-neuron areas in humans there is, however, a rich amount of data proving that a human mirror-neuron system does exist. Evidence comes from neurophysiological and brain-imaging studies (Buccino et al. 2001; Fadiga et al. 2005; Avikainen et al. 2002, see Rizzolatti and Craighero 2004 for a review). This unified representation may subserve the learning of goal-directed actions during development and the recognition of motor acts, when visually perceived.

The existence of multiple motor and premotor cortical areas that differ in some of their properties is well known in primates, but is less clear in small animals. In rats, intracorticali microstimulation reveals in the frontal cortex two separated motor representations of the anterior limb (Neafsey et al. 1986) which are located in different cytoarchitectonic areas (Rouiller et al. 1993) and receive different cortical and thalamic inputs (Wang and Kurata 1998). Some literature data (Neafsey et al. 1986; Rouiller et al. 1993) suggest that these areas (called M1 and NMC, respectively), might be the homologues of primate's primary motor and premotor cortical areas. In fact, NMC seems to participate in preparation and performance of complex coordinated movements by participating in programming and planning of movements. In addition, reciprocal cortico-cortical connections of the rostral forelimb area (RFA) share some pattern with the hodology of primate's motor areas, suggesting that rat's RFA may be considered a far precursor of primate's supplementary/premotor cortex (Wang and Kurata 1998). However, data about the functional characteristics of premotor cortex in rats are not numerous and, more importantly, nothing is known about the existence of motor-resonant systems, like primates' mirror neurons. On the other hand, rats continuously act on objects, interact with other individuals, clean their fur or scratch their skin and, in fact, actions represent the only way they have to manifest their desires and goals. It is therefore plausible that,

considering their manual dexterity and their strong social behaviour, these animals possess some mirror-like neurons in their premotor cortex.

In recent years a new paradigm of learning in small animals was developed through observational training, in which rats repeatedly observed companion rats performing different spatial tasks (Leggio et al. 2003). In some of these experiments animals were actually tested in the tasks they had previously only observed. The results obtained indicate that rats can learn complex behavioral strategies by observing some conspecifics performing the same task. Furthermore, acquisition of the single facets that form the behavioral repertoire can be separately studied as well as the role of particular brain areas (Petrosini et al. 2003). It's well known the ability of rats to manipulate food as well as their capability to retrieve food also when is attached at the end of a long string. (Molinari et al. 1990; Zhuravin and Bures 1988). Thus, a number of such behavioral tasks can be used to investigate electrical activity in the premotor cortex and to elucidate the role of mirror resonant system in rats in these conditions.

Considering that the development of the motor control during ontogenesis is one the most actual problems in the neurobiology and physiology. Despite this interest, only few data have been obtained on functional maturation of motor areas in rat pup cortex (Golikova, 1990). The discovery of mirror neurons in rat's premotor cortex could fundament to study ontogenetic peculiarities of motor resonant system formation. Although extracellular single-unit recordings in restrained, anesthetized animals have long been used in neurophysiological investigations, more recently, modified methods of single-unit recordings in freely behaving animals have converted this classic approach to a powerful new tool to study motor and cognitive behaviours. Another newly developed technique, the multi-electrode single-unit recording in freely behaving animals, is even more powerful in neural circuit studies. With this sophisticated approach, patterns of electrical activity of individual neurons from different areas forming a specific neural circuit can be measured simultaneously during specific behavioural events. This method is therefore indicated to analyse changes in the spatiotemporal patterns of neuronal activity related to goal-directed behaviours.

Methods

Behavioural paradigm and equipment: The main goal of the experiments is to record neuronal activity in rats during hand action execution and observation. To reach this goal, we composed our activity from two different options. The first one was dedicated to design and build a special cage in which rats have to perform free behaviours while the neuronal electrical activity is recorded. This cage must contain two animals, the actor and the observer and, has been conceived in order to allow the observer to easily see the performing rat through a transparent wall. The second task that we carried out was related to proper signals acquisition and analysis. The cage was built with Plexiglas. Dimensions are: length=80 cm, height=45 cm and width=40 cm. The cage is divided into three compartiments by walls made of the same material (Fig. 13, A). The first (equal to ½ size of the cage) is for the rat from which action observation-related neuronal electrical activity has to be registered. Taking into account the big mass of the wires and connectors coming from the microelectrode array connecting the array to the preamplifier and to the amplifier, we designed a special mechanical arm which holds these wires keeping and balances their weight. The remaining space inside the cage was then divided

into two further sectors (see Fig.13, B).

Figure 13. The cage for training and neuronal recording. **A**, frontal view; **B**, top view. The leftmost sector shown in B contains the observing rat; the lower-right sector contains the actor rat which retrieves food from the container visible in the separation.

The partition between these two sectors has one small window (diameter, 25 mm; distance from the floor, 70 mm) allowing the access to a small platform attached to the separation wall. During the experiments a piece of food is positioned on the platform, close to the window, and the actor rat has to grasp this food with its forearm (see Fig. 14, some coloured keys are placed on the platform to make it evident).

Figure 14. Left, the food-containing platform. Right, the cage hosting the rat #1 (left side, the 'spectator') and #2 (right side, the 'actor').

All the rats pertaining to the experimental group (Long-Evans strain) have been previously trained to grasp the pieces of food through the window. The experiments were performed daily from 10.00 to 12.30 a.m. after light food deprivation (food was removed from the cage at 6.00 p.m. the day before the experiment). On average, each rat remained inside the cage for 46±6 min and performed 94±13 grasping movements. The second rat (which also underwent the same food deprivation) was looking at the conspecific from the left compartment of the cage.

The second part of the work consisted in the setup of the recording apparatus. Utah microelectrode array (3x3 mm array containing 36 microelectrodes, Cyberkinetics Inc., USA) have been selected for the experiment (see Figure 15). The insertion of the microelectrode array was performed in deep anaesthesia induced by i.m. ketamine by using a specially designed pneumatic gun (Fig. 16, A) and the multipolar connector was screwed to the skull by using four titanium screws. The operated rats were ready for the experiment after a 7 days recovery period.

A **B**

Figure 15. The Utah 6x6 microelectrodes array (**A** and **B -** bottom and side views, respectively).

A **B**

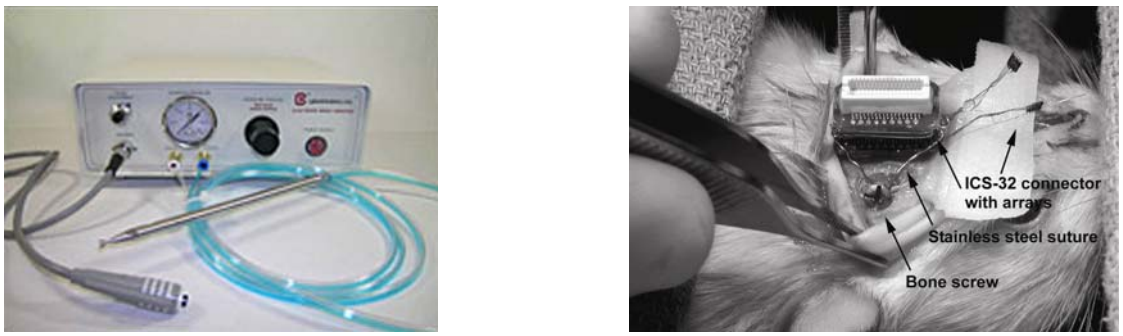

Figure 16. A, the pneumatic device used to push the microelectrode array inside the cortex minimizing tissue damages. B, the connector screwed to the skull.

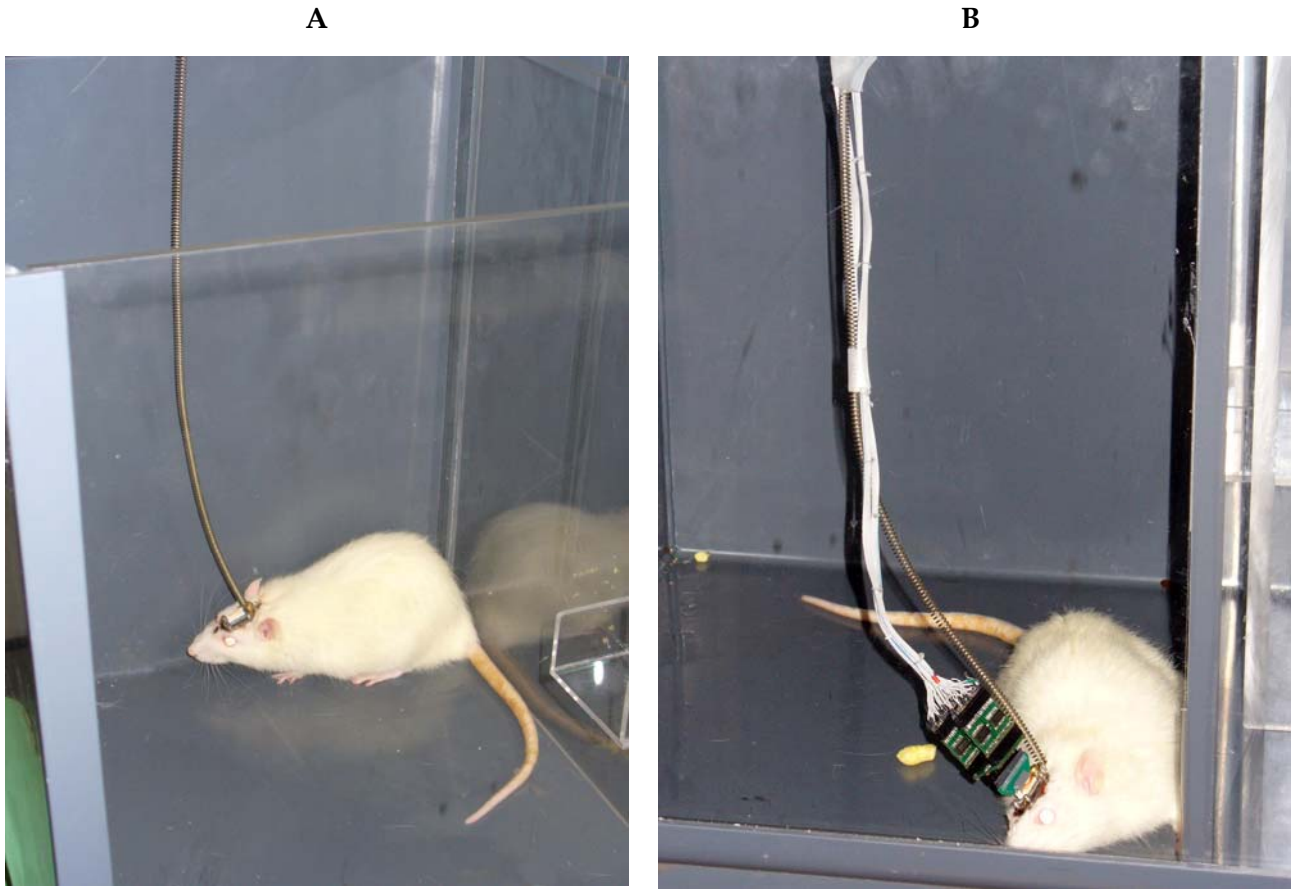

Figure 17. The preamplifiers connected to the head of the rat during recordings. Note the spiral spring providing the necessary rigidity to the system

Electronics: A 32-channels differential amplifier (with respect to a common reference) was designed and built at UNIFE. The data acquisition system for recording and processing neural signals for the 32 extracellular electrodes could be easily extended up to 128 extracellular electrodes by additional modules. Acquisition of signals is triggered by the 'actor' rat by means of a specially designed TTL-trigger (Fig. 9). The acquisition starts at the moment at which the rat touches the food. Miniature low-noise and low input bias current preamplifiers (based on TLC 2272) were fixed on the head of the animal before experiments and connected to the multielectrode microarray through a ICS-32 connector (Ciberkinetics, Inc.) (Fig. 17). After the preamplification stage, the signals reach the amplifier by a thin and flexible 36-wires flat cable. The full amplification gain has been set to x10000. The main unit containing the last-stage amplifiers (fully battery powered), is composed of four compact 8-channel processing boards (Fig. 18). The front-end modules amplify the signals and transmit them to a host PC system via a National Instruments SH100100 shielded cable. A Digital Acquisition Card (PCI-6071, National Instruments, 16-Bit, up to 1.25 MS/s, 64 analog inputs), was used to digitize the input signals. In our configuration, 32-channels were reserved for the acquisition of signals from

electrodes, 1 additional channel was used for the trigger and 2 channels were used as technical references (to control the power supply voltage and current).

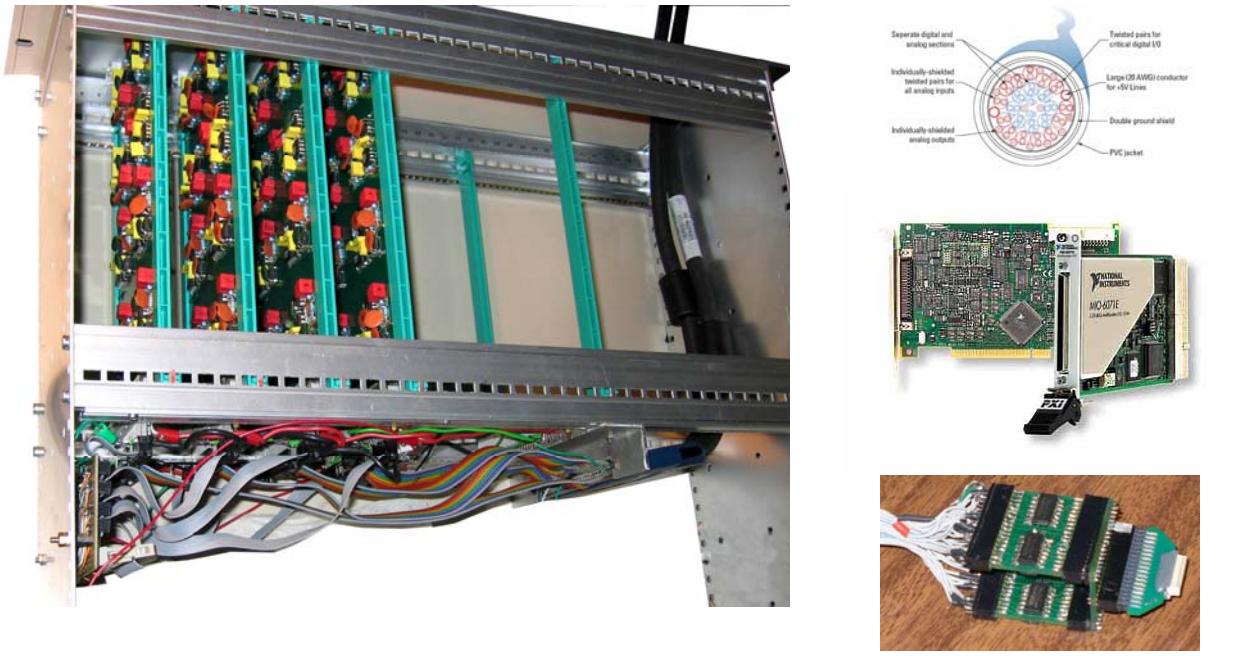

Figure 18. Overview of the multichannel acquisition system for single unit recordings in small animals. Left: the main unit, with 4 boards each hosting 8 last-stage x 10,000 amplifiers. Its rightmost compartment is reserved for the batteries. Right, upper: the shielded cable connecting amplifiers and D/A Converter (SH100100, National Instruments). Right, middle: Digital Acquisition Card (PCI-6071E, National Instruments). Right, lower: preamplifiers head stage (2 boards hosting each 16 preamplifiers connected to a miniature ICS-32 male connector).

Software: The software interface we setup at UNIFE runs on a PC (Windows XP Pro) allowing the user to configure the data processing, to visualize and to analyze the incoming data. The graphical interface is user-friendly and is entirely written in LabView 7.0 (National Instruments Inc.). In order to simplify the description the software package will be called here as 'Neuro-RAT'. The flexible digital architecture of the Neuro-RAT program allows the user to perform a variety of different on-line and off-line analyses, from simple data streaming and storage, to on-line filtering and spike sorting. The program contains three main parts: a) monitoring; b) acquisition; c) analysis.

The Monitoring part is designed for real-time observation of the activity as recorded from all the recording microelectrodes shown by colour-coding the neural activity (Fig. 19). It is therefore capable to detect spikes in all active electrodes and, moreover, to monitor one selected channel with different timescale. We found colour-coding rather helpful because it allows to quickly select and display the electrodes showing the better correlation between neuronal discharge and animal behaviour. At the same time, it helps to determine electrodes showing

noisy or corrupted activity. Another interface window (Fig.19, B) allows to visualize raw-signal from 8 different electrodes user-selectable from the 64 array.

A **B**

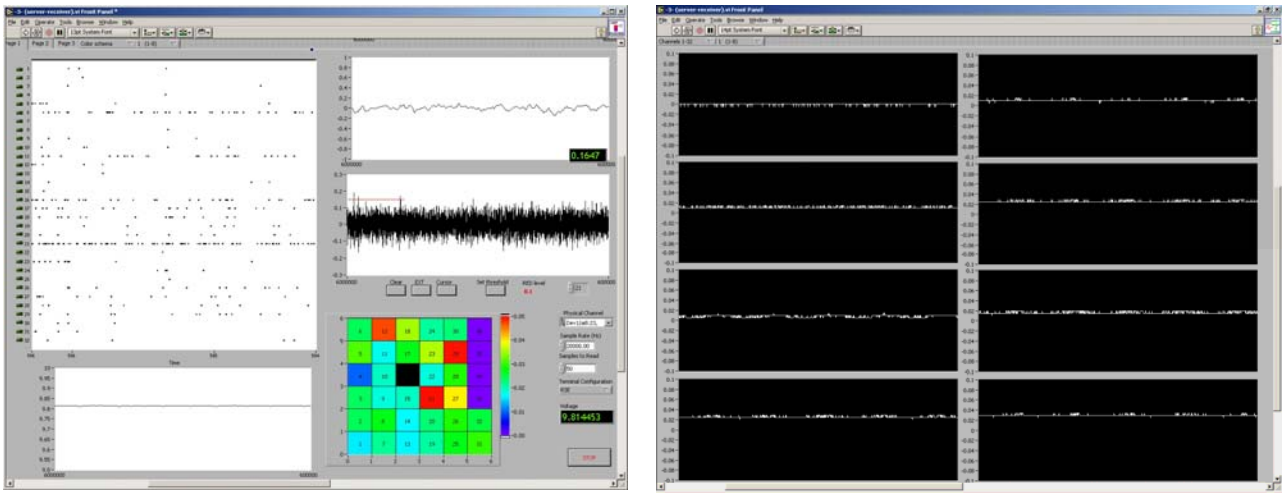

Figure 19. The main interface windows of the Monitoring component of Neuro-RAT. Note in A the color coded array where each position shows the activity of the corresponding microelectrode.

A schematic view of the Acquisition and Analysis component of Neuro-RAT is shown in Fig. 20. The Analysis part of Neuro-RAT allows to separate single units from polispike recordings and its Interface window is shown in Fig. 21.

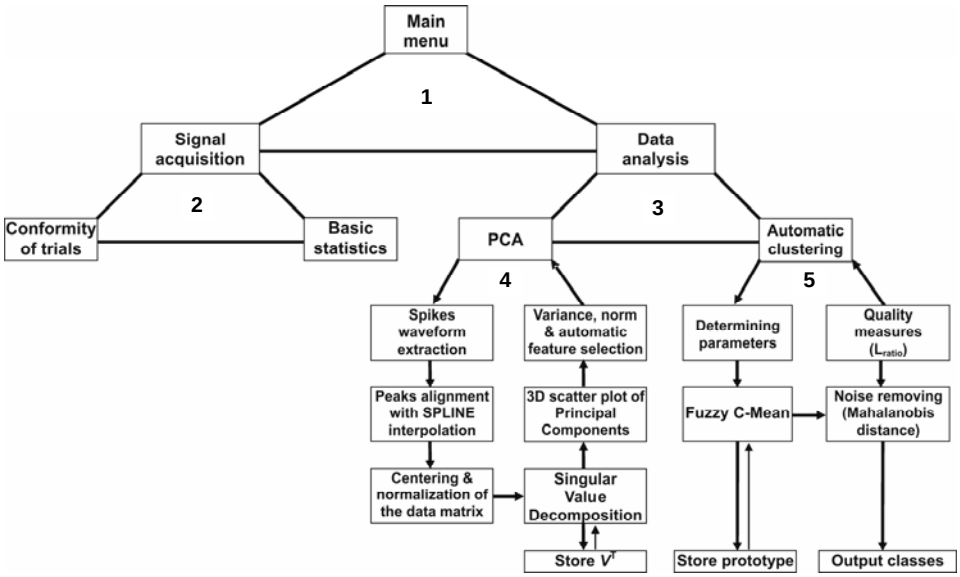

Figure 20. Block-diagram of Aquisition and Analysis part of Neuro-RAT program. The main menu (1) that is at the top level of the program, allows user to initiate new records (2) and to get fast access to any stage of the data processing (3). All other modules of the program are loop-structured and prompt the user to execute the procedure when necessary. Dynamic links between modules and storage of critical parameters of during PCA (Principal Components Analysis, 4) and FCM (Fuzzy C-Mean, 5) allows the program to solve the invariance problem during Principal Component Analysis, automatically select the features to be used in classification, to choose the best settings for clustering (new or previously calculated for a given recording site) and to remove the noise.

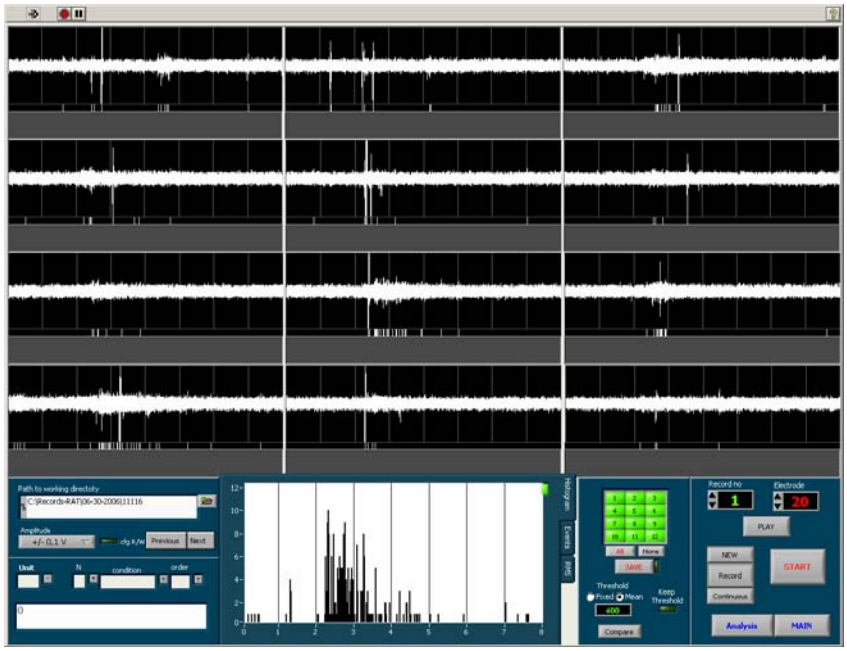

Figure 21. Interface window for the Data acquisition component of Neuro-RAT. The architecture of the user-interface window showing polyspikes acquired during twelve trials is shown. Raw data from the electrode and additional hardware information (i.e. trigger signals) are extracted and visualized. The resulting peristimulus histogram of spikes occurrence (as revealed by the spike sorting module) is shown below the rasters.

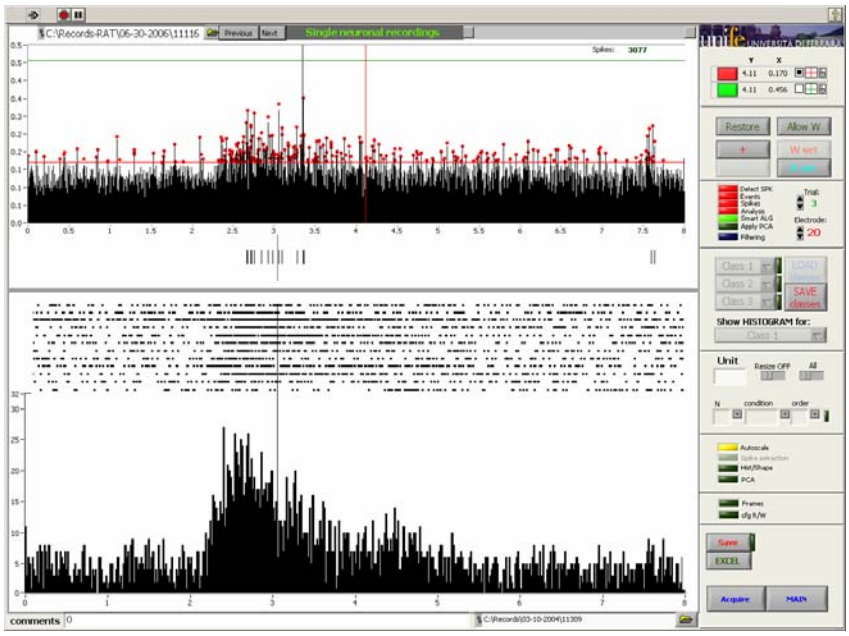

Figure 22. Interface window for the Data Analysis component. Top, the interactive thresholding used for the spike sorting algorithm. Bottom, the peristimulus histogram built from the spikes selected by the thresholding procedure. Note that this amplitude-threshold criterion is too permissive and pools together spikes coming from different neurons.
To obtain in-depth spike sorting, a dedicated part of Neuro-RAT performs Fuzzy C-Mean Classification of Principal Components in multi-dimensional space.

It should be stressed that, the possibilities and functions of the Neuro-RAT software are integrated by filters, smoothing algorithms signal and other useful math tools, implemented available when needed.

Current state of the art and perspectives:

1) Preliminary exploration and functional characterization of rat premotor cortex by intracortical microstimulation: done.

2) Setup of the training procedure of Long-Evans rats: done.

3) Setup of surgical implant: done.

4) Readiness of preamplifiers: 90% (a lighter cable is under construction).

5) Readiness of last-stage amplifiers – 100%.

6) Readiness of acquisition hard & software – 100%.

7) Readiness of analysis software – 90%.

The project is proceeding as expected. The extensive mapping of at least six animals will be finished by the end of the third year of the RobotCub IP.

2.3 Schemas for artefacts

2.3.1 Cortico-spinal (CS) excitability during interception with precision grip (UNIFE)

Interception in humans is a complex visuo-motor task that requires in few hundreds of milliseconds to detect and process visual motion information, to estimate future position of objects in space and time, to transform visual information into an appropriate motor action and to trigger this action in advance, to compensate for physiological and biomechanical delays.

Despite this complexity, humans demonstrate rather good performance in interceptive actions, especially in high-speed ball games (Bootsma & van Wieringen, 1990; McLeod, 1987) but also in laboratory environment (Day & Lyon, 2000; Soechting & Lacquaniti, 1983). One of the critical point is to be able to estimate the time remaining before contact (or time to contact, TTC) in order to trigger the action at the right time. Thirty years of research in this field has led to the proposal that humans use anticipatory mechanisms based on on-line visual information (Lee, 1976) that can be combined with *a priori* implicit knowledge of the rules of physics for the target motion (Lacquaniti, Carrozzo & Borghese, 1993; McIntyre, Zago, Berthoz & Lacquaniti, 2001). By this mean, an estimate of TTC can be updated and improved on line from object appearance until the time at which the action must be triggered.

If the psychophysics of this mechanism is well documented, our knowledges in the physiology of interception are rather poor. However, recent experiment in monkeys ((Merchant, Battaglia-Mayer & Georgopoulos, 2004; Port, Kruse, Lee & Georgopoulos, 2001)) have shown that the activity of neurons in the primary motor cortex (M1) during interception is modulated by the stimulus parameters and especially by an estimate of TTC. At UNIFE we began a series of experiments in order to investigate the excitability of the cortico-spinal (CS) system in humans during the interception of a falling object and its relationship to the target parameters. The hypothesis is that CS excitability should increase as the estimate of TTC is updated until it reach the threshold value at which the muscular activity is triggered.

It is known that action, observation of action and internal simulation of action share some common neural mechanisms and substrate in humans (Decety, 1996; Fadiga, Fogassi, Pavesi & Rizzolatti, 1995; Rizzolatti & Craighero, 2004). Moreover, it has been shown that the timing of simulated actions is similar to the timing of real actions (Decety, Jeannerod & Prablanc, 1989) and that the temporal parameter of actions are coded in motor cortex during action observation (Gangitano, Mottaghy & Pascual-Leone, 2001). Thus, a second aspect of the project was then to determine if similar modulations of the CS excitability could be seen during execution, observation and simulation of an interceptive action.

Methods

We used transcranial magnetic stimulation (TMS), as this technique has already shown to be relevant for testing CS excitability modulation in all these tasks (Fadiga et al., 1995; Fadiga et al., 1999).

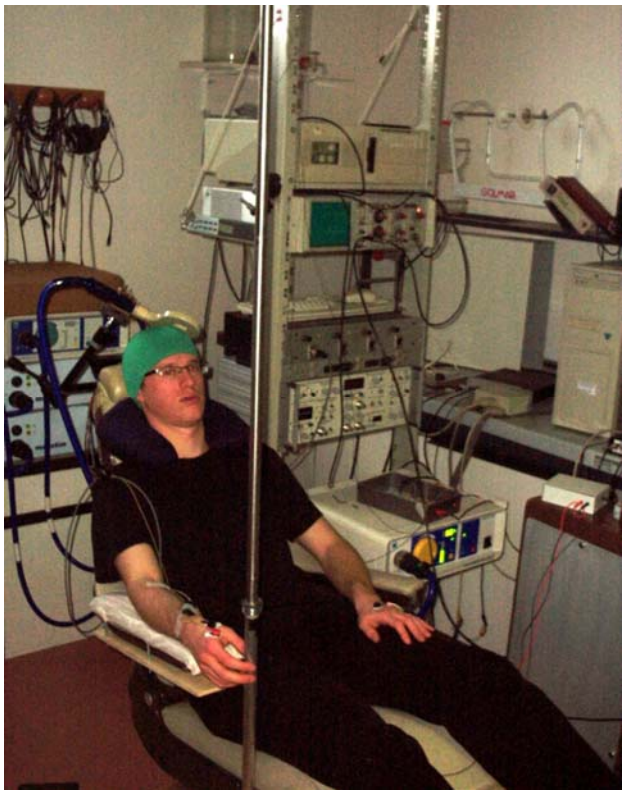

Figure 23. The experimental setup

To this purpose, single pulse TMS applied at different timings during the fall of the target was used to assess the time-course of CS excitability through the amplitude of moto evoked potentials (MEP). MEPs were recorded from the right first dorsal interosseus (FDI) muscle while the subject try to intercept with a precision grip a bar sliding down along a vertical bar (see Figure 23). In a first experiment, single pulse were delivered at -200 ms, 0 ms, +100 ms and +200 ms relative to the release of the target bar. CS excitability was computed as MEP area and compared to a baseline level recorded while subject was at rest. Four experimental conditions have been studied: Execution, No-Go (subjects were instructed to refrain from grasping), Simulation (motor imagery of the grasping movement triggered at the instant of object's fall), and Observation of others (while performing the same grasping movement).

Results

The results (see Fig. 24) showed clear modulation of CS excitability during *Execution* and *No-go* but no significant modulation were found in other conditions. CS excitability started to

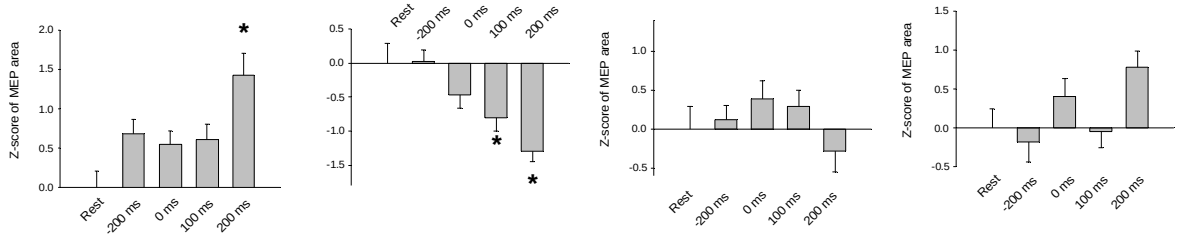

Figure 24. From left to right, Z-score of MEP area in the Execution, No-go, Observation and Simulation conditions. Asterisks signal significant ($p<0.05$) difference relative to baseline.

increase before target release and then slightly decrease at release to increase again until 200 ms. However, despite we found a significant effect of ST (one way ANOVA, $F(4,52)=4.57$; $p<.05$) on MEP area, a Newman-Keuls post-hoc analysis demonstrated that only MEP evoked when TMS pulse was delivered at 200 ms were significantly larger than those evoked at rest and at all other latencies except than at time of release. In summary, CS excitability increases above baseline between 100 and 200 ms after ball release.

During the No-go condition, we observed a general decrease of the CS excitability relative to the *Rest* condition. The one way ANOVA revealed a significant effect of ST ($F(4,52) = 5.8$, $p < 0.05$) and Newman-Keuls post-hoc analysis demonstrated that MEPs evoked when stimulation occurred at 100 and 200 ms after release were significantly smaller than the ones evoked at other latencies and during *Rest* ($p < 0.05$) but not significantly different from each other.

In summary of the first experiment, we found a facilitation of cortico-spinal excitability 200 ms after target release in the *Execution* condition whereas a global inhibition was seen during the *No-go* condition, being significant from 100 ms after release. During *Observation*, despite no significant modulation of MEP area relative to the *Rest* condition, we observe a specific inhibition of CS system at 200 ms, that is when CS excitability increase significantly in the *Execution* condition. During action simulation, no significant difference was found relative to Rest but slight increases of CS excitability were observed at ST 0 and 200 ms relative to target release.

The increase of CS excitability in time during the *Execution* condition reflects the characteristics of interceptive task in which, in contrary to reaction time tasks, the action must be triggered in response to an internal signal (TTC threshold) and not an external one (stimulus). This internal signal should reach its threshold value at about 250 ms as EMG activity began at 280 ms in average. It can be assumed that the CS excitability is rising whereas the TTC

estimate is updated in order to be closer from motor threshold at the triggering time. On the other hand, the decreasing CS excitability during the *No-go* condition is likely reflecting a mechanism dedicated to lower the sensitivity of motor cortex to neural command triggered by the stimulus.

Previous (submitted) data in MEG shown remarkably similar activations during catching and a No-go condition along the dorsal visuo-motor pathways suggesting a stimulus- rather than a task-driven processing. The absence of significant modulation in the *Observation* condition could be expected as TMS pulses were applied before the action begins to be in line with the stimulation time in the Execution condition. A second experiment with different time of stimulation has been performed and results are under process. Finally, the absence of modulation in the simulation condition is difficult to explain. Contribution of M1 to motor imagery is demonstrated by some studies and not by others (see (Lotze et al., 2006)). The observation of M1 activation during motor imagery seems to depend on methodological considerations and our lack of results could be attributed to the difficulty to simulate the task.

2.3.2 Robotic implementation of models of sensory-motor coordination for reaching, grasping and tracking tasks. (SSSA, UNIZH, UNISAL)

The availability of robotic platforms with adequate levels of anthropomorphism, in the sensory systems and in the kinematic structure, allows an experimental investigation of the models of sensory-motor coordination in reaching and grasping.

The SSSA humanoid robot.

The SSSA humanoid robot mimics human mechanisms of perception and action, and can implement neurophysiological models of sensory-motor coordination, for experimental validation. The system is composed of sensors and actuators replicating some level of anthropomorphism, in the physical structure and/or in the functionality. It is worth noting that their specifications were defined together by roboticists and neuroscientists (Dario et al., 2005). The platform is constituted by a 1-link trunk which supports one arm/hand system and a neck/head system (see Fig.1). The 2-dof trunk is part of the arm (Dexter arm, by S.M. Scienzia Machinale srl, Pisa, Italy) which has in total 8 dofs, and integrates the 4 motors of the three-fingered hand on the forearm. The arm structure is anthropomorphic in reproducing a 2-dof shoulder, a 1-dof elbow and a 3-dof wrist (Zollo et al., 2003). The mechanical transmission system is realized through steel cables, which allow the 6 distal motors to be located on the first link, which represents the trunk, by achieving low weight and low inertia for the distal joints. The proprioceptive information for the arm 8 joints are given by a measure of the power consumption of each joint as well as joint positions provided by incremental encoders located on each motor. The hand is has anthropomorphic dimensions and weight (Roccella et al., 2004). Each finger consists of 3 underactuated dofs driven by a single cable allowing flexion/extension. A 2-dofs trapezo-metacarpal joint at the base of the palm allows thumb opposition movement (adduction/abduction). In total the hand has 10 dofs, 6 of which are underactuated. The perception system of the hand includes proprioceptive and exteroceptive sensory systems, and in particular: 9 position Hall-effect sensors, 3 for each finger, one per phalanx; 4 motor encoders; 3 3D force sensor, one for each finger, embedded in the fingertips providing the three force components of the contact; 9 ON/OFF contact sensors, 3 for each finger, one per phalanx. The anthropomorphic robotic head has been designed on the basis of the physical structure and performance of the human head in terms of dofs, ranges of motion, speeds and accelerations (Dario et al., 2005). The head has a total of 7 dofs equipped with incremental encoders for measuring the positions of all the joints as proprioceptive information: 4 dofs on the neck (1 yaw, 2 pitches at different heights, 1 roll), 1 dof for a common eye tilt movement and 2 dofs for independent eye pan movements. The 4 dofs on the neck allow the head to perform dorsal/ventral and right/left neck flexion movements as well as neck rotation. The 2 dofs performing pan movement of the eye permit vergence of the two eyes, thus allowing foveation of targets. The performance of the head allows performing human eye movements such as smooth pursuit and saccades. The head is equipped with 2 cameras providing retina-like images, i.e. space variant image whose resolution is higher in the centre (fovea) and degrades towards periphery, as an imitation of images generated onto the human retina (Sandini & Metta, 2003).

Functional biologically-plausible models of sensory-motor mapping and of learning of sensory-motor coordination have been implemented on different parts of the ARTS humanoid platform. Such models have been adapted from the DIRECT (Direction to Rotation Effector Control Transform), proposed in (Bullock et al., 1993). The implementation of these sensory-motor coordination models on the ARTS humanoid is based on self-organizing neural networks that learn how to coordinate motor actions with sensory feedbacks.

Figure 25. The ARTS humanoid robotic platform.

The model builds a mapping between the positions of the robot in the external space (Cartesian space), as given by the sensory systems, and in the internal space (joint space), as given by the proprioceptive systems. The neural networks start with few information about the robot kinematics, like the number of DOFs and the maximum ranges of motion. During an initial learning phase, associations are created between spatial directions of movements and joint rotations, through random endogenous movements whose effects are detected by vision or touch (similarly to human infants). After learning, the built associations are used to set the proper joint rotation in order to reach a target position. This model has been implemented with Grossberg's outstar cells and Growing Neural Gas (GNG) Networks, as proposed by Bernd Fritzke (Fritzke, 1994). Differently from other techniques, these networks do not have predefined dimension nor topology and can grow, reduce, and re-configure in order to better solve the problem they are designed and trained for. Based on this model, we developed and experimentally validated a neurocontroller for positioning and orienting the robot hand in the 3-dimensional Cartesian space (Asuni et al., 2006; Asuni et al., 2005(b)) and a neurocontroller for

gazing a point in the three-dimensional space, with the robot head, by controlling the neck and eye movements (Asuni et al., 2005(a)). An adaptation of the model includes predictive control of grasping and has been implemented on the ARTS humanoid to obtain 'adaptable grasping', that is the robot was capable of looking at an object, determining the position of the hand for grasping, and accomplish the grasping action by using the tactile perception with an expected perception control loop (Laschi et al., 2006). An alternative biological model (Goossens & Van Opstal, 1997) has been implemented for the coordination of the ARTS humanoid neck and eye movements (Maini et al., 2006).

The UNIZH approach to grasping.

At UNIZH, we investigated how the shape adaptation can be taken over by morphological computation performed by the morphology of the hand, the elasticity of the tendons, and the deformability of the material covering the finger tips, as the hand interacts with the shape of an object. When the hand is closed, the fingers will, because of its anthropomorphic morphology, automatically come together. For grasping an object, a simple control scheme, a "close" is applied. Because of the morphology of the hand, the elastic tendons, and the deformable finger tips, the hand will automatically self-adapt to the object it is grasping. Thus, there is no need for the agent to "know" beforehand what the shape of the to-be-grasped object will be. The shape adaptation is taken over by morphological computation performed by the morphology of the hand, the elasticity of the tendons, and the deformability of the finger tips, as the hand interacts with the shape of the object. Because of this morphological computation, control of grasping is very simple, or in other words, very little brain power is required for grasping. (Pfeifer et al., 2006; Pfeifer et al., in press). We also implemented a learning mechanism in order that the robotic hand can learn to grasp objects by itself as described in WP2 Cognitive development (Gomez et al, 2005 and Gomez et al, 2006).

If the robotic hand actively manipulates an object, there are likely to be correlations in the sensorimotor space. This "good" sensory-motor data can be exploited for perceptual categorization, adaptation, and learning. In a previous series of studies, we have investigated how the usage of correlation, entropy, and mutual information can be employed (a) to segment an observed behaviour into distinct behavioural units, (b) to analyze the informational relationship between the different components of the sensory-motor apparatus, and (c) to identify patterns (or fingerprints) in the sensorimotor interaction between the agent and its local environment. These methods were applied to real robots (Lungarella and Pfeifer, 2001; teBoekhorst et al., 2003) and simulated robotic agents (Lungarella et al., 2005; Gomez et al., 2005; Tarapore et al., 2006) and we are using them now in experiments where the robotic hand is involved in grasping tasks (Lungarella and Gomez, in preparation).

The UNIZH approach to Tracking.

In order to detect objects moving in the environment we have implemented 2 different systems:

The first one is based on elementary motion detectors (EMDs) based on the well-known elementary motion detector of the spatio-temporal correlation type (Marr, 1982), a description of the model implemented, can be found in (Iida, 2003), that successfully implemented a biologically inspired model of the bee's visual "odeometer" based on EMDs. The model was used to estimate the distance traveled based on the accumulated amount of optical flow measured by EMDs. Fig. 1c and 1d show the EMDs responding to motion.

The second one is based on the optic flow extraction. We used the generalized gradient method based on Spatio-Temporal Filtering (Sobey and Srinivasan, 1991; Nagai et al., 1999). A detailed explanation can be found in Fig. 2 and for an example of the performance see Fig 1b.

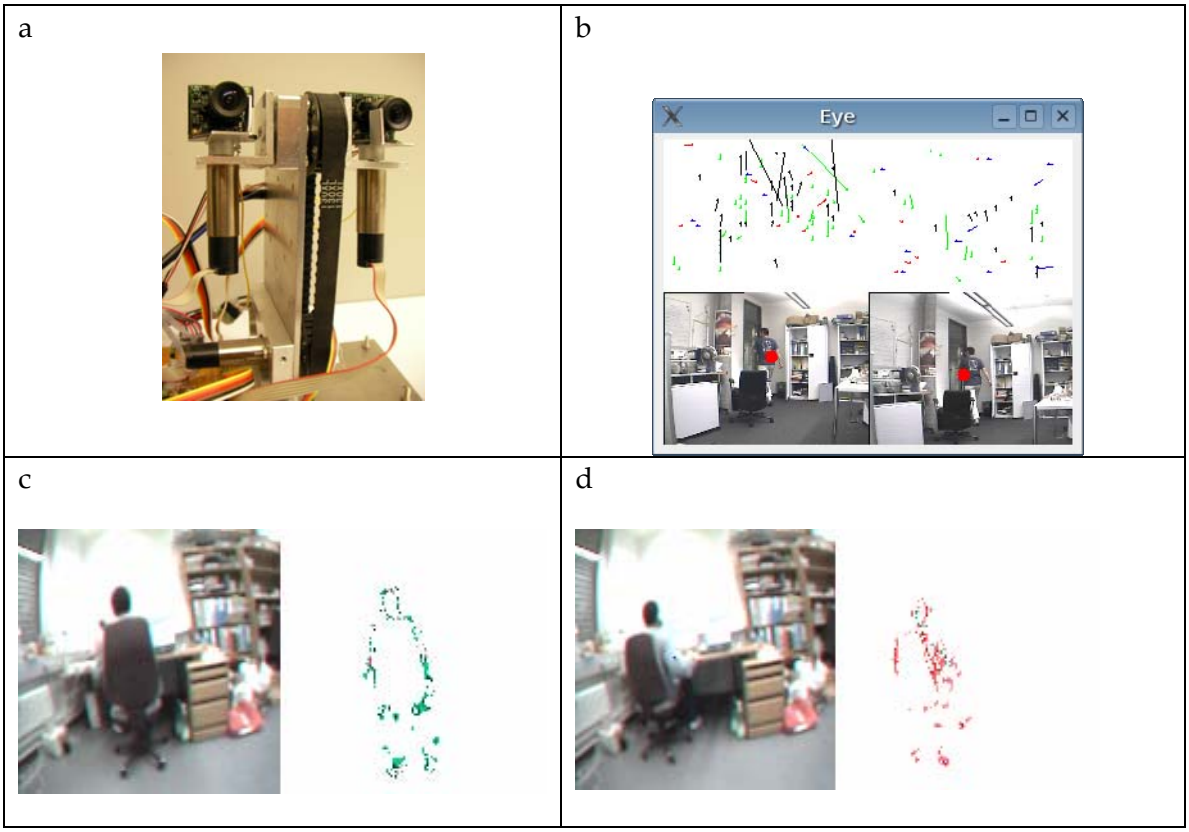

Figure 26. Active vision system. (a) Hardware implementation (b) the lower part consists on the left and right images captured by the cameras, the upper part are the corresponding optical flow. The red dots are the centroid of the motion (i.e., where the robot should gaze). (c-d) EMDs reacting to motion towards the right side of the image (green dots) and to motion to the left direction (red dots).

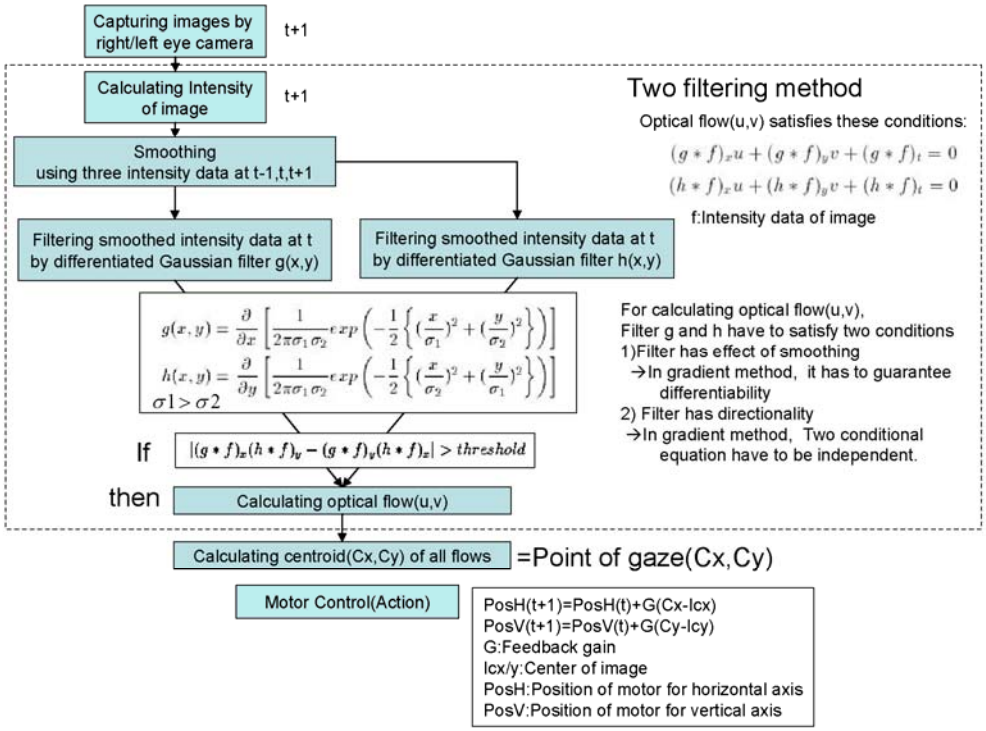

Figure 27. Optical flow extraction.

The contribution of UNISAL to track the acting hand (UNISAL, UNIUP, UNIFE).

At UNISAL, the efforts concerning WP3 have been directed towards:

i) Development of a input tracker glove in conjunction with UNIUP looking at the development of technology to accurately track hand actions in infants up to 24 months. This work has produced a new miniaturised wireless sensory glove able to track the motions of the all finger and the thumb. The current work is developing the software interface and refining the glove design for ease of use and acceptance by the child. These refinements have been based on initial trials with children. It is expected that a new version with testing will be completed within the next recording period permitting the collection of real data.

ii) To permit a greater more accurate analysis than is currently available from glove systems a new high resolution finger tracking systems has been designed and is undergoing testing. This system has been developed based on input from UNIFE. At this time the system has been design and tested with operational software showing accurate 6 dof tracking (accuracy better than 0.1 mm at finger tip). With further development this will be integrated with the work at UNIFE and UNIUP.

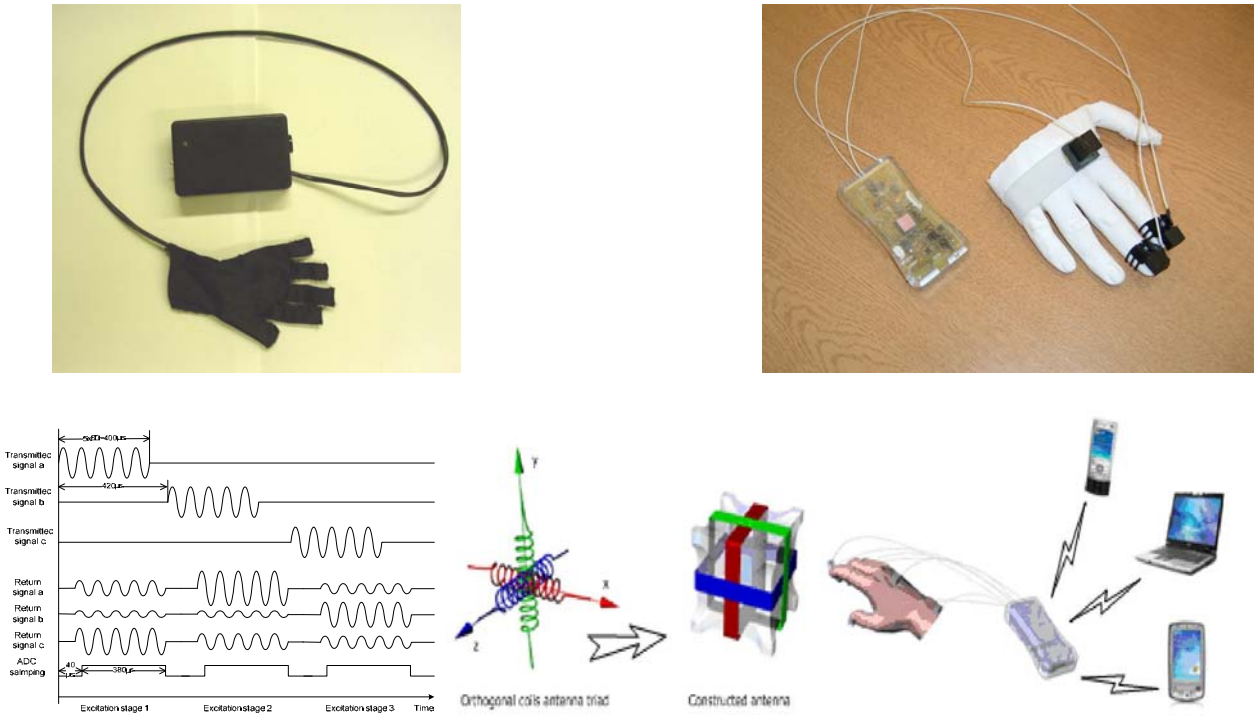

Figure 28. The two hand tracking systems developed at UNISAL with UNIUP (left) and UNIFE (right). This second tracker, in particular, associates high precision to small dimensions. The signal relative to fingertips positions can be remotely transmitted via WiFi of Bluetooth protocols.

iii) At the same time, UNISAL is continuing its work on the development of an understanding of the sensory systems for legs, hips, feet and the sensory requirements of the iCUB. The data relative to this approach will be presented in the final version of this Deliverable 3.1 (month 30).

2.3.3 Sensorimotor Integration of gravity models. (UGDIST)

The work for WP3 at UGDIST has proceeded along two main lines of research. We investigated the acquisition and construction of internal models both in humans and robots. In particular, as a starting point, we concentrated on the acquisition of models of the gravity load during point-to-point movements: i.e. reaching. In the following we illustrate these two aspects.

Gravity models in humans

Introduction. We have designed a series of experiments with the aim of understanding which strategy do humans use to predict the trajectories of flying objects and to catch them. A number of different hypotheses have been proposed to explain this kind of prediction. Our version states that humans build internal models of the dynamics of the flying object and then use this model to intercept it. This point of view is connected with a wider theory in motor control. In fact Mussa Ivaldi and others [2000] proved that a subject moving in a force field, builds an internal model of that field and adopts this model to correctly adapt his movements against the perturbing force. There are already evidences of the existence of an internal model of gravity [McIntyre et al. 2001], [Zago et al., 2004] and a recent work by Hayhoe and others [2005] provides further evidence of the existence of internal models of more sophisticated dynamic properties of the environment.

Methods. Our experiments are organized as follows: the subject looks at a computer screen and moves a magnetic tracker vertically to drive a small paddle up and down on the right side of the screen. His task is to intercept a ball with the paddle which crosses the scene following a parabolic path. The last part of the ball trajectory is hidden in order to force the subject to use prediction. The subjects are divided in two groups: a test group and a control one. To the test group are shown trials (15 blocks of trials, 65 each) in which the parabolic trajectories of the ball are always different, yet generated by the same dynamical system. In particular the ball moves in a force field similar to the gravitational one, characterized by a constant acceleration. The test group is further divided in two parts, according to the direction of the acceleration: downward versus upward direction. During the 14th block the model is suddenly abandoned and the acceleration is randomly chosen. The control group must cope with trajectories which are always parabolic, but which have not an underlying model: each trial presents a different acceleration, both in modulus and direction [upward - downward].

Results. The mean error (distance between the arrival point of the ball and the corresponding position of the paddle) recorded during the experiments are summarized in Figure . From statistical analysis (two ways ANOVA with blocks and condition) results that the constant acceleration case allows for better performances than the ”random” case, in which the only way to preview the arrival point of the ball is to observe its trajectory and extrapolate. This could indicate that the subject infers the unifying characteristic of the trajectories by building an internal dynamic model of the ball and learning its parameters.

In addition the subjects seem to score a better performance when there is coherence between visual and motor inputs. When the ball is subjected to a constant force field directed in the same direction of gravity (the field felt by the subject) errors are lower, thus indicating a strong link between action and perception. These results look promising although it is fair to be said that they are substantially preliminary.

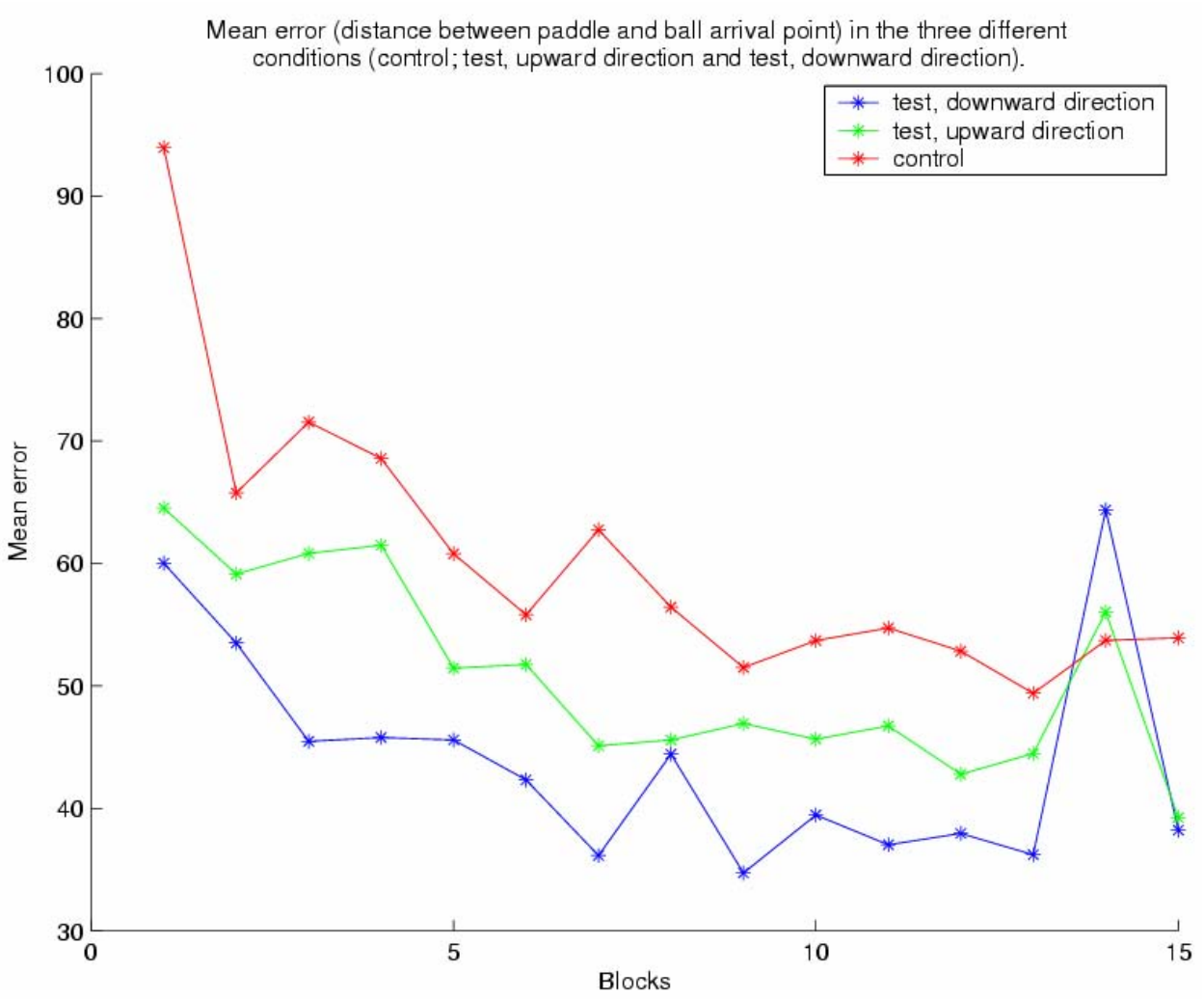

Figure 29. Mean Error (distance between paddle and ball arrival point) in the three different conditions (red = control, green = test, upward direction, blue = test, downward direction).

Gravity models in robots

During the execution of (even simple) arm movements, the effects of gravity need to be taken into account in order to avoid undesired. Therefore, the issue of gravity compensation has always been crucial in the field of robotics [Murray et a. 1994]. Different gravity compensation techniques have been proposed in literature. Among these various techniques, we here focus on model based gravity compensation, limiting our attention on arm point-to-point movements. The main section is divided into three subsections. First, we describe a dynamical model of the arm dynamics. Then, we show how the model can be written in a parametric way. Finally, in

the last subsection, we show some experimental results on the how to compensate gravity on a real robot.

Model of the arm. We model the dynamics of the arm as a fully actuated kinematic chain with n degrees of freedom corresponding to n revolute joints. It is well known in literature that such model can be expressed as follows:

$$M(q)\ddot{q} + C(q,\dot{q})\dot{q} + g(q) = u$$

where q are the generalized coordinates which describe the pose of the kinematic chain, u are the control variables (nominally the torques applied at the joints) and the quantities M, C and g are the inertia, Coriolis and gravitational components.

Parametric model of the arm. In this section, we describe the above dynamic equation in a parametric way. The considered parameters are the masses, the inertias and the center of mass positions for each of the n links which compose the controlled arm. The vector with components represented by these parameters will be denoted p and is composed by the link masses (m_0, m_1, …), the link center of mass positions (c_{0x}, c_{0y}, c_{0z}, c_{1x}, c_{1y}, c_{1z}, …), the link lengths (l_0, l_1, …), and the link inertia tensors (I_{0xx}, I_{0xy}, I_{0xz}, I_{0yy}, I_{0yz}, I_{0zz}, I_{1xx}, I_{1xy}, I_{1xz}, I_{1yy}, I_{1yz}, I_{1zz},…). Obviously, the matrices M, C and g depend on the given vector of parameters, i.e.:

$$M(q,p)\ddot{q} + C(q,\dot{q},p)\dot{q} + g_p(q,p) = u$$

Interestingly, it can be proven that the above parametric dynamics can be rewritten as (see [1] for details):

$$M(q,p)\ddot{q} + C(q,\dot{q},p)\dot{q} + g_p(q,p) = \sum_{j=1}^{J} \Psi_j(p) Y^j(\ddot{q},\dot{q},q)$$

for suitably chosen functions Y^j and Ψ^j. As a special case we have that the gravity term g can be written as:

$$g(q,p) = \sum_{j=1}^{J} \Psi_j(p) Y^j(0,0,q) = \sum_{j=1}^{J} \alpha_j g^j(q)$$

where $\alpha_j=\Psi^j(q)$.Therefore, the effects of gravity on a robotic arm can always be expressed as the linear superposition of terms $g^j(q)$ which do not depend on the dynamical properties of the system. Interestingly enough, this observation has strong connections with the "spinal filed" theory (see [Mussa-Ivaldi et al. 2000] and [Nori et al. 2006] for details) but these connections will not be discussed here being out of our main focus. What is worth saying is that the gravitational properties of the controlled system are represented by mixing coefficients α_j.

Experiments. We designed a set of experiments in order to test if the model:

$$g(q,p) = \sum_{j=1}^{J} \alpha_j g^j(q)$$

agrees with the experimental data taken from the arm of our robot, James (see Figure 30). This test is necessary since the above model is based on a set of assumptions which cannot be completely fulfilled by a real manipulator. In this specific example the arm is four degrees of freedom (three degrees of freedom in the shoulder and one degrees of freedom in the arm) and given the kinematics of the arm we have J=7 and :

J	$g^j(q)$
1	-cos(q1)
2	sin(q1)cos(q2)
3	-sin(q1)sin(q2)
4	sin(q1)cos(q2)cos(q3)-cos(q1)sin(q3)
5	-sin(q1)cos(q2)sin(q3)-cos(q1)cos(q3)
6	[sin(q1)cos(q2)cos(q3)-cos(q1)sin(q3)]cos(q4)-sin(q1)sin(q2)sin(q4)
7	[-sin(q1)cos(q2)cos(q3)+cos(q1)sin(q3)]sin(q4)-sin(q1)sin(q2)cos(q4)

Practically, we can measure the value of g(q,p) at different configurations of the arm by measuring the torques u which has to be applied at the joints in order to keep the system in the specific configuration with zero velocity. We have:

$$g(q^i, p) = u^i$$

where $q^1, q^2, \ldots, q^N$ is a set of configurations and u^i are the torques necessary to counterbalance gravity in order to maintain the configuration q^i. To verify the validity of our model we have to check whether there exists a set of mixing coefficients $\alpha_1, \alpha_2, \ldots, \alpha_7$ that satisfy the following equations:

$$u^i = \sum_{j=1}^{7} \alpha_j g^j(q^i)$$

Obviously, given a sufficient number of measurements (u^i, q^i) the above equations cannot be exactly fulfilled by real data, which are always affected by noise. Therefore, the adopted solution was to estimate the parameters with a least squares procedure:

$$\alpha = \arg\min_{\alpha} \sum_{k=1}^{K} \left\| \sum_{j=1}^{23} \alpha_j g^j(q_i) - u^i \right\|^2$$

and to verify the validity of the estimated parameters on new data samples. Results are shown

in Figure . Training the model with two hundred measurements (u^1, q^1) … (u^{200}, q^{200}) was sufficient to obtain good predictive capabilities thus showing that the model is in good agreement with the real system.

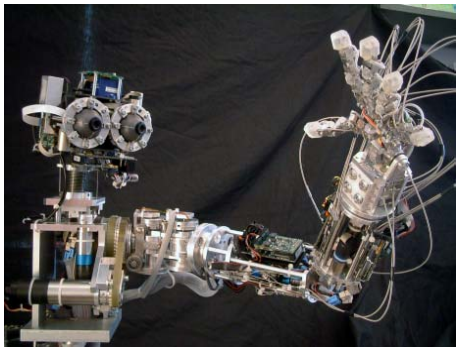

Figure 30. The picture shows our robotic platform, James.

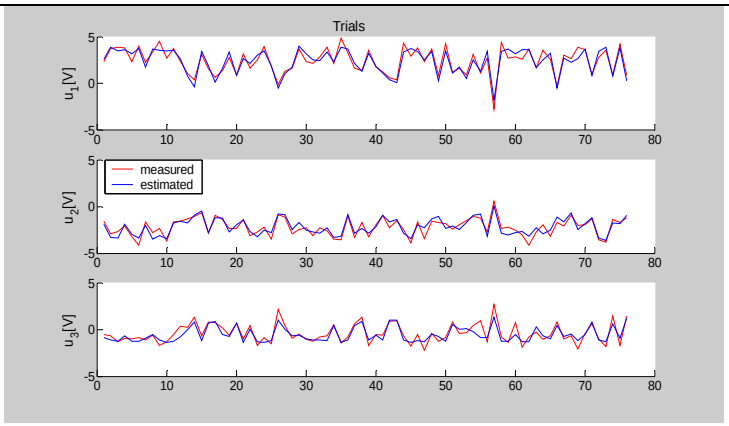

Figure 31. Test of the predictive capabilities of the parametric model. On the horizontal axis, a total of 75 different postures q^1, q^2, …, q^{75} have been considered for testing. For each of these postures we considered the torques necessary to keep the arm at rest (vertical axis). The blue line corresponds to the estimated compensation; the red line instead is the measured compensation.

Non-parametric approximation. The same data were also processed by a non-parametric method which is based on Gaussian processes for regression, a kernel method based on Bayesian inference. The specific algorithm is incremental and sparsifies the solution; it also estimates the hyper-parameters of the algorithm by optimizing a specific quantity (called marginal likelihood). We leave any further detail of the method to the reference in [Csato' et al. 2002] and only show here the result of the approximation of the gravity data from James. The results in the following figures Figure 31 and Figure 32 show that non-parametric estimation is efficient and it can be a good alternative to internal model acquisition. We will explore both possibilities in the future with extensions to the full dynamical model of the robot and its links to other sensing modalities: i.e. vision, vestibular, etc.

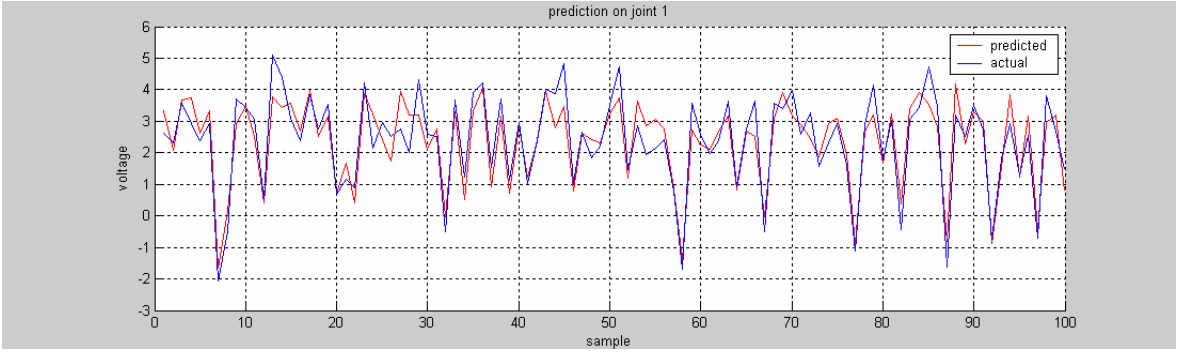

Figure 31. Prediction for joint 1, on a random subset of the available data.

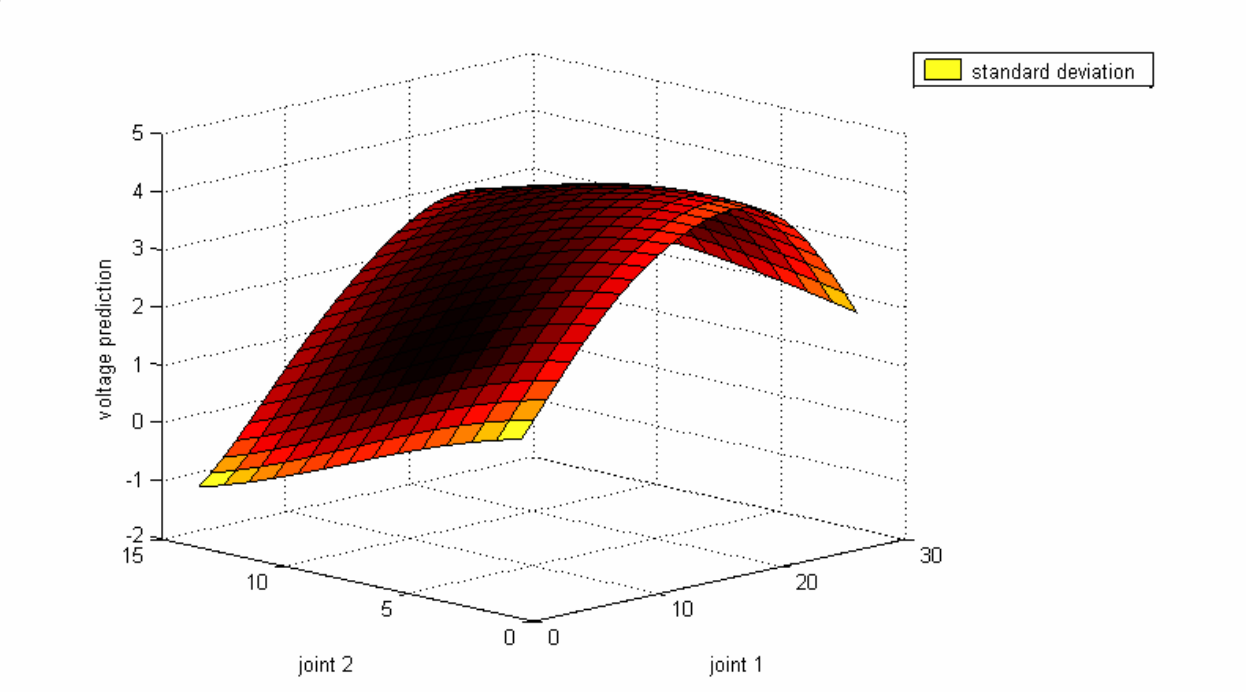

Figure 32. Plot of the predicted function; the shading represents the standard deviation of the prediction. Note how uncertainty grows toward the borders of the region where training points are not available.

2.3.4 Sensorimotor Integration and cortical sensorimotor maps. (UNIHER)

The work at Hertfordshire has addressed the fundamental question: How can raw, uninterpreted information from unknown sensors come to be used by a developing embodied agent with no prior knowledge of its motor capabilities? The approach to answer this in RobotCub is to pursue the development of artificial cortex using information theory as a means for self-organizing sensorimotor structures grounded in experience.

In nature, cognitive structures appear to be organized in the course of evolution and also in the course of development so as to reflect information-theoretic relations arising in the interaction of sensors, actuators, and the environment (including the social environment). Information distance (rather than mutual information or other measures such as Hamming distance) appears to lead to the best structured cortex-like maps of sensorimotor variables [see the paper below]. (For two jointly distributed random variables (e.g. two sensors), information distance is defined as the sum of their conditional entropies $d(X,Y)=H(X|Y)+H(Y|X)$. This satisfies the mathematical axioms for a metric, inducing a geometric structure on the agent's set of sensorimotor variables.) Sensory fields may be constructed on the basis of information methods [Olsson et al. 2004] and then used to autonomously discover sensorimotor laws, e.g. optical or tactile flow and visually guided movement [Olsson et al. 2006]. The particular environment experienced and changes in it can shape the sensorimotor maps and their unfolding in ontogeny [Olsson et al. 2006]. Details were reported in D3.2 "Initial results of experiments on the functional organization of the somatotopic maps and on the cortical representation of movements (report)", and also published as [Olsson et al. 2006a].

More recent work on the informational relationships between the agent, its actions, and the environment [see the paper below] considers a number of statistical measures to compute the informational distance between sensors including the information metric, correlation coefficient, Hellinger distance, Kullback-Leibler, and Jensen-Shannon divergence. The methods are compared using the sensory reconstruction method to fund spatial positions of visual sensors of different modalities in a sensor integration task. The results show how the information metric together with adaptive entropy maximization captures relations not found by the other measures for the construction of somatosensoritopic maps and the development of cross-modal sensory integration. Moreover, these methods are extended to temporally extended experience in WP6, where they are applied to interaction.

2.3.5 Work done by IST on sensorimotor maps. (IST)

The IST group has been addressing the problem of learning sensory-motor maps of high dimension robotic systems. Sensory-motor maps are the mathematical relationships between the information coming from the sensors and the actuators of the robotic system. For instance, one map may determine how visual perception of the robots' hand (image coordinates and velocities) relates to robots' arm motor actions (angular positions and velocities of arm joints).

One of the biggest challenges in the analysis of high dimension systems arises from the existence of redundancies in the motor space, e.g. several arm configurations result in the same hand position. This is advantageous in many situations because we can use the redundant (free) degrees of freedom to avoid obstacles, minimize energy consumption, achieve more comfortable postures, and many others. However, conventional learning mechanisms associating sensory to motor information may not work under these circumstances because the sensory motor maps are no longer unambiguous. In the context of redundant systems we have worked in the above mentioned problems. In particular we are interested in learning the sensory-motor maps, but, at the same time, to use the redundancy to achieve secondary tasks, such as obstacle avoidance and energy minimization. We present three approaches to deal with this problem.

Another problem addressed in this report is related to the learning the sensory motor maps in a way the fully the constraints existing in the joint sensory-motor data. Most existing works to date try to learn either forward (motor-to-sensory) or inverse (sensory-to-motor) maps, which mask some of the underlying structure in the data, mainly when there are redundant degrees of freedom or perceptual aliasing. We propose a manifold learning method, and associated data query and retrieve algorithms, that have the potential ability to address these problems. We present some encouraging results on its application to simulated kinematics and, in future work, will perform tests on real robotics platforms.

2.3.5.1 Minimum Order Sensory Motor Maps

A “Minimum Order Sensory Motor Map (SMM)” is a map that takes the desired image configuration and the Degrees Of Redundancy (DOR) as input variables, while the non-redundant Degrees of Freedom are viewed as outputs. Since the DORs are not frozen in this process, they can be used to solve additional tasks or criteria. This method provides a global solution for positioning a robot in the workspace, without the need to move in an incremental way. We provide examples where these tasks correspond to optimization criteria that can be solved online. We show how to learn the “Minimum Order SMM” using a local statistical learning method. Extensive experimental results with a humanoid robot are discussed to validate the approach, showing how to learn the Minimum Order SMM of a redundant system and using the redundancy to accomplish auxiliary tasks.

Mathematical Formulation

In this section we show how to define a Sensory-Motor Map that explicitly takes the DOR into consideration, thus allowing the completion of several simultaneous tasks.

Let us define a *SMM* that maps a vector of control variables *(n,r)* to a vector of image point features *I*, where *n* is a minimum set of degrees of freedom that spans the full output space and r is a set of redundant degrees of freedom. Note that there are several partitions of the input space, into redundant versus non-redundant degrees of freedom that can give this same property. This forward model can thus be written as:

$$I = f(n, r)$$

and allows predicting the image configuration of the robot given a set of motor commands. In many cases, we are more interested in the inverse map, i.e. computing the motor commands that drive the robot to a desired image configuration, *I*. If there were an inverse mapping $(n, r) = f^{-1}(I)$, this problem could be solved in a straight forward manner. However, as the dimension of the input space is larger than that of the output space, there are many input combinations that generate the same image point features. In other words, because of the DOR, *f(n, r)* is not bijective and, therefore, not invertible.

We built a cost function, *K*, with two terms: one weighting the error in the position of the end effector (data fitness) and another one corresponding to the weights on the control (regularization term).

$$K(I^*, n, r) = \lambda \left\| I - I^* \right\|^2 + c(n, r)$$

This cost function expresses that we are willing to accept some error in the position if another task can be solved at the same time, in this case control costs. Examples of control cost criteria *c* can be ``Comfort'' (e.g. distance to joint limits), Energy minimization (e.g. the position with lower momentum) or Minimum motion (i.e. minimize total motion from current to desired position), posture control, amongst others.

Finding the Solution

The regularized solution can be found by minimizing the defined cost as follows:

$$(\hat{n}, \hat{r}) = \arg\min_{n,r} (\lambda \left\| I - I^* \right\|^2 + c(n, r))$$

where *I* can be computed with the forward model. This formula integrates two terms: one describing the task part and another related to posture control.

There are two important observations to this formulation. Firstly, the optimization is

done with respect to all control variables, which translates into a significant computational cost. Secondly, the DORs are not treated as such, since they undergo exactly the same process as the non-redundant DOFs.

The consequence of this approach is that the extra degrees of freedom are frozen from the beginning and can no longer be used for a different purpose during execution. In a way, redundancy is lost. Instead, in our approach, we would like to keep the redundant degrees of freedom free for solving additional tasks online. In essence, we split the problem in two steps. Firstly, we define a ``Minimal Order Sensory Motor Map'', $n = g(I, r)$. By taking the DORs as input (independent variables) instead of output signals, the problem of computing the non-redundant DOFs becomes well posed. The DORs, *r*, are left unconstrained and can be fixed during runtime, when a secondary task or optimization criterion is specified.

The definition of the ``Minimum Order SMM'' allows us to use the redundancy to meet additional criteria or task-constraints, that can be changed online. The DORs can be determined as the solution of a new optimization problem, with cost function *L*:

$$\hat{r} = \arg\min_{r}(L(I^{*}, r))$$

Note that, in contrast with the previous case, this optimization is done with respect to the redundant degrees of freedom, only. The optimization complexity is thus substantially lower and lends itself to be used as an online process. In general, the solutions in the two cases are not the same, because different local minima could be reached and the criteria are slightly different.

Our approach guarantees zero prediction error, because the *Minimum Order SMM* allows us to determine the values of *n* corresponding to the exact image position, for the selected redundant degrees of freedom. This solution is similar to the first (regularized) problem when λ becomes large. If the *Minimum Order SMM* is not exact, then it will introduce some error in the final image configuration.

Results

The following figure shows the minimization in energy obtained when holding the robot hand in a pre-defined position.

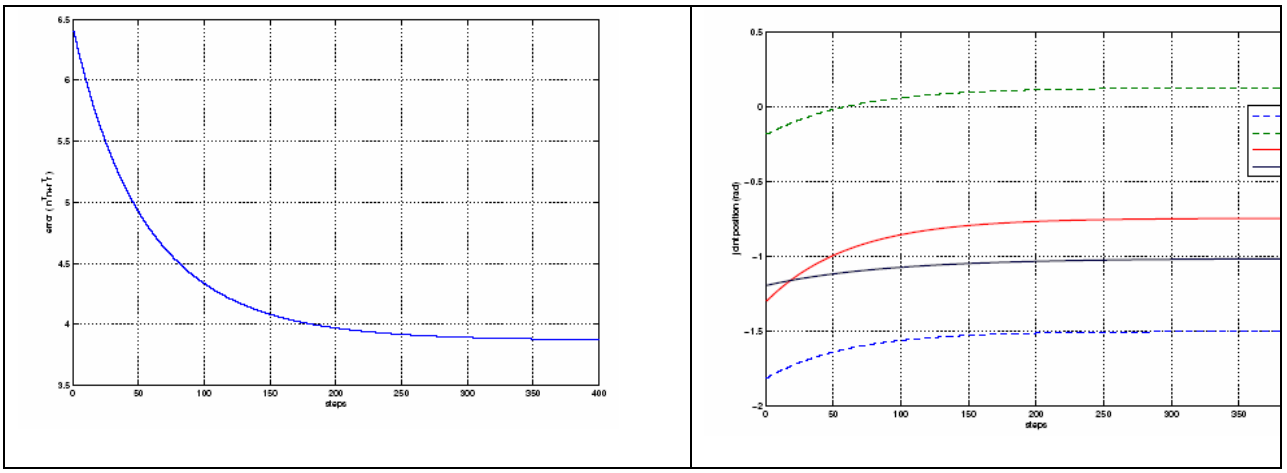

Figure 1 Minimization in energy obtained when holding the robot hand in a pre-defined position (left). Motion of the joints to achieve the result.

2.3.5.2 Visual Controlled Uncalibrated Redundancy Control

Visual servoing methods provide very efficient and robust solutions to control robot motions. They provide high accuracy for the final pose and good robustness to camera calibration and other settings. The redundancy formulation presented in the previous section can be extended to the Visual Servoing framework, to compute a control law that realizes a main task, while simultaneously taking supplementary constraints into account. It can be used when the main task does not constrain all the robot degrees of freedom (DOF). A secondary task can then be added to meet a second objective without disturbing higher priority tasks.

The control law for the second task is computed in the within the set of motions that do not change the primary task. This is achieved by projecting motion hypotheses into the set of motions constituting the null space of the first task, thus leaving the first tasks unmodified. The computation of the projection operator is based on the jacobian of the first task. This approach involves the computation of the task jacobian, linking the evolution of the visual features to the robot articular motion. It thus requires knowledge about the camera world and world-actuator transformations that influence the interaction matrix (relating image and camera velocities) and the robot jacobian (relating end-effector and joint velocities). Such transformations are usually obtained during an offline calibration phase.

However, full system calibration (and even a coarse one) is not always possible and/or desirable. Some robots may lack proprioceptive sensors to provide the necessary information and some parameters may vary over time, due to malfunction, changes in mechanical parts or modification in the camera lenses. Even when calibration information is available, the analytic computation of the interaction matrix often requires an estimate of the depth of the tracked features. For all these reasons, a perfect computation of the task jacobian can be very difficult or even impossible in practice.

Redundancy formulation for two tasks.

Let q be the articular vector of the robot. Let e_1 and e_2 be two tasks,

$$\mathbf{J_i} = \frac{\partial \mathbf{e_i}}{\partial \mathbf{q}} \ (i = 1, 2)$$

Their jacobian is defined by:

$$\dot{\mathbf{e}}_\mathbf{i} = \frac{\partial \mathbf{e_i}}{\partial \mathbf{q}} \dot{\mathbf{q}} = \mathbf{J_i} \dot{\mathbf{q}}$$

Since the robot is controlled using its articulation velocity $\dot{q}$, the jacobian has to be (pseudo-) inverted. The general solution (with i = 1) is:

$$\dot{q} = J_1^+ \dot{e}_1 + P_1 z$$

where P_1 is the orthogonal projection operator on the null space of J_1 and J_1^+ is the pseudo-inverse of J_1. Vector *z* can be used to apply a secondary command, that will not disturb e_1. Here, z is used to carry out at best a task e_2. With further algebraic manipulations we have:

$$\dot{e}_2 = J_2 J_1^+ \dot{e}_1 + J_2 P_1 z$$

By inverting this last equation, and introducing the computed *z*, we finally get:

$$\dot{q} = J_1^+ \dot{e}_1 + P_1 (J_2 P_1)^+ (\dot{e}_2 - J_2 J_1^+ \dot{e}_1)$$

Results

We have tested several estimation methods for J and the results are the following

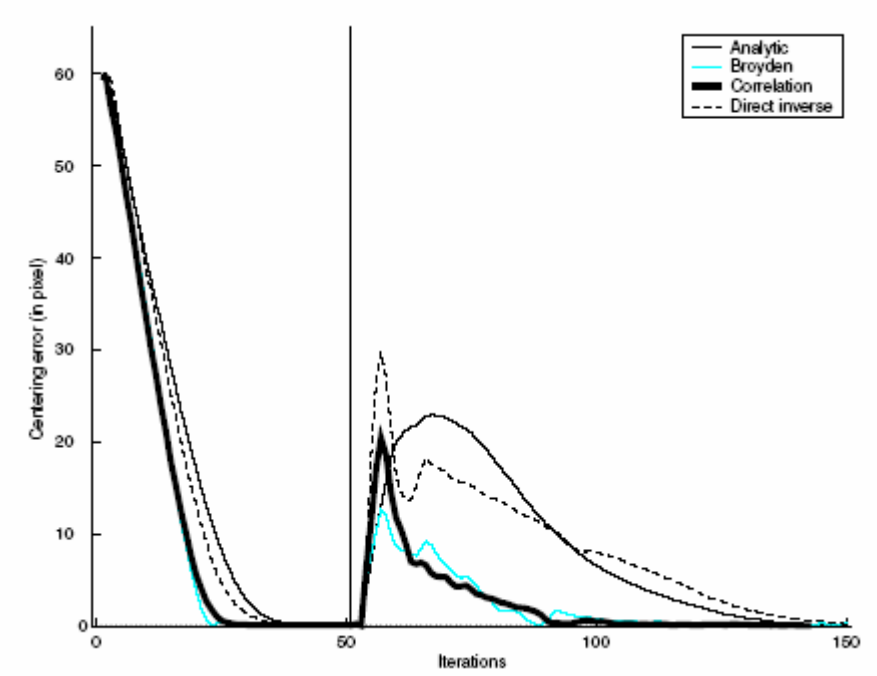

Figure 2 – Results of task sequencing. The vertical line shows the time instant when the second task was activated.

From the results show in Figure 2 we can see that when a second task is activated there is a small perturbation on the first task that is rapidly reduced to zero.

2.3.5.3 Joint representation of sensory-motor relations

Learning a structure jointly representing both sensory and motor information can provide significant advantages, if such knowledge can later be used to recover any (partial) map between perception and action. In this section we present a new approach to work with unknown redundant systems. For this we have developed:

- An online algorithm that learns the input-output constraints of a generic smooth map (manifold);

- A method that, given a partial set of input-output variables, provides an estimate of the

remaining ones, using the learned constraints.

Referring to our problem, the manifold estimate can be used to obtain the direct and inverse robot kinematics, i.e., to provide an estimate of the observed variables given an actuation value, or, inversely, obtain the actuators position that leads to a desired observation. This constitutes a new approach to learn forward-backward models, allowing to easily recovering the relationship among any set of variables. The key point of our approach is to consider the problem from an unsupervised learning point of view, where data points consist of vectors containing both input and output variables. These vectors define a surface that can be seen as the graphic of a function.

Consider D_c to be the number of controlled — or independent — variables and D_o the number of observed variables. A point x belonging to the manifold in a $D = D_c + D_o$ dimensional space will lie in a sub-space of dimension D_c. This manifold can be represented by the implicit function

$H(x) = 0$

where $H(x)$ imposes the $D - D_c$ restrictions arising from kinematics considerations. Note that the dimension of the manifold is D_c because this corresponds to the number of independent variables. The observed variables are generic smooth, frequently non-injective functions of the independent variables. In almost all cases these manifolds are highly nonlinear, hard to parameterize without any a priori knowledge.

However, they are smooth and so can be approximated by local linear parameterizations estimated from sample data. Unsupervised learning of a D_c-dimensional manifold in a D-dimensional space can be interpreted as a probability density estimation problem: given a set of (possibly corrupted with noise) sample points x_i belonging to the manifold, i = 1 . . .N, estimate the probability of a point x belonging

to the manifold, i.e.,

$p(H(x) = 0 \mid x_1, x_2, \ldots, x_N)$

After estimating the manifold, and given a partial set of input-output variables, we can query for an estimate of the remaining ones. Suppose data points x are divided into a query component and an answer component, $x = [x^T_q \; x^T_a]^T$, such that $D_q + D_a = D$, where D_q is the query dimension and D_a is the answer dimension, not necessarily equal to D_c and D_o. The answer component is the set x_a of elements of x to be estimated given a specific value of the remaining elements x_q. For instance, for a forward kinematics problem x_q corresponds to the actuation variables, while for an inverse kinematics problem x_q matches the observed variables. Note that if the dimension of the query exceeds D_c, the manifold dimension, the estimation problem is over-determined and a solution may not exist. Conversely, if the dimension of the query is lower than D_c, the estimation problem is under-determined and a continuum of solutions exist — in this case, as will be explained later, our algorithm will provide multiple answers that can be interpreted as a sampling of that continuous solution. The M local models that describe the learned manifold can be used to provide an estimate x_a for a specific query x_q. For a single

model m, we can choose the estimate of x_a to be the value that maximizes the likelihood of the data point x given model m, i.e., that maximizes $p(x|m)$. Maximization of this likelihood can be achieved by minimizing the corresponding Mahalanobis distance to the center of the model m_1:

$J_1 = (x - \mu)^T C^{-1}(x - \mu)$

The data is characterized by its first (mean ◎) and second order (covariance matrix C) moments. Consider the following decomposition for the covariance matrix:

$$C^{-1} = \begin{bmatrix} C_{qq} & C_{qa} \\ C_{aq} & C_{aa} \end{bmatrix}$$

where C_{qq}, C_{qa}, C_{aq} and C_{aa} are, respectively, of dimensions $D_q \times D_q$,

$D_q \times D_a$, $D_a \times D_q$ and $D_a \times D_a$. Then after some simple calculations we get the estimate

$$\hat{x}_a(x_q) = -C_{aa}^{-1} C_{aq}(x_q - \mu_q) + \mu_a$$

The following experiment shows a simple example of a sensory-motor relation. We can see that the correct relation (in blue) is accurately estimated (red lines) and that a one-to-many relation can be recovered.

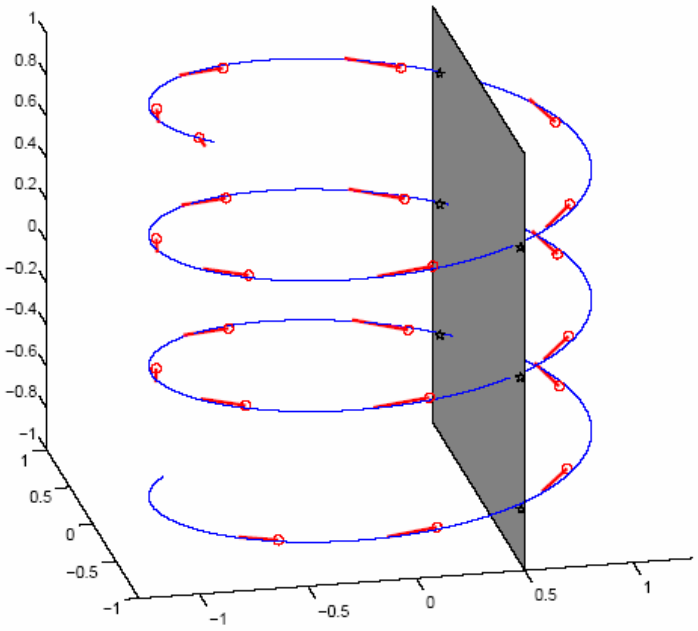

Fig. 4. Recovering the forward model embedded in the manifold. With $x_q = 0.5$ the six possible outcomes are successfully estimated (represented in the figure by black asterisks).

In future work we will apply and evaluate the performance of the proposed model to data

obtained from redundant robots with multiple degree of freedom.

4 Conclusions

This deliverable presents the current state of the art of experiments and models on sensorimotor integration together with some demos on infants crawling modelling. This is the final version of the Deliverable that has been provided at month 36 and includes all the contributions to Workpackage 3 provided by RobotCub partners during the first phase of the project. As soon as the artefact will be ready, new experiments, testing sensorimotor coordination directly on the platform will be carried out on the basis of the current experience.

5 References

Adolphs R, Tranel D and Damasio AR. Dissociable neural systems for recognizing emotions. Brain Cogn 52: 61-9, 2003.

Altschuler, E.L., A. Vankov, V. Wang, V.S. Ramachandran, J.A. Pineda, Person See, Person, poster session presented at the 27th Annual Meeting of the Society for Neuroscience, New Orleans, LA, November 1997.

Asuni G, G. Teti, C. Laschi, E. Guglielmelli, P. Dario, 2005(a). "A Robotic Head Neuro-controller Based on Biologically-Inspired Neural Models", *IEEE International Conference on Robotics and Automation – ICRA 2005*, Barcelona, Spain, April 18-22, 2005, pp.2373-2378.

Asuni G, G. Teti, C. Laschi, E. Guglielmelli, P. Dario, 2005(b). "A Bio-Inspired Sensory-Motor Neural Model for a Neuro-Robotic Manipulation Platform", *IEEE International Conference on Advanced Robotics – ICAR 2005*, Seattle, WA, USA, July 18-20, 2005.

Asuni G, G. Teti, C. Laschi, E. Guglielmelli, P. Dario, 2006. "Extension to End-effector Position and Orientation Control of a Learning-based Neurocontroller for a Humanoid Arm", *IEEE/RSJ International Conference on Intelligent Robots and Systems (IROS 2006)*, Beijing, China, October 9-15, 2006.

Avikainen S, Forss N and Hari R. Modulated activation of the human SI and SII cortices during observation of hand actions. Neuroimage 15: 640-6, 2002.

Baron-Choen, S, A.M. Leslie, U. Frith, *Cognition*, **21**, 37, 1985.

Bootsma, R. & van Wieringen, P. (1990). Visual control of an attacking forehand drive in table tennis. , 16, 21-29.

Brighina, F., La Bua, V., Oliveri, M., Piazza, A. & Fierro, B. (2000). Magnetic stimulation study during observation of motor tasks. J Neurol Sci, 174, 122-6.

Buccino G, Binkofski F, Fink GR, Fadiga L, Fogassi L, Gallese V, Seitz RJ, Zilles K, Rizzolatti G and Freund HJ. Action observation activates premotor and parietal areas in a somatotopic manner: an fMRI study. Eur J Neurosci 13: 400-4, 2001.

Bullock D, S. Grossberg, and F. H. Guenther, 1993. "A self-organizing neural model of motor equivalent reaching and tool use by a multijoint arm", *Journal of Cognitive Neuroscience*, 5(4):408–435, 1993.

Carr L, Iacoboni M, Dubeau MC, Mazziotta JC and Lenzi GL. Neural mechanisms of empathy in humans: a relay from neural systems for imitation to limbic areas. Proc Natl Acad Sci U S A 100: 5497-502, 2003.

Corbetta M., F. M. Miezin, S. Dobmeyer, G. L. Shulman, and S. E. Petersen. Selective and divided attention during visual discriminations of shape, color, and speed: functional anatomy by positron emission tomography. *J Neurosci.*, 11:2383.2402, 1991

Corbetta M., F. M. Miezin, S. Dobmeyer, G. L. Shulman, and S. E. Petersen. Attentional modulation of neural processing of shape, color, and velocity in humans. *Science*, 248:1556.9, 1990

Craighero L.. Nascimben, and L. Fadiga. Eye position affects orienting of visuospatial attention. *Current Biology*, 14:331.333, 2004.

Csato', L., and M. Opper. Sparse On-Line Gaussian Processes. Neural Computation, 14, 641–668, 2002.

Dapretto, M. et al., *Nature Neuroscience,* **9**, 28 (2006).

Dario P, M.C. Carrozza, E. Guglielmelli, C. Laschi, A. Menciassi, S. Micera, F. Vecchi, 2005. "Robotics as a "Future and Emerging Technology: biomimetics, cybernetics and neuro-robotics in European projects", *IEEE Robotics and Automation Magazine*, Vol.12, No.2, June 2005, pp.29-43.

Day, B. & Lyon, I. (2000). Voluntary modification of automatic arm movements evoked by motion of a visual target. Exp Brain Res, 130, 159-168.

Decety J., D. Perani, M. Jeannerod, V. Bettinardi, B. Tadary, B. Woods, and J. C. Mazziotta. Mapping motor representations with PET. *Nature*, 371:600.602, 1994.

Decety, J. (1996). Do imagined and executed actions share the same neural substrate?. Brain Res Cogn Brain Res, 3, 87-93.

Decety, J., Jeannerod, M. & Prablanc, C. (1989). The timing of mentally represented actions. Behav Brain Res, 34, 35-42.

Del Bianco S, F. Martelli and G. Zaccanti "Penetration depth of light re-emitted by a diffusive medium: theoretical and experimental investigation", Phys. Med. Biol. **47**, 4131-44 (2002). Di Pellegrino, G., Fadiga, L., Fogassi, L., Gallese, V. & Rizzolatti, G. (1992). Understanding motor events: a neurophysiological study. Exp Brain Res, 91, 176-80.

Esslen M, Pascual-Marqui RD, Hell D, Kochi K and Lehmann D. Brain areas and time course of emotional processing. Neuroimage 21: 1189-203, 2004.

Fadiga L, Craighero L and Olivier E. Human motor cortex excitability during the perception of others' action. Curr Opin Neurobiol 15: 213-8, 2005.

Fadiga L, Fogassi L, Gallese V, Rizzolatti G. Visuomotor neurons: ambiguity of the discharge or 'motor' perception? Int J Psychophysiol, 35:165-77, 2000.

Fadiga, L., Buccino, G., Craighero, L., Fogassi, L., Gallese, V. & Pavesi, G. (1999). Corticospinal excitability is specifically modulated by motor imagery: a magnetic stimulation study. Neuropsychologia, 37, 147-58.

Fadiga, L., Fogassi, L., Pavesi, G. & Rizzolatti, G. (1995). Motor facilitation during action observation: a magnetic stimulation study. J Neurophysiol, 73, 2608-11.

Ferrari PF, Gallese V, Rizzolatti G and Fogassi L. Mirror neurons responding to the observation of ingestive and communicative mouth actions in the monkey ventral premotor cortex. Eur J Neurosci 17: 1703-14, 2003.

Flanagan, J. R., R.S. Johansson, *Nature*, **424**, 769 (2003)

Fogassi L, Gallese V, Fadiga L and Rizzolatti G. Neurons responding to the sight of goal directed hand/arm actions in the parietal area PF (7b) of the macaque monkey. Society of Neuroscience Abstracts 24: 255, 1998.

Fogassi L, Gallese V, Fadiga L, Luppino G, Matelli M, Rizzolatti G. Coding of peripersonal space in inferior premotor cortex (area F4). J Neurophysiol, 76:141-57, 1996.

Frith, U., *Autism: Explaining the Enigma* (Blackwell Publishing, 2003).

Fritzke B, 1994. "Growing cell structures a self-organizing network for unsupervised and supervised learning", Neural Networks, 7(9):1441–1460, 1994. ICSI TR-93-026.C.

Gallese, V. & Goldman, A. (1998). Mirror neurons and the simulation theory of mind-reading. Trends in cognitive science, 2, 493-501.

Gallese, V., Fadiga, L., Fogassi, L. & Rizzolatti, G. (1996). Action recognition in the premotor cortex. Brain, 119 (Pt 2), 593-609.

Gangitano, M., Mottaghy, F. M. & Pascual-Leone, A. (2001). Phase-specific modulation of cortical motor output during movement observation. Neuroreport, 12, 1489-92.

Gangitano, M., Mottaghy, F. M. & Pascual-Leone, A. (2004). Modulation of premotor mirror neuron activity during observation of unpredictable grasping movements. Eur J Neurosci, 20, 2193-2202.

Gergely G. *et al*. (1995) Taking the intentional stance at 12 months of age. *Cognition* **56**, 165-193

Golikova T.V. Vibrissa inputs into motor cortex in adult and developing rats. Zh. Evol. Biohim. Fisiol. 26: 193-199, 1990.

Gomez, G., Hernandez, A., Eggenberger Hotz, P. (2006). An adaptive neural controller for a tendon driven robotic hand. In Proceedings of the 9th International Conference on Intelligent Autonomous Systems (IAS-9). T. Arai et al. (Eds.), IOS Press, Tokyo, Japan, pp. 298-307.

Gomez, G., Hernandez, A., Eggenberger Hotz, P., and Pfeifer, R. (2005). An adaptive learning mechanism for teaching a robot to grasp. International Symposium on Adaptive Motion of Animals and Machines (AMAM 2005).

Gomez, G., Lungarella, M. and Tarapore, D. (2005). Information-theoretic approach to embodied category learning. Proc. of 10th Int. Conf. on Artificial Life and Robotics. (AROB 10): Proceedings of the 10th Int. Symp. on Artificial Life and Robotics, Beppu, Oita, Japan. pp. 332-337.

Goossens H.H. and Van Opstal A.J., 1997. "Human eye-head coordination in two dimensions under different sensorimotor conditions", *Exp. Brain Res*.1997, Vol. 114, pp. 542–560.

Grafton S. T., M. A. Arbib, L. Fadiga, and G. Rizzolatti. Localization of grasp representations in humans by PET: 2. observation compared with imagination. *Experimental Brain Research*, 112:103.111, 1996.

Hayhoe MM., Mennie, N., Sullivan, B. & Gorgos, K. The role of Internal Models and Prediction in Catching balls. American Association for Artificial Intelligence (AAAI), 2005 Fall Symposium, From Reactive to Anticipatory Cognitive Embodied Systems. Conference paper.

Hepp-Reymond MC, Husler EJ, Maier MA, Ql HX. Force-related neuronal activity in two regions of the primate ventral premotor cortex. Can J Physiol Pharmacol, 1994; 72: 571-9.

Iida, F. (2003) Biologically inspired visual odometer for navigation of a flying robot, Robotics and Autonomous Systems, Vol 44/3-4, pp. 201-208

Koelsch S, Fritz T, V Cramon DY, Muller K and Friederici AD. Investigating emotion with music: an fMRI study. Hum Brain Mapp 27: 239-50, 2006.

Kohler E, Keysers Cm, Umiltà A, Fogassi L, Gallese V, Rizzolatti G. Hearing sounds, understanding actions: Action representation in mirror neurons. Science, 297, 846-848, 2002

Kozlowski, K. Modelling and Identification in Robotics. Springer-Verlag, 1998. Murray, R.M., Z. Li, and S.S. Sastry. A Mathematical Introduction to Robotic Manipulation. CRC Press, 1994.

Lacquaniti, F., Carrozzo, M. & Borghese, N. (1993). The role of vision in tuning anticipatory motor responses of the limbs. In A. Berthoz (Ed.), Multisensory control of movement (Volume , pp. 379-393). Oxford University Press, Oxford.

Laschi, G. Asuni, G. Teti, M.C. Carrozza, P. Dario, E. Guglielmelli, R. Johansson, 2006. "A Bio-inspired Neural Sensory-Motor Coordination Scheme for Robot Reaching and Preshaping", *IEEE/RAS-EMBS International Conference on Biomedical Robotics and Biomechatronics*, Pisa, Italy, February 20-22, 2006.

Lee, D. (1976). A theory of visual control of bracking based on information about time-to-collision. Perception, 5, 437-459.

Leggio MG, Graziano A, Mandolesi L, Molinari M, Neri P and Petrosini L. A new paradigm to analyze observational learning in rats. Brain Res Brain Res Protoc 12: 83-90, 2003.

Lopes M, Santos-Victor J, Learning sensory-motor maps for redundant robots. Proc. IEEE/RSJ International Conference on Intelligent Robots and Systems, IROS, Beijing, China, Oct. 9-15, 2006.

Lopes M and Damas B, The manifold structure of sensory-motor coordination. IEEE – Intelligent Robotic Systems (IROS'07), 2007.

Lotze, M., Heymans, U., Birbaumer, N., Veit, R., Erb, M., Flor, H. & Halsband, U. (2006). Differential cerebral activation during observation of expressive gestures and motor acts. Neuropsychologia, , .

Lungarella, M. and Gomez, G. (In preparation). Information transfer at multiple scales. To be submitted to Physical Review E.

Lungarella, M. and Pfeifer, R. (2001). Robots as cognitive tools: Information-theoretic analysis of sensory-motor data. In Proceedings of the 2nd International Conference on Humanoid Robotics, Waseda, Japan.

Lungarella, M., Pegors, T., Bulwinkle, D. and Sporns, O. (2005). Methods for quantifying the information structure of sensory and motor data. Neuroinformatics, 3(3):243-262.

Maeda, F., Kleiner-Fisman, G. & Pascual-Leone, A. (2002). Motor facilitation while observing hand actions: specificity of the effect and role of observer's orientation. J Neurophysiol, 87, 1329-35.

Maini E.S., G. Teti, C. Laschi, M. Rubino, P. Dario, 2006. "Bio-inspired control of eye-head coordination in a robotic anthropomorphic head", *IEEE/RAS-EMBS International Conference on Biomedical Robotics and Biomechatronics*, Pisa, Italy, February 20-22, 2006.

Mansard N, Lopes M, Santos-Victor J, Chaumette F, Jacobian Learning Methods for Tasks Sequencing in Visual Servoing, Proc. IEEE/RSJ International Conference on Intelligent Robots and Systems, IROS, Beijing, China, Oct. 9-15, 2006.

Marr, D. (1982). Vision. A computational investigation into the human representation and processing of visual information. W. H. Freeman and Company.

Martelli F, S. Del Bianco and G. Zaccanti, "Perturbation model for light propagation through diffusive layered media", Phys. Med. Biol. **50**, 2159-2166 (2005). McIntyre, J., Zago, M., Berthoz, A., & Lacquaniti, F. (2001). Does the brain model Newton's laws? Nature Neuroscience, 4, 693-694.

McLeod, P. (1987). Visual reaction time and high-speed ball games. Perception, 16, 49-59.

Merchant, H., Battaglia-Mayer, A. & Georgopoulos, A. (2004). Neural responses during

interception of real and apparent circularly moving stimuli in motor cortex and area 7a. Cereb Cortex, 14, 314-331.

Molinari M, Petrosini L and Gremoli T. Hemicerebellectomy and motor behaviour in rats. II. Effects of cerebellar lesion performed at different developmental stages. Exp Brain Res 82: 483-92, 1990.

Murata A, Fadiga L, Fogassi L, Gallese V, Raos V, Rizzolatti G. Object representation in the ventral premotor cortex (area F5) of the monkey. J Neurophysiol. 1997;78:2226-30.

Mussa-Ivaldi F.A., E. Bizzi. Motor learning through the combination of primitives. Philosophical transactions of the Royal Society: biological sciences. Vol 335: Issue 1404 Dec 2000. Pag 1755-1769.

Nagai, A., Kuno, Y. and Shirai¡, Y. (1999) Detection of Moving Objects against a Changing Background.Systems and Computers in Japan, Vol. 30, No. 11, pp. 107-116.

Neafsey EJ, Bold EL, Haas G, Hurley-Gius KM, Quirk G, Sievert CF and Terreberry RR. The organization of the rat motor cortex: a microstimulation mapping study. Brain Res 396: 77-96, 1986.

Nishitani, N., S. Avikainen, R. Hari, *Ann. Neurol.*, **55**, 558 (2004).

Nori, F., G. Metta, L. Jamone, and G. Sandini. Adaptive combination of motor primitives. Proceedings of AISB'06, Adaptation in Artificial and Biological Systems.

Oberman, L..M. et al., *Cognitive Brain Research*, **24**, 190(2005).

Olsson L., C. L. Nehaniv, & D. Polani, "Sensory Channel Group and Structure from Uninterpreted Sensor Data", IEEE NASA/DoD Conference on Evolvable Hardware 2004, IEEE Computer Society, pp. 153-160, 2004.

Olsson L., C. L. Nehaniv, & D. Polani, From Unknown Sensors and Actuators to Actions Grounded in Sensorimotor Perceptions, Connection Science, special issue on Developmental Robotics (D. Bank & L. Meeden, guest eds.), volume 18(2), 2006.

Parsons L. M., P. T. Fox, J. H. Downs, T. Glass, T. B. Hirsch, C. C. Martin, P. A. Jerabek, and J. L. Lancaster. Use of implicit motor imagery for visual shape discrimination as revealed by PET. *Nature*, 375:54.58, 1995.

Petrosini L, Graziano A, Mandolesi L, Neri P, Molinari M and Leggio MG. Watch how to do it! New advances in learning by observation. Brain Res Brain Res Rev 42: 252-64, 2003.

Pfeifer, R., Iida, F., and Gomez, G. (2006). Morphological computation for adaptive behavior and cognition. International Congress Series 1291: 22-29.

Pfeifer, R., Iida, F., and Gomez, G. (In press). Designing intelligent robots – on the implications of embodiment. To appear in the International Journal of the Robotics Society of Japan.

Port, N., Kruse, W., Lee, D. & Georgopoulos, A. (2001). Motor cortical activity during interception of moving targets. J Cogn Neurosci, 13, 306-318.

Posner M. I. and S. Dehaene. Attentional networks. *Trends Neurosci.*, 17:75.9, 1994.

Posner M. I. and S. E. Petersen. The attention system of the human brain. *Annu Rev Neurosci.*, 13:25.42, 1990.

Posner M. I., S. E. Petersen, P. T. Fox, and M. E. Raichle. Localization of cognitive operations in the human brain. *Science*, 240(1627-31), 1988

Premack, D. Woodruff, G. (1978). Does the chimpanzee have a theory of mind?. Behav Brain Sci, 1, 515.

Rizzolatti G, Camarda R, Fogassi L, Gentilucci M, Luppino G, Matelli M. Functional organization of inferior area 6 in the macaque monkey: II. Area F5 and the control of distal movements. Experimental Brain Research, 71:491–507, 1988.

Rizzolatti G, Fadiga L, Fogassi L and Gallese V. Resonance behaviors and mirror neurons. Arch Ital Biol 137: 85-100, 1999.

Rizzolatti G, Fadiga L. Grasping objects and grasping action meanings: the dual role of monkey rostroventral premotor cortex (area F5). In: G. R. Bock & J. A. Goode (Eds.), Sensory Guidance of Movement, Novartis Foundation Symposium (pp. 81-103). Chichester: John Wiley and Sons, 1998.

Rizzolatti G, Luppino G and Matelli M. The organization of the cortical motor system: new concepts. Electroencephalogr Clin Neurophysiol 106: 283-96, 1998.

Rizzolatti G. and R. Camarda. Neural circuits for spatial attention and unilateral neglect. In M. Jeannerod, editor, *Neurophysiological and neuropsychological aspects of spatial neglect*, pages 289.313, Amsterdam, 1987. North-Holland.

Rizzolatti G., L. Riggio, and B. M. Sheliga. Space and selective attention. In C. Umiltà and M. Moscovitch, editors, *Attention and performance XV*, pages 231.265, Cambridge, MA, 1994. MIT Press.

Rizzolatti G., L. Riggio, I. Dascola, and Umilta C. Reorienting attention across the horizontal and vertical meridians: evidence in favor of a premotor theory of attention. *Neuropsychologia*, 25:31.40, 1987.

Rizzolatti, G. & Craighero, L. (2004). The mirror-neuron system. , 27, 169-192.

Rizzolatti, G., Fadiga, L., Gallese, V. & Fogassi, L. (1996). Premotor cortex and the recognition of motor actions. Brain Res Cogn Brain Res, 3, 131-41.

Roccella S, M.C. Carrozza, G. Cappiello, P. Dario, J.J. Cabibihan, M. Zecca, H. Miwa, K. Itoh, M. Matsumoto, A. Takanishi, 2004. “Design, fabrication and preliminary results of a novel

anthropomorphic hand for humanoid robotics: RCH-1", *2004 IEEE/RSJ International Conference on Intelligent Robots and Systems*, Sendai, Japan, September 28 - October 2, 2004, Page(s):266 - 271 vol.1.

Rouiller EM, Moret V and Liang F. Comparison of the connectional properties of the two forelimb areas of the rat sensorimotor cortex: support for the presence of a premotor or supplementary motor cortical area. Somatosens Mot Res 10: 269-89, 1993.

Sandini G, G. Metta, 2003. "Retina-like sensors: motivations, technology and applications", in *Sensors and Sensing in Biology and Engineering*, by Friedrich G. Barth, Timothy W. Secomb, and Joseph A. C. Humphrey, (Ed.s), Springer Verlag, 1st edition, March 28, 2003, pp.109-125.

Selb J, J. J. Stott, M. A. Franceschini, A. G. Sorensen, and D. A. Boas, "Improved sensitivity to cerebral hemodynamics during brain activation with a time-gated optical system: analytical model and experimental validation", J. Biomed Opt. **10**, 11013 (2005). Sheliga B. M., L. Riggio, L. Craighero, and G. Rizzolatti. Spatial attention and eye movements. *Exp Brain Res*, 105:261.75, 1995b.

Sheliga B.M., L. Riggio, L. Craighero, and G. Rizzolatti. Spatial attention-determined modifications in saccade trajectories. *Neuroreport*, 6:585.8, 1995a.

Sirigu A., J. R. Duhamel, L. Cohen, B. Pillon, B. Dubois, and Y. Agid. The mental representation of hand movements after parietal cortex damage. *Science*, 273:1564.1568, 1996

Sobey, P. and Srinivasan, M. V. (1991). Measurement of optical flow by a generalized gradient scheme. J. Opt. Soc. Am. A 8, 1488.

Soechting, J. & Lacquaniti, F. (1983). Modification of trajectory of a pointing movement in response to a change in target location. , 49, 548-564.

Steinbrink H, H. Wabnitz, A. Obrig, Villringer and H. Rinneberg, "Determining changes in NIR absorption using a layered model of the human head", Phys. Med. Biol. **46**, 879-896 (2001). Strafella, A. P. & Paus, T. (2000). Modulation of cortical excitability during action observation: a transcranial magnetic stimulation study. Neuroreport, 11, 2289-92.

Tarapore, D., Lungarella, M. and Gomez, G. (2006). Quantifying patterns of agent-environment interaction. Robotics and Autonomous Systems, 54(2):150-158.

Te Boekhorst, R., Lungarella,M., and Pfeifer, R. (2003). Dimensionality reduction through sensory-motor coordination. In Kaynak,O., Alpaydin, E., Oja, E., and Xu, L. (Eds). Proc. of the Joint Int. Conf. ICANN/ICONIP, pp 496-503.

Theoret, H. et al., *Current Biology*, **15**, 84 (2005).

Uller C. (2003) Disposition to recognize goals in infant chimpanzees. *Animal Cognition*

Umilta, M., Kohler, E., Gallese, V., Fogassi, L., Fadiga, L., Keysers, C. & Rizzolatti, G. (2001). I know what you are doing. a neurophysiological study. Neuron, 31, 155-165.

Wang Y and Kurata K. Quantitative analyses of thalamic and cortical origins of neurons projecting to the rostral and caudal forelimb motor areas in the cerebral cortex of rats. Brain Res 781: 135-47, 1998.

Wimmer, H., J. Perner, *Cognition*, **13**, 103 (1983).

Xiao D and Barbas H. Circuits through prefrontal cortex, basal ganglia, and ventral anterior nucleus map pathways beyond motor control. Thalamus & Related Systems. 2: 325–343, 2004.

Zago, M., Bosco, G., Maffei, V., Iosa, M., Ivanenko, Y. P., & Lacquaniti, F. (2004). Internal models of target motion: Expected dynamics overrides measured kinematics in timing manual interceptions. Journal of Neurophysiology, 91, 1620-1634.

Zhuravin IA and Bures J. Changes of cortical and caudatal unit activity accompanying operant slowing of the extension phase of reaching in rats. Int J Neurosci 39: 147-52, 1988.

Zollo L, B. Siciliano, C. Laschi, G. Teti, P. Dario, 2003. "An Experimental Study on Compliance Control for a Redundant Personal Robot Arm," Robotics and Autonomous Systems, vol. 44, pp. 101–129, 2003.

6 Appendices

Measuring Informational Distances Between Sensors and Sensor Integration

Lars Olsson*, Chrystopher L. Nehaniv*† and Daniel Polani*†
Adaptive Systems* and Algorithms† Research Groups
School of Computer Science, University of Hertfordshire
United Kingdom
{L.A.Olsson, C.L.Nehaniv, D.Polani}@herts.ac.uk

Abstract

In embodied artificial intelligence is it of interest to study the informational relationships between the agent, its actions, and the environment. This paper presents a number of statistical measures to compute the informational distance between sensors including the information metric, correlation coefficient, Hellinger distance, Kullback-Leibler, and Jensen-Shannon divergence. The methods are compared using the sensory reconstruction method to find spatial positions of visual sensors of different modalities in a sensor integration task. The results show how the information metric can find relations not found by the other measures.

Introduction

In the early 1960s H. B. Barlow suggested (Barlow, 1961) that the visual system of animals "knows" about the structure of natural signals and uses this knowledge to represent visual signals. Ever since then neuroscientists have analysed the informational relationships between organisms and their environment. In recent years, with the advent of embodied artifical intelligence, there has also been an increased interest in robotics and artificial intelligence to study the informational relations between the agent, its environment, and how the actions of the agent affect its sensory input. It is believed that this research can give us new principles and quantitative measures which can be used to build robots that can exploit bootstrapping (Prince et al., 2005) and continously learn, develop, and adapt depending on their particular environment, environment, and task to perform. This paper presents some work in this area and presents a number of methods for computing the distance between sensors and how these methods can be useful for sensor integration of different sensor modalities.

The informational relationships between sensors are dependent on the particular embodiment of an agent. Thus, these relationships can be useful for the agent to learn about its own body, the potential actions it can perform, and how the sensors relate to its particular environment. In (Olsson et al., 2004b) the sensory reconstruction method, first described by Pierce and Kuipers (1997), was applied to robots and extended by considering the informational relations between sensors. The results showed how the visual field could be reconstructed from raw and uninterpreted sensor data and how some symmetry of the physical body of the robot could be found in the created sensoritopic maps. This method was also used in (Olsson et al., 2005b) to show how a robot can develop from no knowledge of its sensors and actuators to perform visually guided movement.

One other aspect of the information available in an agent's sensors is that the particular actions of the agent can have an impact on the nature and statistical structure of its sensoric input. This has been studied in a number of papers since (Lungarella and Pfeifer, 2001); see for example (Sporns and Pegors, 2003, 2004; Lungarella et al., 2005). The results show how saliency guided movement decreases the entropy of the input while increasing the statistical dependencies between the sensors. The specific environment of an agent also limits in principle what an agent can know about the world and the physical and informational relationships of its sensors (Olsson et al., 2004a).

Information-theoretic measures have also been used to classify behaviour and interactions with the environment using raw and uninterpreted sensor data from the agent. In (Tarapore et al., 2004) the statistical structure of the sensoric input was used to fingerprint interactions and environments. Mirza et al. (2005b) considered how the informational relationships between its sensors, as well as actuators, can be used to build histories of interaction by classifying trajectories in the sensorimotor phase space. In (Kaplan and Hafner, 2005) the authors also considered clustering behaviours by the informational distances between sensors by considering configurations of matrices of information distances between all pairs of sensors.

One important issue in this research is what measures to use to quantify the informational relationships. In (Lungarella et al., 2005) the authors present a number of methods for quantifying informational structure in sensor and motor data. The focus is on integration, i.e., how much information two or more sources have in common. In this paper we focus on the opposite, i.e., how to compute how different two

or more sources are. Following (Olsson et al., 2004b), several papers including (Olsson et al., 2004a, 2005b,c,a, 2006; Mirza et al., 2005a,b; Kaplan and Hafner, 2005; Hafner and Kaplan, 2005) have used the information distance metric disucssed by Crutchfield (1990) to compute the informational distance between sensors. An important question the authors have received several times in reviews of papers and in discussions is "why the information metric?". This is a good question and in this paper we present a number of alternative distance measures suggested by colleagues and reviewers as well as the information metric. To compare the potential utility of the methods we apply them as the distance measure used in the sensory reconstruction method (Pierce and Kuipers, 1997; Olsson et al., 2004b). In the experiment the sensors of the visual field of a robot is split into three different modalities: red, blue, and green, and the problem is to find the relationships between sensors, including which sensors come from the same pixel in the camera. This is an example of sensor integration. The results show how the information metric performs better in this problem as it measures both linear as well as non-linear relationships between sensors.

The rest of this paper is structured as follows. The next section presents a number of methods to compute the distance between two sensors. Then a short introduction to the sensory reconstruction method is given before the results of the experiments are presented. The final section concludes the paper.

Measuring the Distance Between Sensors

In this section we present a number of methods for computing the distance between two sensors S_x and S_y. Each sensor can assume one of a discrete number of values (continuous values are discretized) $S_x^t \in \mathcal{X}$ at each time step t where $\mathcal{X}$ is the alphabet of possible values. Thus, each sensor can be viewed as a time series of data $\{S_x^1, S_x^2, \ldots, S_x^T\}$ with T elements. Each sensor can also be viewed as a random variable X drawn from a particular probability distribution $p_x(x)$, where $p_x(x)$ is estimated from the time series of data. Similarly the joint probability distribution $p_{x,y}(x,y)$ is estimated from the sensors S_x and S_y.

A distance measure $d(X,Y)$ is a distance function on a set of points, mapping pairs of points (X,Y) to non-negative real numbers. A *distance metric* in the mathematical sense also needs to satisfy the three following properties:

- $d(X,Y) = d(Y,X)$ (Symmetry).
- $d(X,Y) = 0 \quad \text{iff} \quad Y = X$ (Equivalence).
- $d(X,Z) \leq d(X,Y) + d(Y,Z)$. (Triangle Inequality).

If (2) fails but (1) and (3) hold, then we have a pseudo-metric, from which one canonically obtains a metric by identifying points at distance zero from each other. This is done here and in (Crutchfield, 1990).

Why can it be useful to use distance measures which are metrics in the mathematical sense? If a space of information sources has a metric, is it possible to use some of the tools and terminology of geometry. It might also be useful to be able to talk about sensors in terms of spatial relationships. This might be of special importance if the computations are used to actually discover some physical structure or spatial relationships of the sensors, for example as in (Olsson et al., 2004b), where the spatial layout of visual sensors as well as some physical symmetry of a robot was found by information theoretic means.

Distance Measures

The *1-norm distance* used in (Pierce and Kuipers, 1997) is different from the distance measures that follows in that it does not take in to account the probabilites of the different values that a sensor can take. It is normalized between 0.0 and 1.0 and is defined as

$$d_1(S_x,S_y) = \frac{1}{T}\sum_{t=1}^{T} |S_x^t - S_y^t|. \tag{1}$$

The *correlation coefficient* is defined as

$$r = \frac{\sum_{t=1}^{T}(S_x^t - \bar{S}_x)(S_y^t - \bar{S}_y)}{\sqrt{\sum_{t=1}^{T}(S_x^t - \bar{S}_x)^2}\sqrt{\sum_{t=1}^{T}(S_y^t - \bar{S}_y)^2}} \tag{2}$$

where $\bar{S}_x$ and $\bar{S}_y$ are the mean of S_x and S_y respectively. The range of r is $-1.0 \leq r \leq 1.0$, where 1.0 means that they are perfectly correlated in a linear way, 0 that they are not linearly correlated, and -1.0 perfectly negatively correlated. This can be made symmetric by computing the squared correlation coefficient, which is in the range $0 \leq r^2 \leq 1.0$, and then

$$d_{CC}(S_x,S_y) = 1 - r^2_{S_x,S_y}. \tag{3}$$

This is still not a metric since it does not satisfy the triangle inequality (Ernst et al., 2005).

The *information metric* is proved to be a metric in (Crutchfield, 1990) and is defined as the sum of two conditional entropies, or formally

$$d_{IM}(S_x,S_y) = H(X|Y) + H(Y|X), \tag{4}$$

where

$$H(Y|X) = -\sum_{x\in X}\sum_{y\in Y} p(x,y)\log_2 p(y|x). \tag{5}$$

The *Kullback-Leibler divergence* (Cover and Thomas, 1991) is defined as

$$D(p_x||p_y) = \sum_{x\in X} p_x(x)\log_2 \frac{p_x(x)}{p_y(x)}, \tag{6}$$

where $0\log_2\frac{0}{p_y}=0$ and $p_x\ \log_2\frac{p_x}{0}=\infty$. The Kullback-Leibler measure is not a metric because it is not symmetric. It can be made symmetric by adding two Kullback-Leibler measures,

$$d_{KL}(S_x,S_y)=D(p_x||p_y)+D(p_y||p_x), \quad (7)$$

where p_x is the probability distribution associated with sensor S_x and p_y with S_y. This is still not a metric since it does not satisfy the triangle inequality.

The square root of the *Hellinger distance*, also known as *Bhattacharya distance* (Basu et al., 1997) , is a metric and is defined as

$$d_H(S_x,S_y)=\sqrt{\frac{1}{2}\sum_{x\in\mathcal{X}}\left(\sqrt{p_x(x)}-\sqrt{p_y(x)}\right)^2}. \quad (8)$$

Finally, the *Jensen-Shannon divergence*, presented in (Lin, 1991), is defined as

$$d_{JS}(S_x,S_y)=H(\pi_X X+\pi_Y Y)-\pi_X H(X)-\pi_Y H(Y), \quad (9)$$

where $\pi_X,\pi_Y\leq 0, \pi_X+\pi_Y=1$, are the weights associated with the sensors S_x and S_y. In this paper the weights were always $\pi_X=\pi_Y=0.5$. In (Endres and Schindelin, 2003) it was proved that the Jensen-Shannon is the square of a metric, i.e., $\sqrt{d_{JS}}$ is a metric, which was used in the experiments presented in this paper.

Sensory Reconstruction Method

In the sensory reconstruction method (Pierce and Kuipers, 1997; Olsson et al., 2004b) sensoritopic maps are created that show the informational relationships between sensors, where sensors that are informationally related are close to each other in the maps. The sensoritopic maps might also reflect the real physical relations and positions of sensors. For example, if each pixel of a camera is considered a sensor, is it possible to reconstruct the organization of these sensors even though nothing about their positions is known. It is important to note that using only the sensory reconstruction method, only the positional relations between sensors can be found, and not the real physical orientation of the visual layout. To do this requires higher level feature processing and world knowledge or knowledge about the movement of the agent (Olsson et al., 2004b). Figure 1 shows an example of a sensoritopic map for a SONY AIBO robot.

To create a sensoritopic map the value for each sensor at each time step is saved, where in this paper each sensor is a specific pixel in an image captured by the robot. The first step of the method is to compute the distances between each pair of sensors. In the paper by Pierce and Kuipers (1997) the 1-norm distance was used but after (Olsson et al., 2004b) the information metric has been used in a number of papers. In this paper the different distance measures presented

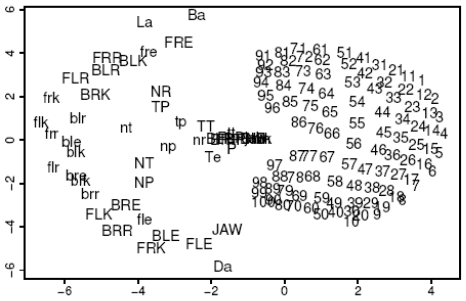

Figure 1: A sensoritopic map created by the sensory reconstruction method taken from (Olsson et al., 2004b) using the information metric. In this example there are 150 sensors, including 100 image sensors that are labeled 1-100 to the right in the map.

in the previous section are used. From the matrix of pairwise distance measurements between the sensors the dimensionality of sensory data (two in this case of a visual field) is computed and a sensoritopic map of that dimensionality can be created, using a number of different methods such as metric-scaling, which positions the sensors in the two dimensions of the metric projection. In our experiments we have used the relaxation algorithm described by Pierce and Kuipers (1997).

Experiment

This section describes the performed experiment and the results.

Method

In our experiments a SONY AIBO robotic dog was placed in a sitting position on a desk in the lab. The robot only moved its head with uniform speed using the pan and tilt motors in eight directions: up, down, left, right, and four diagonal directions. Five sequences of 6000 frames each of visual data was collected from the camera at a resolution of 88 by 72 pixels with 8 bits for each channel (red, green, blue) at an average rate of 20 frames per second. The collected images were downsampled to 8 by 8 pixels using averaging. Each pixel of the image had one red, one green, and one blue sensor. Thus, there is a total of 192 sensors (64 of each modality) where the red sensors are labeled $R1-R64$, the green $G1-G64$, and the blue sensors $B1-B64$. The sensors labeled 1 are located at the upper left corner of the image and 64 at lower right corner. In the collected data the range of

Measure \ Exp.	64R	192RGB	192ARGB
1-norm	0.06 (0.01)	0.32 (0.01)	–
Correlation coefficient	0.19 (0.02)	0.23 (0.03)	0.21 (0.05)
Information metric	0.07 (0.02)	0.12 (0.03)	0.09 (0.03)
Kullback-Leibler	0.37 (0.03)	0.35 (0.01)	0.41 (0.05)
Hellinger	(0.45 (0.05)	0.40 (0.02)	0.46 (0.04)
Jensen-Shannon	0.45 (0.04)	0.39 (0.01)	0.45 (0.04)

Table 1: Average distances between all pairs of correct and reconstructed sensors using equation 10 with standard deviation in parentheses. The column 64R shows the average distances for the 64 red sensors of figure 2 and 192RGB the red, green, and blue sensors of figure 3, both using normal binning. 192ARGB shows the results for the adaptive binning of figure 4.

the blue sensors was slightly lower than the red and green sensors with a slightly smaller variation.

Sensoritopic maps were created from each of the five sequences of data by the sensory reconstruction method using the different distance measures previously described. The presented maps are examples but all maps created using one particular distance measure had the same characteristics as the ones presented here.

Results

Figure 2 shows sensoritopic maps computed with the different distance measures of only the red sensors $R1 - R64$. First, if we look at the maps for the Kullback-Leibler, Hellinger, and Jensen-Shannon distance, we find no real structure. For the correlation coefficient distance, figure 2(b), we find that sensors that are close in the visual field tend to be closer in the sensoritopic map, but it is not very clear. Now, compare this to the sensoritopic maps for both the 1-norm distance, figure 2(a), and the information metric, 2(c). Here the spatial relationships of the red sensors have been found, with sensor $R1$ in the upper left corner and $R64$ in the lower left corner for the 1-norm distance and the $R1$ sensor in lower left corner for the information metric. Since the sensory reconstruction method cannot find the true physical location of sensors but only the spatial relationships both of these maps represent the visual field.

Up until now the term "reconstructed" has been used in an informal way, where a visual field is reconstructed if the sensoritopic map and the real layout of the sensors look similar. One way this similarity can be formally quantified is by

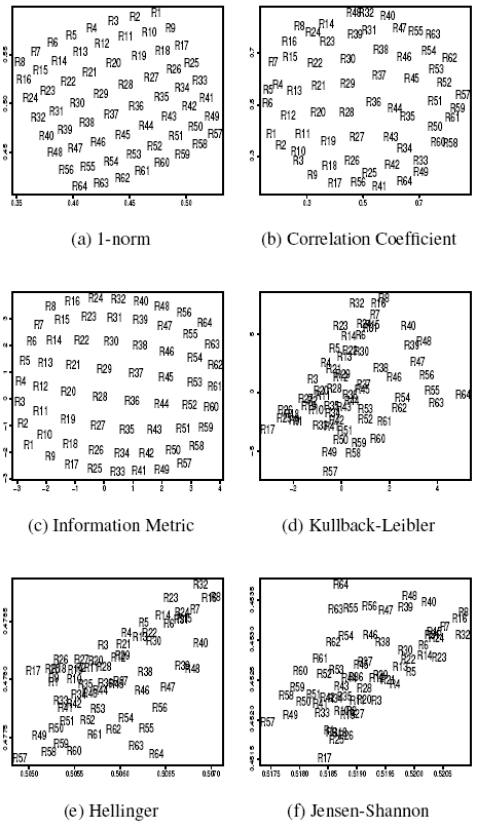

(a) 1-norm (b) Correlation Coefficient

(c) Information Metric (d) Kullback-Leibler

(e) Hellinger (f) Jensen-Shannon

Figure 2: Sensoritopic maps of the red sensors.

computing the relative distances between pairs of sensors in the reconstructed visual field and the real layout of the sensors. Let $r_{i,j}$ be the Euclidean distance between two sensors i and j in the reconstructed map, and $\ell_{i,j}$ the distance between the same two sensors in the real layout, where the x and y coordinates in both cases have been normalised into the range $[0.0, 1.0]$. Now the average distance between all pairs of sensors can be compared,

$$d(r,\ell) = \frac{1}{N^2}\sum_{i,j} |r_{i,j} - \ell_{i,j}|, \qquad (10)$$

where N is the number of sensors. This compares the relative positions of the sensors and not the physical positions, and $d(r,\ell)$ will have a value in the range $[0.0, 1.0]$. A distance of zero means that the relative positions are exactly the same,

and sensors placed at completely random positions will have an average distance of approximately 0.52.

Table 1 shows the average distances for 10 created maps for each of the five sets of data using equation 10. The 64R column shows that the 1-norm and information metric have a significantly lower average distance then the other measures, indicating that using these two measures more accurately reconstructs the real visual field.

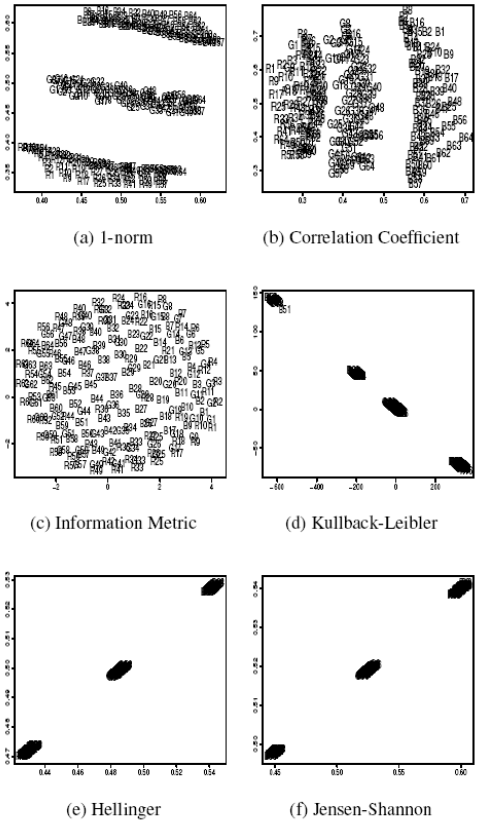

(a) 1-norm (b) Correlation Coefficient

(c) Information Metric (d) Kullback-Leibler

(e) Hellinger (f) Jensen-Shannon

Figure 3: Sensoriopic maps of 192 sensors using uniform binning.

Figure 3 shows sensoritopic maps for all the red, green, and blue sensors, and column 192RGB of table 1 show the corresponding average distances. This is an example of sensor integration where the problem is to find what sensors that are from the same location of the visual field, when the only input data to the system is the raw and unstructured data from the 192 sensors without any classification. The

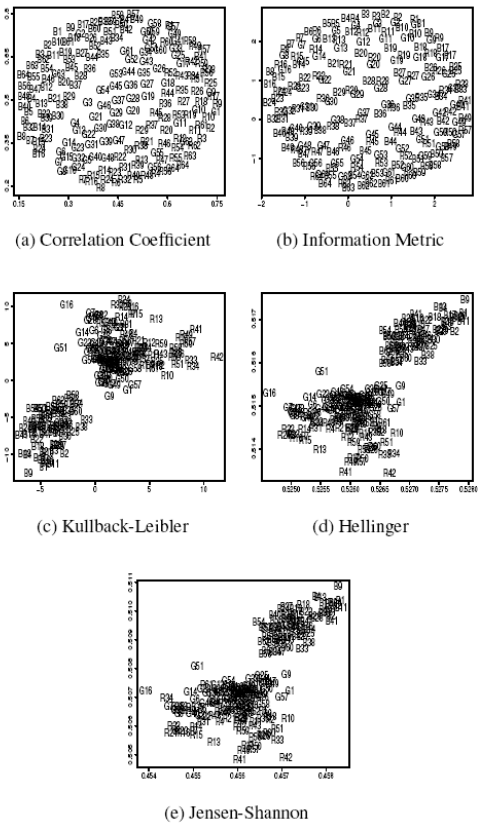

(a) Correlation Coefficient (b) Information Metric

(c) Kullback-Leibler (d) Hellinger

(e) Jensen-Shannon

Figure 4: Sensoriopic maps of 192 sensors using entropy maximization of the sensor data.

Hellinger map and Jensen-Shannon map both contain three clusters, one for each modality. The Kullback-Leibler map is divided in to four clusters. The 1-norm distance shows how structure within the modalities is present but there is no fusion of the sensors from different modalities. The correlation coefficient measure shows a similar structure but there is some overlap between the red and the green sensors. For the information metric, figure 3(c), the situation is different. Here the sensors of different modalities from the same location in the visual field are clustered together. This is an example of autonomous sensory fusion where sensors of different modalities are combined. A well-studied example of this in neuroscience is the optic tectum of the rattlesnake, where nerves from heat-sensitive organs are combined with nerves from the eyes (Newman and Hartline, 1981).

In (Olsson et al., 2005c) it was shown how entropy maximization of the data in individual sensors might be useful to find correlations between sensors of different modalities. Figure 4 shows sensoritopic maps and column 192ARGB of table 1 the average distance computed using the same data as before where it has been preprocessed by maximizing the entropy in each sensor using a window of 100 time steps (see (Olsson et al., 2005c) for details of this method). The 1-norm distance is not included since it is operating on raw sensor values and not on probabilities. The Kullback-Leibler, Hellinger, and Jensen-Shannon measures now cluster the red and green together and the blue in another cluster. The map of the correlation coefficient is similar, albeit with with more structure showing the layout of the individual sensors of the different modalities, as also can be seen in the average distance in table 1. The information metric in figure 4(b) again shows clustering of the different modalities according to their spatial location in the visual field. For example is sensor $R28$ clustered together with $B28$ and $G28$.

Discussion

Why is it the case that the information metric enables the sensory reconstruction method to find these relations between sensors of different modalities when the other measures do not? By considering the individual as well as joint entropies of the sensors the information metric provides a general method for quantifying all functional relationships between sensors, while many other methods only find some relationships. For example, a correlation coefficient approaching 0 does not imply that two variables actually are independent (Steuer et al., 2002).

Conclusions

For purposes of autonomous construction of the relations among sensors in an embodied agent, in this paper we compared the information metric to five other distance measures: the 1-norm distance, the correlation coefficient, Kullback-Leibler divergence, Hellinger distance, and the Jensen-Shannon divergence. Among these the information metric, 1-norm distance, Hellinger distance, and the squared Jensen-Shannon divergence are metrics in the mathematical sense. The comparision was performed by applying the distance measures as the distance measure used in the sensory reconstruction method. The created sensoritopic maps were evaluated by comparing the average spatial distances of the sensors of the reconstructed maps with the spatial distances between the sensors of the real square layout of the sensors.

The results showed that for autonomous construction of the relationships between sensors of different modalties, sensoritopic reconstruction using the information metric was the only successful method, outperforming all the other distance measures. When using sensors from only one modality the average reconstruction distance of the information metric was similar to the 1-norm distance. Among the other proposed measures the correlation coefficient had a shorter average distance than the others, but still significantly greater than the information metric. This is due to the fact that the information metric captures general relationships between sensors and not just linear relationships, as is the case with many other measures.

In recent years there has been an increased interest in studying the informational relationships between robots, their environment, and how their actions affect the information available in their sensors. Here the information metric is useful since it captures general relationships between sensors. This has, for instance, been exploited to discover optical and information flow in sensors of different modalities (Olsson et al., 2005a, 2006), and to build "interpersonal maps" that represent the informational relationships between two agents (Hafner and Kaplan, 2005). It has also been used to study the informational content available to robots in environments with oriented contours (Olsson et al., 2004a), inspired by the developmental studies of kittens reared in restricted visual environments (Wiesel, 1982; Callaway, 1998).

One possible avenue for future research is to study how robots, just like animals, can optimize their sensory system based on the statistics of their specific environments, as well as the actions and embodiment of the particular robot. Here the construction of sensoritopic maps using the information metric can be used as a general method to find the informational relationships between the sensors and the actions of the robot. It would also be of interest to study how a robot actively can shape the informational relationships among its sensors by deliberate actions.

Acknowledgements

The work described in this paper was partially conducted within the EU Integrated Project RobotCub ("Robotic Open-architecture Technology for Cognition, Understanding, and Behaviours") and was funded by the European Commission through the E5 Unit (Cognition) of FP6-IST under Contract FP6-004370.

References

Barlow, H. B. (1961). Possible principles underlying the transformation of sensory messages. *Journal of Sensory Communication*, pages 217–234.

Basu, A., Harris, I. R., and Basu, S. (1997). Minimum distance estimation: The approach using density-based distances. In Maddala, G. S. and Rao, C. R., editors, *Handbook of Statistics*, volume 15, pages 21–48.

Callaway, E. M. (1998). Visual scenes and cortical neurons: What you see is what you get. *Proceedings of the National Academy of Sciences*, 95(7):3344–3345.

Cover, T. M. and Thomas, J. A. (1991). *Elements of Information Theory*. John Wiley & Sons, Inc.

Crutchfield, J. P. (1990). Information and its Metric. In Lam, L. and Morris, H. C., editors, *Nonlinear Structures in Physical Systems – Pattern Formation, Chaos and Waves*, pages 119–130. Springer Verlag.

Endres, D. M. and Schindelin, J. E. (2003). A new metric for probability distributions. *IEEE Transactions on Information theory*, 49(7):1858–1860.

Ernst, J., Nau, G. J., and Bar-Joseph, Z. (2005). Clustering short time series gene expression data. In *Proceedings of ISMB*. to appear.

Hafner, V. and Kaplan, F. (2005). Interpersonal maps and the body correspondance problem. In Demiris, Y., Dautenhahn, K., and Nehaniv, C. L., editors, *Proceedings of the AISB 2005 Third International Symposium on Imitation in Animals and Artifacts*, pages 48–53.

Kaplan, F. and Hafner, V. (2005). Mapping the space of skills: An approach for comparing embodied sensorimotor organizations. In *Proceedings of the 4th IEEE International Conference on Development and Learning (ICDL-05)*, pages 129–134.

Lin, J. (1991). Divergence measures based on the Shannon entropy. *IEEE Transactions on Information Theory*, 37(1):145–151.

Lungarella, M., Pegors, T., Bulwinkle, D., and Sporns, O. (2005). Methods for quantifying the informational structure of sensory and motor data. *Neuroinformatics*, 3(3):243–262.

Lungarella, M. and Pfeifer, R. (2001). Robots as cognitive tools: Information-theoretic analysis of sensory-motor sata. In *Proceedings of the 2nd International Conference on Humanoid Robotics*, pages 245–252.

Mirza, N. A., Nehaniv, C. L., te Boekhorst, R., and Dautenhahn, K. (2005a). Robot self-characterisation of experience using trajectories in sensory-motor phase space. In *Proceedings of the fifth international workshop Epigenetic Robotics*, pages 143–144.

Mirza, N. A., Nehaniv, C. L., te Boekhorst, R., and Dautenhahn, K. (2005b). Using sensory-motor phase-plots to characterise robot-environment interactions. In *Proceedings of the 6th IEEE International Symposium on Computational Intelligence in Robotics and Automation (CIRA-2005)*, pages 581–586.

Newman, E. A. and Hartline, P. H. (1981). Integration of visual and infrared information in bimodal neurons of the rattlesnake optic tectum. *Science*, 213:789–791.

Olsson, L., Nehaniv, C. L., and Polani, D. (2004a). The effects on visual information in a robot in environments with oriented contours. In *Proceedings of the Fourth International Workshop on Epigenetic Robotics*, pages 83–88. Lund University Cognitive Studies.

Olsson, L., Nehaniv, C. L., and Polani, D. (2004b). Sensory channel grouping and structure from uninterpreted sensor data. In *Proceedings of the 2004 NASA/DoD Conference on Evolvable Hardware*, pages 153–160. IEEE Computer Society Press.

Olsson, L., Nehaniv, C. L., and Polani, D. (2005a). Discovering motion flow by temporal-informational correlations in sensors. In *Proceedings of the Fifth International Workshop on Epigenetic Robotics*, pages 117–120. Lund University Cognitive Studies.

Olsson, L., Nehaniv, C. L., and Polani, D. (2005b). From unknown sensors and actuators to visually guided movement. In *Proceedings of the Fourth International Conference on Development and Learning (ICDL 2005)*, pages 1–6. IEEE Computer Society Press.

Olsson, L., Nehaniv, C. L., and Polani, D. (2005c). Sensor adaptation and development in robots by entropy maximization of sensory data. In *Proceedings of the Sixth IEEE International Symposium on Computational Intelligence in Robotics and Automation (CIRA-2005)*, pages 587–592. IEEE Computer Society Press.

Olsson, L., Nehaniv, C. L., and Polani, D. (2006). From unknown sensors and actuators to actions grounded in sensorimotor perceptions. *Connection Science*, 18(2).

Pierce, D. and Kuipers, B. (1997). Map learning with uninterpreted sensors and effectors. *Artificial Intelligence*, 92:169–229.

Prince, C., Helder, N. A., and Hollich, G. J. (2005). Ongoing emergence: A core concept in epigenetic robotics. In *Proceedings of the fifth international workshop Epigenetic Robotics*, pages 63–70.

Sporns, O. and Pegors, T. K. (2003). Generating structure in sensory data through coordinated motor activity. *Proceedings of the International conference Neural Networks*, page 2796.

Sporns, O. and Pegors, T. K. (2004). Information-theoretic aspects of embodied artificial intelligence. *Embodied Artificial Intelligence, LNCS 3139*, pages 74–85.

Steuer, R., Kurths, J., Daub, C. O., J., W., and Selbig, J. (2002). The mutual information: Detecting and evaluating dependencies between variables. *Bioinformatics*, 18:231–240.

Tarapore, G., Lungarella, M., and Gómez, G. (2004). Fingerprinting agent-environment interaction via information theory. In Groen, F., Amato, N., Bonarini, A., Yoshida, E., and Kröse, B., editors, *Proceedings of the 8th International Conference on Intelligent Autonomous Systems, Amsterdam, The Netherlands*, pages 512–520.

Wiesel, T. (1982). Postnatal development of the visual cortex and the influence of environment. *Nature*, 299:583–591.

Proceedings of the 2006 IEEE/RSJ
International Conference on Intelligent Robots and Systems
October 9 - 15, 2006, Beijing, China

Jacobian Learning Methods for Tasks Sequencing in Visual Servoing

Nicolas Mansard[1], Manuel Lopes[2], José Santos-Victor[2], François Chaumette[1]
[1] *IRISA - INRIA Rennes, France*
E-Mail : {nmansard,chaumett}@irisa.fr
[2] *Instituto de Sistemas e Robótica, Instituto Superior Técnico, Lisboa, Portugal*
E-Mail : {macl,jasv}@isr.ist.utl.pt

***Abstract*— In this paper, the coupling between Jacobian learning and task sequencing through the redundancy approach is studied.**

It is well known that visual servoing is robust to modeling errors in the jacobian matrices. This justifies why jacobian estimation does not usually degrade the system convergence. However, we show that this is not true anymore when the redundancy formalism is used. In this case the jacobian matrix is also necessary to compute projection operators for task decomposition, which is quite sensitive to errors. We show that learning improves the servoing performance, when task sequencing is used. Conversely, sequencing improves the convergence of learning, especially for tasks involving several degrees of freedom. Eye-in-hand and eye-to-hand experiments have been performed on two robots with six degrees of freedom.

I. Introduction

Visual servoing methods provide very efficient and robust solutions to control robot motions [7]. It provides high accuracy for the final pose and good robustness to camera calibration and other setting parameters. The redundancy formalism [10], [14] extends the task-function approach [16] to compute a control law that realizes a main task, while simultaneously taking supplementary constraints into account. It can be used when the main task does not constrain all the robot degrees of freedom (DOF). A secondary task can then be added to meet a second objective without disturbing higher priority tasks. The control law for the second task is projected into the set of motions constituting the null space of the first task, thus leaving the first tasks unmodified. The computation of the projection operator is based on the jacobian of the first task.

This approach involves the computation of the task jacobian, linking the evolution of the visual features to the robot articular motion. It thus requires knowledge about the camera-world and world-actuator transformations that influence the interaction matrix (relating image and camera velocities) and the robot jacobian (relating end-effector and joint velocities). Such transformations are usually obtained during an offline calibration phase.

However, full system calibration (and even a coarse one) is not always possible and/or desirable. Some robots may lack proprioceptive sensors to provide the necessary information and some parameters may vary over time, due to malfunction, changes in mechanical parts or modification in the camera lenses. Even when calibration information is available, the analytic computation of the interaction matrix often requires an estimate of the depth of the tracked features. For all these reasons, a perfect computation of the task jacobian can be very difficult or even impossible in practice.

Several methods have already been proposed to estimate the interaction matrix, the robot jacobian or the task jacobian. One of the first works was [6], where robust learning rule was derived and a convergence proof given. This method is based on the Broyden update rule, well known from optimization theory [5] and has been widely used in robotic applications with visual control. In [8], it was used for visually-guided grasping. Ad hoc task sequencing was used in [3] to separate the reaching phase and the grasping phase. Another object-grasping task is presented in [12], where the estimation algorithm is used to provide an approximation of a highly non-linear mapping, using several local linear models. An error function for the jacobian approximation is defined. By minimizing this function with a Newton method, a time-varying system is obtained. This work was applied to both eye-in-hand and eye-to-hand systems with moving targets [15]. It was also suggested to learn the inverse jacobian directly, instead of the jacobian [9], although only an offline formulation was proposed in that work. A complete discussion about adaptive identification methods for slowly varying parameters is presented in [2]. It also presents a new method to improve the robustness of parameter identification, by combining directions with new information with those where the information had been lost and had to be recovered.

All these works are only focused in the jacobian estimation itself. It is well known that visual servoing offers a high level of robustness to jacobian errors. As a consequence, learning the jacobian usually provides satisfactory results. However, when computing the control law for a set of tasks using the redundancy formalism, the jacobian is also used to compute a projection operator. As will be shown in this paper, this computation is not robust at all, and the highest priority task may be strongly disturbed by the projector estimation errors. **Learning the jacobian for a redundancy-based servo scheme turns out to be more demanding than for single-task scheme** and has to be studied with care, which is one of the scope of this paper.

In [13] a solution was presented to stack redundant tasks on top of the others, until all degrees of freedom of the robot

are constrained, and the desired pose is reached. It is based on a generalization of the redundancy approach to several tasks [17].

In this work, we apply the sequencing method to coarsely calibrated systems. Hence, errors in the jacobian will cause errors in the computation of the projection operators, disturbing higher priority tasks. To overcome this problem, we use the disturbance itself as an error signal used to improve the jacobian online. We compare several estimation methods, in order to access their quality in terms of real-parameter estimation and online behavior of the system.

Our results show that it is possible to estimate the jacobian online, in the context of task sequencing for visual servoing. In addition, the learning stability is greatly improved by the task sequencing approach. Hence, **task sequencing and learning are intertwined, mutually constrained processes that bring additional performance and flexibility** to the control of complex robotic systems, when calibration information is unavailable or highly uncertain.

In Section II the stack of tasks structure used to sequence redundant tasks is defined, together with a control law that maintains all the tasks. Section III recalls several jacobian estimation methods, that are discussed in the experiments. Several sets of experiments have been realized to support our conclusions using two different six DOF robots (Section IV).

II. Visual servoing using a stack of tasks

In this section, we recall how to sequence redundant tasks and to maintain the tasks already achieved [13].

A. Redundancy formalism for two tasks

Let $\mathbf{q}$ be the articular vector of the robot. Let $\mathbf{e_1}$ and $\mathbf{e_2}$ be two tasks, $\mathbf{J_i} = \frac{\partial \mathbf{e_i}}{\partial \mathbf{q}}$ $(i = 1, 2)$ their jacobian, defined by:

$$\dot{\mathbf{e_i}} = \frac{\partial \mathbf{e_i}}{\partial \mathbf{q}} \dot{\mathbf{q}} = \mathbf{J_i} \dot{\mathbf{q}} \tag{1}$$

Since the robot is controlled using its articular velocity $\dot{\mathbf{q}}$, (1) has to be inverted. The general solution (with $i = 1$) is:

$$\dot{\mathbf{q}} = \mathbf{J_1^+} \dot{\mathbf{e_1}} + \mathbf{P_1} \mathbf{z} \tag{2}$$

where $\mathbf{P_1}$ is the orthogonal projection operator on the null space of $\mathbf{J_1}$ and $\mathbf{J_1^+}$ is the pseudo-inverse of $\mathbf{J_1}$. Vector $\mathbf{z}$ can be used to apply a secondary command, that will not disturb $\mathbf{e_1}$. Here, $\mathbf{z}$ is used to carry out at best a task $\mathbf{e_2}$. Introducing (2) in (1) (with $i = 2$) gives:

$$\dot{\mathbf{e_2}} = \mathbf{J_2} \mathbf{J_1^+} \dot{\mathbf{e_1}} + \mathbf{J_2} \mathbf{P_1} \mathbf{z} \tag{3}$$

By inverting this last equation, and introducing the computed $\mathbf{z}$ in (2), we finally get:

$$\dot{\mathbf{q}} = \mathbf{J_1^+} \dot{\mathbf{e_1}} + \mathbf{P_1} (\mathbf{J_2} \mathbf{P_1})^+ (\dot{\mathbf{e_2}} - \mathbf{J_2} \mathbf{J_1^+} \dot{\mathbf{e_1}}) \tag{4}$$

Since $\mathbf{P_1}$ is Hermitian and idempotent (it is a projection operator), (4) can be written:

$$\dot{\mathbf{q}} = \mathbf{J_1^+} \dot{\mathbf{e_1}} + \widetilde{\mathbf{J_2}}^+ \widetilde{\dot{\mathbf{e_2}}} \tag{5}$$

where $\widetilde{\mathbf{J_2}} = \mathbf{J_2} \mathbf{P_1}$ is the limited jacobian of the task $\mathbf{e_2}$, giving the available range for the secondary task to be performed without affecting the first task, and $\widetilde{\dot{\mathbf{e}}_2} = \dot{\mathbf{e}}_2 - \mathbf{J_2} \mathbf{J_1^+} \dot{\mathbf{e}}_1$ is the secondary task function, after subtracting the part $\mathbf{J_2} \mathbf{J_1^+} \dot{\mathbf{e}}_1$ already accomplished by the first task. A very good intuitive explanation of this equation is given in [1].

B. Extending the redundancy formalism for several tasks

Let $(\mathbf{e_1}, \mathbf{J_1})$ ... $(\mathbf{e_n}, \mathbf{J_n})$ be n tasks so that Task $\mathbf{e_i}$ should not disturb task $\mathbf{e_j}$ if $i > j$. A recursive extension of (5) is proposed in [17]:

$$\dot{\mathbf{q}}_\mathbf{i} = \dot{\mathbf{q}}_{\mathbf{i-1}} + (\mathbf{J_i} \mathbf{P}^\mathbf{A}_{\mathbf{i-1}})^+ (\dot{\mathbf{e}}_\mathbf{i} - \mathbf{J_i} \dot{\mathbf{q}}_{\mathbf{i-1}}) \tag{6}$$

where $\mathbf{P}^\mathbf{A}_\mathbf{i}$ is the projector onto the null-space of the augmented Jacobian $\mathbf{J}^\mathbf{A}_\mathbf{i} = (\mathbf{J_1}, \dots \mathbf{J_i})$. The recursion is initialized by $\dot{\mathbf{q}}_\mathbf{0} = 0$. The robot velocity is $\dot{\mathbf{q}} = \dot{\mathbf{q}}_\mathbf{n}$.

Using this recursive equation directly, a projector has to be computed on each step of the computation. A recursive formula for the computation of the projector is proposed in [1]. We recall this equation here

$$\mathbf{P}^\mathbf{A}_\mathbf{i} = \mathbf{P}^\mathbf{A}_{\mathbf{i-1}} - \widetilde{\mathbf{J}}_\mathbf{i}^+ \widetilde{\mathbf{J}}_\mathbf{i} \tag{7}$$

where $\widetilde{\mathbf{J}}_\mathbf{i} = \mathbf{J_i} \mathbf{P}^\mathbf{A}_{\mathbf{i-1}}$ is the limited jacobian of the task i. The recursion is initialized by $\mathbf{P}^\mathbf{A}_\mathbf{0} = \mathbf{I}$ (identity matrix).

The control law is finally obtained by setting an exponential decrease for each task:

$$\forall i = 1..n, \quad \dot{\mathbf{e}}_\mathbf{i} = -\lambda_i \mathbf{e_i} \tag{8}$$

where the parameters λ_i are used to tune the convergence speed of each task.

In this control law, two matrices have to be learned: $\mathbf{J_i}$ and $\mathbf{P}^\mathbf{A}_\mathbf{i}$. Since $\mathbf{P}^\mathbf{A}_\mathbf{i}$ can be computed from $\mathbf{J_i}$, we will learn only the jacobian and then compute the projection operator from it. In this sense, the two matrices are learned. The effect of the learning can be considered from two different points of view: convergence of a task while the jacobian is learned online and the disturbances caused upon higher priority tasks due to the effect of learning the projection operator.

C. Application to visual servoing

In this article, we propose an implementation of this control law using visual servoing. The task functions $\mathbf{e_i}$ used in the remainder of the text are computed from visual features:

$$\mathbf{e_i} = \mathbf{s_i} - \mathbf{s_i^*} \tag{9}$$

where $\mathbf{s_i}$ is the current value of the visual features for task $\mathbf{e_i}$ and $\mathbf{s_i^*}$ their desired value.

The interaction matrix $\mathbf{L_{s_i}}$ related to $\mathbf{s_i}$ is defined so that $\dot{\mathbf{s}}_\mathbf{i} = \mathbf{L_{s_i}} \mathbf{v}$, where $\mathbf{v}$ is the camera kinematic screw. From (9), it is clear that the interaction matrix $\mathbf{L_{s_i}}$ and the task jacobian $\mathbf{J_i}$ are linked by the relation:

$$\mathbf{J_i} = \mathbf{L_{s_i}} \mathbf{J_q} \tag{10}$$

where the matrix $\mathbf{J_q}$ denotes the robot jacobian ($\mathbf{v} = \mathbf{J_q} \dot{\mathbf{q}}$). In the following section we will see several methods that can be used to learn the jacobian matrix.

III. JACOBIAN ESTIMATION METHODS

A large amount of information is required to recompute the jacobian at each iteration. As presented just above, the jacobians can be divided in two parts: the articular jacobian $\mathbf{J_q}$, and the interaction matrix $\mathbf{L_s}$ (see (10)). The articular jacobian can only be computed if the full arm-eye calibration is available. Instead, the interaction matrices require some 3D parameters of the observed object. This can be estimated using pose computation (if the object model is available) or using homographies [4] between the image and relevant scene planes. In this last case, the scale parameters cannot be estimated, and the object depth has to be fixed *a priori* or estimated using other methods. All these parameters can lead to errors in the computation of the interaction matrix.

Different approaches can be used to estimate the tasks jacobians. Learning the task jacobian, $\mathbf{J_i}$, is quite difficult, due to the numerous non-linear terms involved in its analytical form. The experiments have proved the extreme difficulty in obtaining a good estimation of $\mathbf{J_i}$. In [12], a mixture of several linear models was described to tackle this problem.

Instead of trying to estimate $\mathbf{J_i}$, we have chosen to use an approximation of the articular jacobian, $\widehat{\mathbf{J_q}}$, computed from coarse robot calibration data. Then, since an approximation of $\mathbf{v}$ can be computed, only the matrices $\widehat{\mathbf{L_{s_i}}}$ need to be estimated. Furthermore, estimating $\mathbf{L_{s_i}}$ will allow to "absorb" some of the errors in $\mathbf{J_q}$, caused by the coarse robot calibration. This solution is also able to take into account the uncertainties in the target model, yielding better results, even when using a properly calibrated robot, as it will be shown in Section IV-B. In the following sub-sections, we present the methods used in the experiments to learn the jacobian.

A. Broyden Update

The first work presented for jacobian estimation in visual servoing was [6]. This method is based on the Broyden update rule. The Jacobian estimation is given by:

$$\hat{\mathbf{J}}(t+1) = \hat{\mathbf{J}}(t) + \alpha \frac{\left(\Delta\mathbf{e} - \hat{\mathbf{J}}(t)\Delta\mathbf{x}\right)\Delta\mathbf{x}^\top}{\Delta\mathbf{x}^\top\Delta\mathbf{x}} \tag{11}$$

After observing some image motion, $\Delta\mathbf{e}$, caused by a motor command $\Delta\mathbf{x}$, the Jacobian is updated directly, with α defining the update speed. This method has several positive aspects: low memory usage because only the last observation is used; low computational cost and a single parameter to be tuned. When the motions are too small, this computation may become unstable. One solution consists in including a regularization term in the denominator to prevent singularities. Alternatively, the learning can simply be switched off, whenever the motion falls below a certain threshold.

In practice, it can be used to compute offline an estimation of the jacobian from a set of simple motions. Or the estimation of the jacobian can be updated online, using at the first iteration the result of the offline learning or an estimation of the analytical jacobian.

B. Correlation

A different approach can be made with least squares estimation [2]. Considering the cost function l as:

$$l = \sum_{i=0}^{t} \gamma^{i-t}(\Delta\mathbf{e} - \mathbf{J}\Delta\mathbf{x})^\top(\Delta\mathbf{e} - \mathbf{J}\Delta\mathbf{x})$$

The minimization off-line gives the usual least squares solution:

$$\mathbf{J} = \mathbf{Q}\mathbf{R}^+$$

where $\mathbf{Q}$ and $\mathbf{R}$ are:

$$\begin{aligned}\mathbf{Q} &= \sum_{i=0}^{t} \lambda^{(t-i)}\boldsymbol{\Delta}\mathbf{e}_i^\top\boldsymbol{\Delta}\mathbf{x}_i \\ \mathbf{R} &= \sum_{i=0}^{t} \lambda^{(t-i)}\boldsymbol{\Delta}\mathbf{x}_i^\top\boldsymbol{\Delta}\mathbf{x}_i\end{aligned}$$

or in an online formulation;

$$\begin{aligned}\mathbf{Q} &= \lambda\mathbf{Q} + \boldsymbol{\Delta}\mathbf{e}_t^\top\boldsymbol{\Delta}\mathbf{x}_t \\ \mathbf{R} &= \lambda\mathbf{R} + \boldsymbol{\Delta}\mathbf{x}_t^\top\boldsymbol{\Delta}\mathbf{x}_t\end{aligned} \tag{12}$$

Like the *Broyden* update, the correlation learning can be used offline or online. However, it can not be used to update an approximation of the analytical jacobian since the two matrices $\mathbf{Q}$ and $\mathbf{R}$ are required. In practice, it is difficult to start the learning online without any offline training. In the experiment, a short offline training composed of some simple motions has always been used to initialize the online learning.

C. Direct-Inverse

Learning the jacobian boils down to minimizing the prediction error of the image velocities. Yet, for control purposes, we need the inverse map $\mathbf{J}^+$, that corresponds to the "reconstruction" of the robot joint velocities from image velocities. Thus, in [9], it was suggested that one should learn the inverse Jacobian directly, instead of the Jacobian. The cost function becomes:

$$l = \sum_{i=0}^{t} \gamma^{i-t}(\Delta\mathbf{x} - \mathbf{H}\Delta\mathbf{e})^\top(\Delta\mathbf{x} - \mathbf{H}\Delta\mathbf{e})$$

where $\mathbf{H} = \mathbf{J}^+$. This cost function can be seen as a reconstruction error, as opposed to the prediction error used before. The main advantage is that we no longer need to invert the Jacobian for computing the control law. An additional benefit is that the least-squares fitting requires the inversion of a smaller, possibly better conditioned, information matrix, R. This is particularly relevant for the task sequencing approach whereby the (sub-)task dimension is much smaller than the control space.

Using the online formulation (12) it is possible to propose an online version of the *direct-inverse* learning method. In the experiment, both the offline and the online version of the method were used. As for the classical correlation method, the online learning can not be initialized from an analytical value of the jacobian, and requires thus a short offline training.

IV. Experiments and results

In this section we present results comparing the quality of tasks sequencing using several methods of jacobian estimation. Two robots with different kinematics and servoing architectures were used for the experiments. We first describe quickly the selected visual features used for the experiments. Four representative experiments are then presented in detail.

A. Visual features for vision-based control

In order to have a better and easier control over the robot trajectory, approximately decoupled tasks were chosen. We have used visual features derived from the image moments. To simplify the image processing as we mainly focus on the control part, we have used a simple white-points-on-black-board target as shown Fig 1. The first task $\mathbf{e_g}$ - *centering* - is based on the position of the center of gravity of the four points. The second task $\mathbf{e_Z}$ - *zooming* - uses the area of the object in the image to control the range between the robot and the target. The third task $\mathbf{e}_\alpha$ - *Z-rotation* - rotates the camera around the optical axis, so that the object will be correctly oriented in the image. It uses the orientation of the object in the image, which can be obtained from the second order moments. The last task $\mathbf{e_R}$ - *perspective correction* - uses third order moments to decouple v_x from ω_y and v_y from ω_x. The reader is invited to refer to [18] for more details.

B. Results

The three first experiments were realized with the robot Baltazar. Baltazar is an anthropomorphic robotic torso [11] equipped with a six DOF arm, an eleven DOF hand and a four DOF head. In the presented experiments, the target was attached to the robot hand. An eye-to-hand visual servo was used to position the hand parallel to the eye image plane, centered at a distance of $20cm$. This robot has a high payload/weight ratio causing some elasticities, its motors are equipped with position sensors but the lack of an home sensor causes some errors if a precise calibration is needed. The camera is coarsely calibrated and for the experiments a $4.5mm$ lens had to be used. Figure 1 presents the robot and the initial and final hand position. The total motion is about $30cm$ corresponding to a maximum joint translation of $90\,dg$.

The first experiment includes a comparison of the estimation methods presented in Section III. The second experiment shows that it is possible to correct the robot (coarse) calibration by learning only the interaction matrix when realizing a full sequencing. The third experiment is a first step to show (experimentally) that the trajectory obtained when applying a sequencing control law provides a very good dataset for learning. The last experiment was realized on an accurately calibrated robot (see Section IV-F). It shows that a small uncertainty can result in a big perturbation, and that the online estimation is able to provide a nearly perfect behavior.

C. Experiment 1 - online learning

In this first experiment, the stack has two tasks: centering ($\mathbf{e_g}$) and Z-rotation ($\mathbf{e}_\alpha$). The goal consists in testing how the

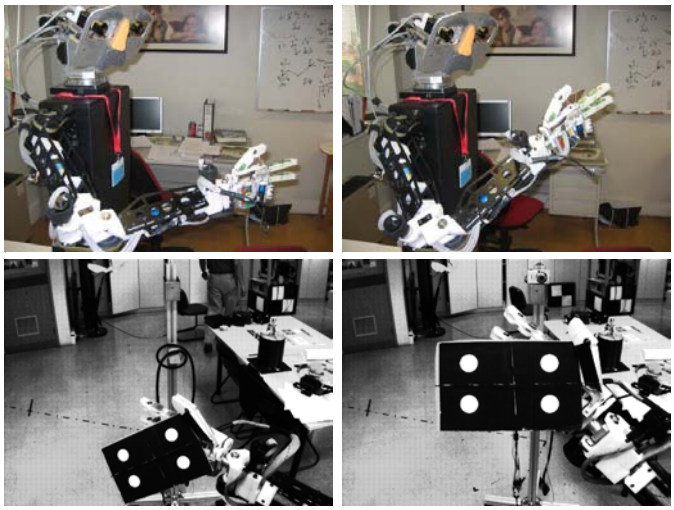

Fig. 1. Initial and final position. Top: outside view, Down: camera view

jacobian estimation errors influence the task sequencing, due to errors introduced in the projection operator. When the jacobian of the first task is mis-estimated, the centering is lost with the activation of the second task. When the error increases, the target moves further away from the image center, and could even leave the image if the disturbance is too strong (which results of course in the visual servoing failure).

Figure 2 presents the evolution of the error for the first task using analytic/offline learning versus online estimation methods. Figure 3 shows the result for the second (rotation) task. Offline learning relies on simple motions of the arm, done during approximately 250 iterations. Online learning was carried out at every frame.

As can be seen in Fig. 2, analytic or offline learning are worse, in terms of having a larger perturbation and longer convergence times. The perturbation is very important and it can not be reduced before the secondary task completion.

On the opposit, online estimation methods lead to much better results, outperforming the results with the analytical jacobian. Although a large disturbance appears when the second task is added, it is quickly reduced afterward. For online estimation, the amplitude of the perturbation ranged from 20 to 30 pixels. *Broyden* and *Correlation* methods were able to eliminate the error after 30 iterations. The maximal perturbation is equivalent to the one obtained with analytic computation, but the duration is much shorter.

The online *Direct-inverse* method was unable to reduce the error as fast as the two other methods or the analytic version, whatever the tuning realized. The advantage of directly minimizing the reconstruction errors instead of the prediction error does not appear significant in this setting. Indeed, to compute the projection it is necessary to have the direct map and the result, in the end, is worst.

It is also interesting to see that the task-error convergence is very similar for all methods (for Task $\mathbf{e_g}$, Fig. 2 before Iteration 50, and for Task $\mathbf{e}_\alpha$, Fig. 3). This emphasizes that the

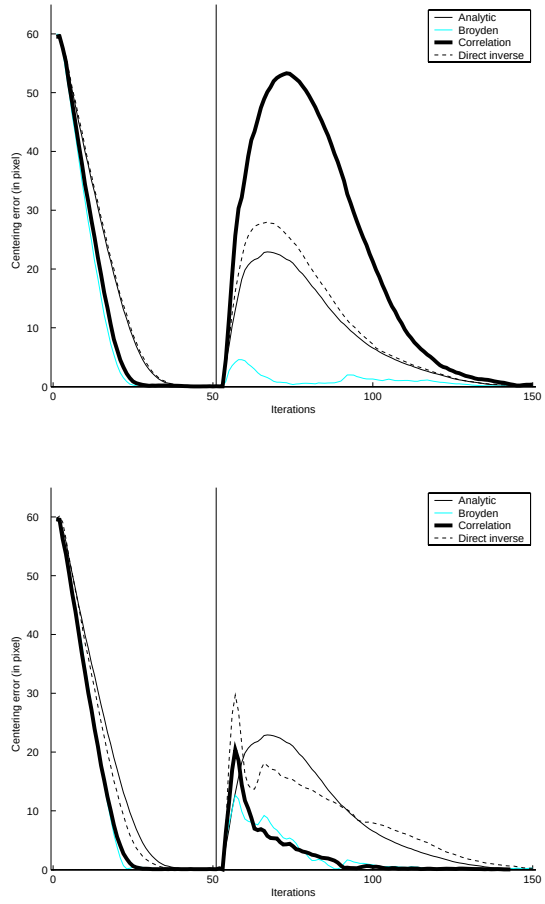

Fig. 2. Temporal evolution of the image error during servoing using offline (top) or online (bottom) learning methods. The vertical line shows the time instant where the second task started.

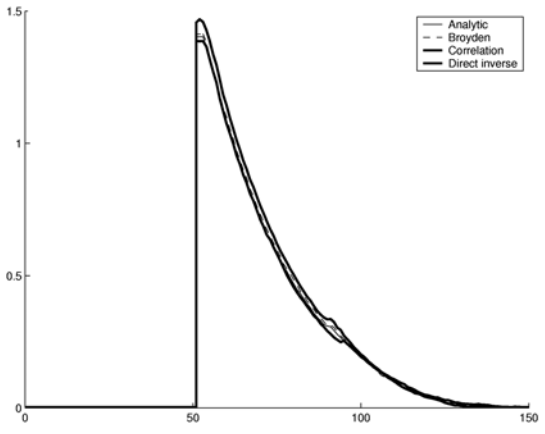

Fig. 3. Convergence rates for the second task (rotation) while trying to keep the centering at zero (refer to Figure 2). Due to robustness to jacobian error, the convergences are the same for all the tasks.

reduction of the perturbation is not made at the cost of worse convergence. The convergence is very robust to jacobian error, since all the task convergences are the same. It is nevertheless not true for the projection operator estimation, which is very sensitive and requires an accurate estimation.

Finally, we can note from several experiments starting from different initial positions and using different tasks that the online *Correlation* method produced better results in sense of perturbation amplitude, perturbation average and perturbation-correction time, when properly tuned. However, it is not as robust to gain-tuning as the *Broyden* approach that could solve the task in all situations with the same parameters settings (note the *Broyden* performances for offline learning).

D. Experiment 2 - generalization to more tasks

To verify that the method it is possible to learn all tasks, a complete sequence was done, consisting in: centering, zooming, Z-rotation and perspective. All online learning methods have been able to achieve the sequencing. The lowest perturbations were obtained using the *Correlation* method. Figure 4 cares the results of this method (on the bottom) with the analytical one (on the top). The vertical lines represent the time instant where a new task is added to the stack, after all the tasks already in the stack have converged to zero. It is interesting to see that in a badly calibrated system, the learning scheme yields better results than using the analytic solution, in terms of convergence speed, amplitude and average of the perturbations.

E. Experiment 3 - better learning through task sequencing

A very important point was to note that learning improves the sequencing quality by reducing convergence time and the size of the perturbations. At the same time, the sequencing generates more efficient trajectories for learning. This experiment tests the hypothesis that learning four simpler tasks in sequence is easier than learning four tasks at the same time.

We compared the learning when running the robot under three different control laws. During the first run, task sequencing was used, in the same way as in previous experiments. In the second trial, all tasks are active at the same time. In other words, the same formalism is used but every task is active from the beginning, as opposed to starting a new task only after all the previous ones are completed. The last trial consisted on classical visual servoing, using only one single task of full rank. The condition number of the full-rank jacobian matrix was then estimated at each iteration. When a sequencing was used, the jacobians of all tasks were piled up and the overall condition number evaluated.

For *Correlation* and *Direct-inverse* methods, the condition number was the same for the three experiments. For these learning methods, the sequencing does not improve the learning.

On the opposite, the hypothesis has turned out to be correct when using *Broyden* algorithm. Figure 5 shows that for the *Broyden* method, the condition number of the matrices are much worse for the full task and convergence cannot be attained.

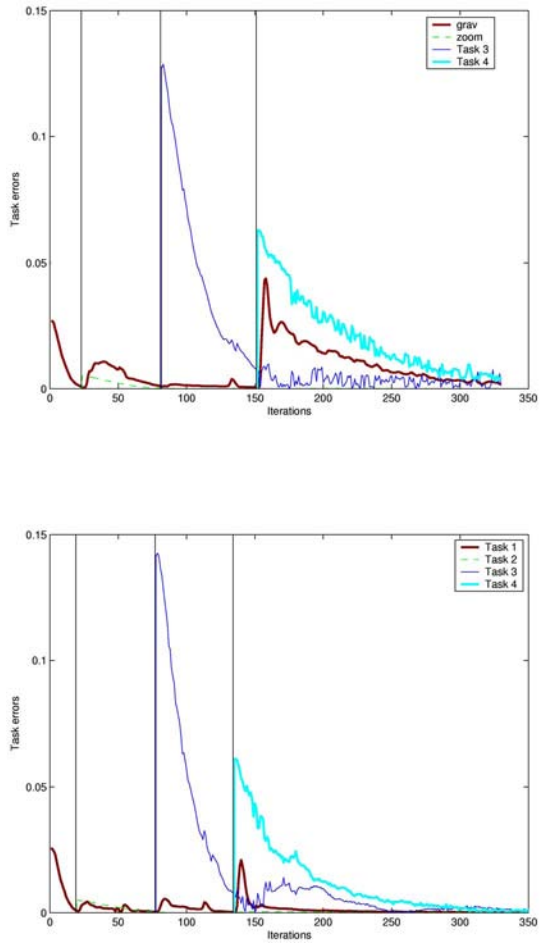

Fig. 4. Results for a sequence of four tasks. Top: Analytic method. Bottom: *Correlation*. The vertical line shows the time instant where a new task is added in the stack. Due to calibration errors, the analytical solution is not able to ensure the stack priorities. When a perturbation appears, it is not corrected until the active task has converged. The online estimation is able to quickly correct the perturbations. The perturbation average is thus much lower. The perturbation amplitudes are also lower.

F. Experiment 4 - calibrated robot

The last experiment was realized with an industrial robot. This robot is a six-DOF eye-in-hand robot with a very low payload/weight ratio. It has position and home sensors and its high repeatability allows to do a very precise calibration. Full, accurate calibration is available and the articular jacobian is no longer an approximation. However, the depth of the target is unknown and must be estimated to compute the correct jacobians. Mis-estimating depth induces scale errors in the interaction matrices.

The experiments consist in a sequencing of the four tasks. The tasks were introduced in the same order as before, at fixed time for a better comparison ($\mathbf{e_g}$ at $t = 0$, $\mathbf{e}_\alpha$ at $t = 150$, $\mathbf{e_Z}$ at $t = 60$, and $\mathbf{e_R}$ at $t = 110$). For each experiment, we vary the method used to compute the interaction matrix. The evolution of the perturbation norm is shown on Fig. 6 for each estimation scheme. The complete results are detailed for the *Broyden* method in Fig. 7.

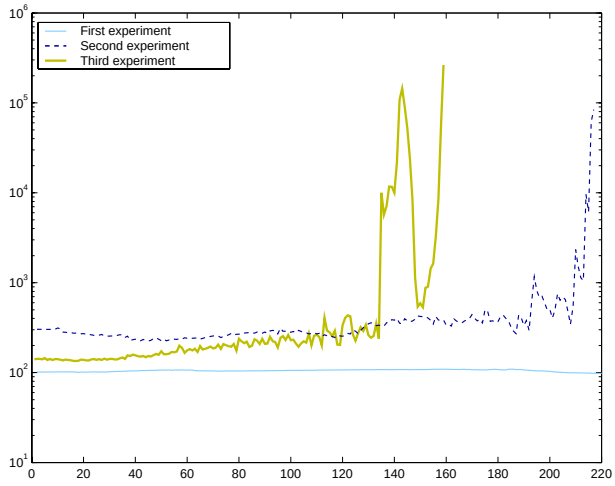

Fig. 5. Condition-number evolution of the estimated interaction matrix during the servo. The matrix is learned from three different trajectories. The first one is a sequencing as done above (first experiment). The second uses the stack of task (control law (**??**)), but all the tasks were activated at the same time at the first iteration (that is to say, no task sequencing). The last one is obtained from a classical visual servoing using a six-DOF task composed of all the visual features (third experiment). The matrix learned from a classical servo has a very large condition number. It increases until the servo becomes impossible. The learning realized from sequencing provides a properly conditioned matrix.

The first test ("current") shows that a perfect behavior is obtained when all the required knowledge is available. Depth was estimated with a pose computation algorithm, using the object geometric model and camera calibration. In the second trial ("misestimated"), depth was mis-estimated by a factor of 2. In the third experiment ("desired"), the interaction matrices were computed at the desired position using the desired depth. As can be shown on the top of Fig. 6, inaccuracies in the projection operators introduce large perturbations.

In a second set of experiments presented on the bottom of Fig. 6, we analyze the use of estimated jacobian matrices. The first two trials use both the online and offline versions of the *Correlation*. The third one starts with the analytical matrix, that is updated with the *Broyden* rules. These methods are compared with the same analytic version ("curent") as before.

Figure 6 shows the perturbations for each estimation scheme. As expected, the use of the "perfect" analytical solution leads to better results than the versions with estimated jacobians. However, the use of an estimation of the jacobian matrix (such as the matrix computed at the desired value, or from a misestimated depth parameter) produces large perturbations during a long time. It is also true when used the results of some offline learning. On the opposite, the use of online estimations always outperforms approximations the analytical jacobian. The best behavior is obtained with the *Broyden* algorithm, using the true interaction matrix as initialization. It provides a robust and fast online estimation without the need of a first offline learning.

Finally, Fig. 7 shows the results using the *Broyden* method. We can note that the perturbation amplitudes are very small (almost invisible) for all tasks. They are also quickly reduced.

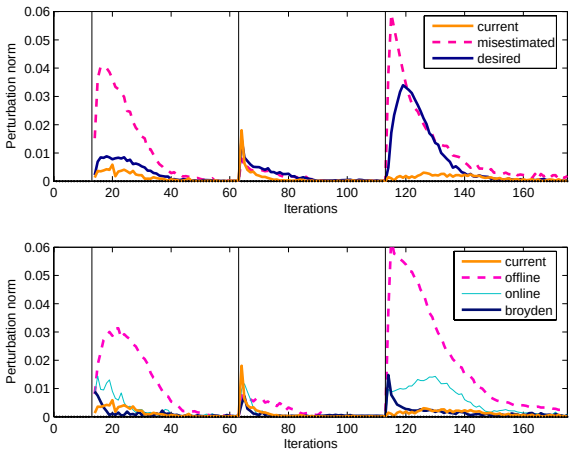

Fig. 6. Perturbation norm (i.e. norm of the error of the tasks already completed) during the positioning. Top: results obtained with the true jacobian ("current") and two approximate versions where the depth is misestimated by a factor of 2 or set to the desired value in the goal position. Bottom: comparison of the true jacobian version ("current") with learned jacobians (Correlation offline and online) and Broyden. Approximations in the analytic solution (on the top) can generate disturbance that are reduced using a learning scheme (on the bottom).

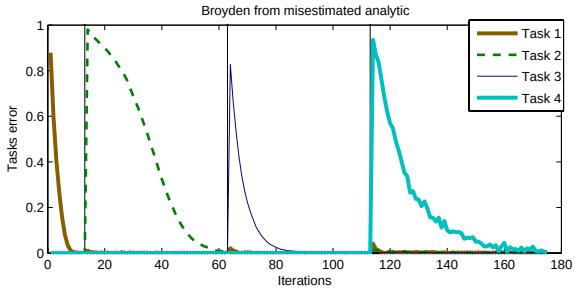

Fig. 7. Correcting a depth mis-estimation by an online estimation of the interaction matrix. Results for a sequence of four tasks sequencing on the full-calibrated robot Afma6. The jacobian estimation method is *Broyden*, using the analytical solution as an initialization of the learning.

V. Conclusion

In this paper several learning methods have been tested for jacobian estimation in task sequencing. The tested methods were *Broyden* method, *Correlation* method and *Direct-inverse* method. The *Direct-inverse* method was adapted to have an online update rule. All methods were able to learn the jacobian and accomplish the sequence of tasks, both in eye-in-hand and eye-to-hand configuration.

Of course, if all the necessary knowledge is present (that is if the system is perfectly modeled and calibrated), the control scheme using the analytical jacobian performs better than any learning-based scheme. However, as soon as some errors or misestimations appear in the model, the performances of the analytical solution become lower while the learning improves the quality of the servo. If the calibration is not accurate, the learning methods perform always better.

When comparing the learning schemes, an online update of the jacobian produces better results than an offline learning when considering the number of iterations required to nullify the perturbation, and also when considering the perturbation amplitude. In terms of comparison, the best estimation was obtained using the *Correlation* method. But it requires a tuning and a training step. Another very interesting solution is to use the analytical approximation of the jacobian to initialize the *Broyden* online learning. This solution is very robust, it does not require any tuning, and can perform all the tasks with the same parameters. Moreover, it does not require any offline learning phase.

It was verified that learning improves the task sequencing by reducing the perturbations. It was also shown that the sequencing helps the learning by estimating a mixture of smaller subtasks successively. The condition number of the obtained jacobian, and the stability of the global system (control+learning) are more satisfactory.

References

[1] P. Baerlocher and R. Boulic. An inverse kinematic architecture enforcing an arbitrary number of strict priority levels. *The Visual Computer*, 6(20), 2004.

[2] M. De Mathelin and R. Lozano. Robust adaptive identification of slowly time-varying parameters with bounded disturbances. *Automatica*, 35:1291–1305, 1999.

[3] Z. Dodds, M. Jägersand, G. Hager, and K. Toyama. A hierarchical vision architecture for robotic manipulation tasks. In *Proc. of Int. conf. on Computer Vision Systems*, 1999.

[4] O. Faugeras. *Three-dimensional computer vision: a geometric viewpoint*. MIT Press, Cambridge, Massachusetts, 1993.

[5] R. Fletcher. *Practical Methods of Optimization*. Chichester, 2nd edition, 1987.

[6] K. Hosoda and M. Asada. Versatile visual servoing without knowledge of true jacobian. In *IROS*, pages 186–193, Munchen, Germany, Sep. 1994.

[7] S. Hutchinson, G. Hager, and P. Corke. A tutorial on visual servo control. *IEEE Trans. on Robotics and Automation*, 12(5):651–670, October 1996.

[8] M. Jagersand and R.C. Nelson. On-line estimation of visual-motor models using active vision. In *ARPA Image Understanding Workshop*, pages 677–682, 1996.

[9] J. T. Lapresté, F. Jurie, M. Dhome, and F. Chaumette. An efficient method to compute the inverse jacobian matrix in visual servoing. In *ICRA*, 2004.

[10] A. Liegeois. Automatic supervisory control of the configuration and behavior of multibody mechanisms. *IEEE Trans. on Systems, Man and Cybernetics*, 7(12):868–871, December 1977.

[11] M. Lopes, R. Beira, M. Praça, and J. Santos-Victor. An anthropomorphic robot torso for imitation: design and experiments. In *IROS*, Sendai, Japan, 2004.

[12] M. Lopes, A. Bernardino, and J. Santos-Victor. A developmental roadmap for task learning by imitation in humanoid robots. In Y. Demiris, editor, *AISB - Third Int. Symp. on Imitation in Animals and Artifacts*, Hatfield, Uk, April 2005.

[13] N. Mansard and F. Chaumette. Visual servoing sequencing able to avoid obstacles. In *ICRA*, Barcelona, Spain, April 2005.

[14] E. Marchand and G. Hager. Dynamic sensor planning in visual servoing. In *IROS*, volume 3, pages 1988–1993, Leuven, Belgium, May 1998.

[15] J. A. Piepmeier, B. A. Gumpert, and H. Lipkin. Uncalibrated eye-in-hand visual servoing. In *ICRA*, 2002.

[16] C. Samson, M. Le Borgne, and B. Espiau. *Robot Control: the Task Function Approach*. Clarendon Press, Oxford, United Kingdom, 1991.

[17] B. Siciliano and J-J. Slotine. A general framework for managing multiple tasks in highly redundant robotic systems. In *ICAR'91*, pages 1211 – 1216, 1991.

[18] O. Tahri and F. Chaumette. Point-based and region-based image moments for visual servoing of planar objects. *IEEE Transactions on Robotics*, 21(6):1116–1127, December 2005.

Proceedings of the 2006 IEEE/RSJ
International Conference on Intelligent Robots and Systems
October 9 - 15, 2006, Beijing, China

Learning Sensory-Motor Maps for Redundant Robots

Manuel Lopes José Santos-Victor
Instituto de Sistemas e Robótica, Instituto Superior Técnico, Lisboa, Portugal
http://vislab.isr.ist.utl.pt
{macl,jasv}@isr.ist.utl.pt

***Abstract*— Humanoid robots are routinely engaged in tasks requiring the coordination between multiple degrees of freedom and sensory inputs, often achieved through the use of sensory-motor maps (SMMs).**

Most of the times, humanoid robots have more degrees of freedom (DOFs) available than those necessary to solve specific tasks. Notwithstanding, the majority of approaches for learning these SMMs do not take that into account. At most, the redundant degrees of freedom (degrees of redundancy, DOR) are "frozen" with some auxiliary criteria or heuristic rule.

We present a solution to the problem of learning the forward/backward model, when the map is not injective, as in redundant robots. We propose the use of a "Minimum order SMM" that takes the desired image configuration and the DORs as input variables, while the non-redundant *DOFs* are viewed as outputs. Since the DORs are not frozen in this process, they can be used to solve additional tasks or criteria. This method provides a global solution for positioning a robot in the workspace, without the need to move in an incremental way. We provide examples where these tasks correspond to optimization criteria that can be solved online.

We show how to learn the "Minimum Order SMM" using a local statistical learning method. Extensive experimental results with a humanoid robot are discussed to validate the approach, showing how to learn the *Minimum Order SMM* of a redundant system and using the redundancy to accomplish auxiliary tasks.

I. Introduction

Humanoid robots must routinely coordinate the head and the arm. For this purpose, the robot must have a way to predict what will happen in the world if some action is made (forward model), and what action can change the world in a pre-defined manner (backward model). Usually, the correspondence between perception and action is called a *Sensory-Motor Map* (SMM) and it can be interpreted in terms of forward/inverse kinematics of robotic manipulators jointly with a camera. In this work, the SMM is used to predict the image resulting from the robot moving the arm to a certain posture, or the inverse association, by determining which motor command causes the arm to reach a specified appearance.

Quite often, humanoid robots have more degrees of freedom than those strictly necessary to accomplish a certain task. For example, Figure 1 shows several positions of an humanoid robot, where the wrist position is always the same, but the posture of the arm changes. In terms of input-output map, this redundancy translates into the fact that several different inputs yield the same observation or output. If the backward model is obtained by inverting the forward model, this causes a problem, because the function is no longer invertible. Also, if it is desired to learn the inverse model common algorithms will fail because the dataset is incoherent. Hence, to learn this map for a redundant systems requires the adoption of some extra assumptions. However, this strategy effectively "freezes" the redundant degrees of freedom, that can no longer be used for any additional task.

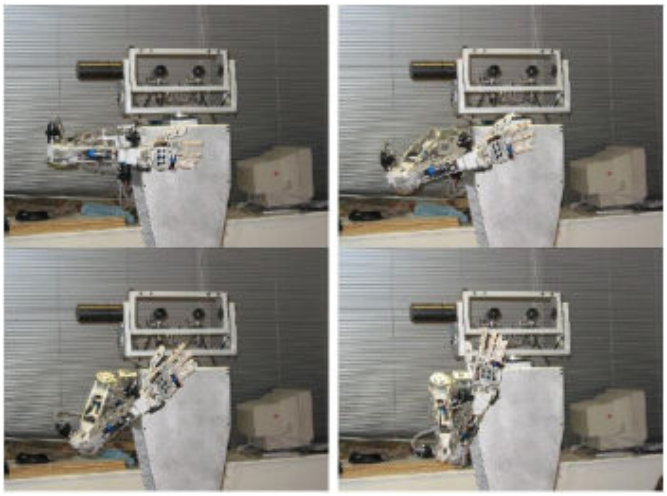

Fig. 1. Redundancy of the robotic system, the $3D$ position of the wrist is the same but the arm configuration is different

This work presents a solution for learning perception-action maps when redundant degrees of freedom exist (also known as degrees of redundancy, DOR). As we do not restrict the output of the system at learning time, the extra degrees of freedom stay free for online selection, and so they can be used to fulfill a secondary task or to meet an additional criterion or constraint, like e.g energy minimization. For this we propose the use of a "Reduced order SMM" that takes the image configuration and DORs as input variables, and the non-redundant DOFs as outputs.

We also present a methodology for estimating the "Reduced Order SMM" automatically. As the map should be differentiable, the function fitting method for estimating the map must be chosen carefully. We choose a local learning method with

1-4244-0259-X/06/$20.00 ©2006 IEEE

differentiable kernels [1], [2].

Several applications have already been proposed, using the SMM perspective. A neural-network architecture was used in [3] to coordinate a binocular head with a three-DOF arm in a reaching task. As the open loop motion can have some error, this work also included some error correction methods by executing a closed loop visual servoing.

Correspondences between perception and action can also relate dynamic properties. In [4], a statistical learning method is used to learn an inverse kinematic function for an highly redundant humanoid robot, engaged in imitation tasks. In this case, a map from positions and velocities is related to image velocities, enabling the robot to repeat arm gestures. The trajectories for learning are hand-coded trajectories, the authors comment that this approach solves the problem of robot singularities, because only seen motions are learned, and so no infinite velocities appear.

The robot jacobian matrix [5] is very often used for control purposes. This matrix relates the cartesian velocity of the end-effector with the corresponding joint velocities. To move in a desired position the inverse jacobian should be evaluated. Some other methods can be used to do this inversion when the jacobian is not square [6]. A well known approach is the damped least-squares, where the inversion is made jointly with an energy minimization [7], originally introduced to solve the problem of controlling robots near singularities.

With redundant robots, the extra degrees of freedom can be used to solve other task, provided that the corresponding motion is done along a direction in the null space of the main motion, this is called the redundancy formalism as proposed in [8], [9]. Several criteria can be used to choose this secondary task. This formalism is very well described in [10] for humanoid animations. In humanoids, several conflicting constraints may frequently occur, like the position of the hands, feet and head in a dance posture. With the redundancy formalism these constraints can be dealt with. In a similar application to ours, the work of [11] presents a robot under visual control, where redundancy is used to obtain better trajectories in a visual servoing task.

We can find examples in the literature on work done in closed kinematic chains. Modeling the musculo-skeletal human system [12] requires some constraints, because the muscles only work by contraction, which must be taken into account when computing the solution. Other works have dealt with planning in humanoid robots. A system able to decompose the forces in order to act both the task domain, but also and independently in the robot posture is presented in [13].

Some methods have already been proposed to estimate the interaction or the jacobian matrix of robots. One of the first works was [14], where a very robust learning rule was derived and a convergence proof given. This method is based on the Broyden update rule already known from optimization theory [15]. It has been widely used in real robotic applications based on visual control. In [16], it was used for a grasping task guided by visual servoing. As the jacobian depends strongly on the current position, it must be evaluated at each time instant. For object-grasping task in [17] an estimation algorithm is used to provide an approximation of this highly non-linear mapping using several local linear models.

Our approach is different from these approaches in several ways:

- Includes visual information in the loop
- No knowledge about the system kinematics is needed. The sensory-motor map is learned with a self-exploration phase.
- The map is global and not a local approximation. This means that we can go directly to a position in an open-loop fashion if we want.
- Several criteria can be used as secondary task without having to learn a new map.

This paper is organized as follows: Section II describes the use of statistical learning methods in redundant robots. Section III shows how to use local regression methods to learn the partial backward model. Section IV is devoted to experiments done with a humanoid torso with 10 DOF, that evaluates the quality of our approach. Finally some conclusions and future work are done. As an annex, we have the deduction of the jacobian of the local learning method.

II. Sensory-motor Coordination with Control Optimization

In this section we show how to define a Sensory-Motor Map that explicitly takes the DOR into consideration, thus allowing the completion of several simultaneous tasks.

Let us define a *SMM* that maps a vector of control variables (n,r) to a vector of image point features $\mathcal{I}$, where n is a minimum set of degrees of freedom that spans the full output space and r is a set of redundant degrees of freedom. Note that there are several partitions of the input space, into redundant versus non-redundant degrees of freedom, that can give this same property. It is possible to find automatically the redundancy by analyzing the correlation matrix for the jacobian estimation [18]. This forward model can thus be written as:

$$\mathcal{I} = f(n, r)$$

and allows to predict the image configuration of the robot given a set of motor commands.

In many cases, we are more interested in the inverse map, i.e. computing the motor commands that drive the robot to a desired image configuration, $\mathcal{I}$. If there were an inverse mapping $(n, r) = f^{-1}(\mathcal{I})$, this problem could be solved in a straight forward manner. However, as the dimension of the input space is larger than that of the output space, there are many input combinations that generate the same image point features. In other words, because of the DOR, $f(n, r)$ is not bijective and, therefore, not invertible.

Fig. 1 shows an example of redundancy, where, for this robot the $3D$ position of the wrist is controlled with 4 DOFs, thus remaining one DOR.

To put the problem in another perspective, we can say that finding the robot joint angles to move the arm to a desired image configuration $\mathcal{I}$ is an ill-posed problem when the arm has redundant degrees of freedom, [19], because multiple solutions exist.

One approach to solve ill-posed problems, [20], [21], consists in using additional constraints that restrain the set of admissible solutions, in such a way that the solution sought becomes unique in this reduced solution space. In our case, this corresponds to recast the original problem to that of moving the robot to a desired image position $\mathcal{I}^*$ while, at the same time, minimizing some auxiliary criterion, $c(n, r)$.

We built a cost function, $\mathcal{K}$, with two terms: one weighting the error in the position of the end effector (data fitness) and another one corresponding to the weights on the control (regularization term).

$$\mathcal{K}(\mathcal{I}^*, n, r) = \lambda \left\| \mathcal{I} - \mathcal{I}^* \right\|^2 + c(n, r) \tag{1}$$

This cost function expresses that we are willing to accept some error in the position if another task can be solved at the same time, in this case control costs. Examples of control cost criteria c can be "Comfort" (e.g. distance to joint limits), Energy minimization (e.g. the position with lower momentum) or Minimum motion (i.e. minimize total motion from current to desired position), posture control, amongst others.

The regularized solution can be found by minimizing the cost defined in Equation (1), as follows:

$$(\hat{n}, \hat{r}) = \arg\min_{n,r} \left(\lambda \left\| \mathcal{I} - \mathcal{I}^* \right\|^2 + c(n, r) \right) \tag{2}$$

where $\mathcal{I}$ can be computed with the forward model $\mathcal{I} = f(n, r)$. Similarly to [13], this formula integrates two terms: one describing the task part and another related to posture control.

There are two important observations to this formulation. Firstly, the optimization is done with respect to all control variables, which translates into a significant computational cost. Secondly, the DORs are not treated as such, since they undergo exactly the same process as the non-redundant DOFs.

The consequence of this approach is that the extra degrees of freedom are frozen from the beginning and can no longer be used for a different purpose during execution. In a way, redundancy is lost.

Instead, in our approach, we would like to keep the redundant degrees of freedom free for solving additional tasks online. In essence, we split the problem in two steps. Firstly, we define a "Minimal Order Sensory Motor Map", $g(\mathcal{I}, r)$, that relates n and $(\mathcal{I}, r)$:

$$n = g(\mathcal{I}, r) \tag{3}$$

By taking the DORs as input (independent variables) instead of output signals, the problem of computing the non-redundant DOFs becomes well posed. The DORs, r, are left unconstrained and can be fixed during runtime, when a secondary task or optimization criterion is specified.

The definition of the "Minimum Order SMM" allows us to use the redundancy to meet additional criteria or task-constraints, that can be changed online. The DORs can be determined as the solution of a new optimization problem, with cost function $\mathcal{L}$:

$$\hat{r} \quad = \quad \arg\min_{r} \mathcal{L}(\mathcal{I}^*, r) \tag{4}$$

The optimization is done with a gradient-descendant method with following update step:

$$r_{t+1} = r_t - \alpha \nabla_r \mathcal{L}(\mathcal{I}, r)$$

Note that, in contrast with the previous case, this optimization is done with respect to the redundant degrees of freedom, only. The optimization complexity is thus substantially lower and lends itself to be used as an online process. In general, the solutions in the two cases are not the same, because different local minima could be reached and the criteria are slightly different.

Our approach guarantees zero prediction error, because the *Minimum Order SMM* allows us to determine the values of n corresponding to the exact image position, for the selected redundant degrees of freedom. This solution is similar to the first (regularized) problem when λ becomes large. If the *Minimum Order SMM* is not exact, then it will introduce some error in the final image configuration.

For clarity, we summarize the final algorithm.

1) Select the desired image configuration, $\mathcal{I}^*$
2) Select and initial motor command (n, r)
3) Select the secondary task optimization criterion
4) Solve the optimization of Equation (4) for r and use $g(.)$ to compute n.
5) Move the arm to the obtained solution, (n, r)
6) Observe $\mathcal{I}$ and possibly adjust the function $g(\mathcal{I}, n)$
7) If some extra precision is needed, go to 4

There are several important differences in our approach whem compared to other methods based on the robot Jacobian. The *Minimum Order SMM* provides directly the goal position corresponding to the desired redundant joint position. It is then possible to move the robot directly (i.e. in an open-loop fashion) to the goal position, avoiding incremental steps. The posture optimization is done iteratively with the previous update rule. Therefore, the motion goes along the optimization path or directly to the convergence point. This is the case because no visual feedback is necessary to the algorithm. If extra precision is needed, then a visual feedback loop needs to be added.

An example, where the secondary goal is to maintain the control variables as near zero as possible, is presented next:

$$\begin{aligned} \mathcal{L}(\mathcal{I}^*, r) &= \|n\|^2 + \|r\|^2 \\ &= \|g(\mathcal{I}^*, r)\|^2 + \|r\|^2 \end{aligned} \tag{5}$$

Differentiating this cost function yields:

$$\nabla_r \mathcal{L}(\mathcal{I}, r) = 2 \left(\frac{\partial g(\mathcal{I}, r)}{\partial r} g(\mathcal{I}, r) + r \right)$$

The derivation of $\frac{\partial g(\mathcal{I}, r)}{\partial r}$ is presented as an appendix.

We have seen how the introduction of the *Minimum Order SMM* allows us to use the system redundancy to solve additional tasks online, as opposed to freezing the DORs in a regularized solution to the initial ill-posed problem. In the next section, we will see how to estimate the *Minimum Order SMM* $g(\mathcal{I}, n)$ online.

III. Learning the Minimum Order SMM through Local Regression

In the previous section we have seen how to partition the redundant and non-redundant degrees of freedom to build a Minimum Order SMM, $g(\mathcal{I}, r)$ that allows for the computation of the non-redundant DOFs leaving the DORs unconstrained. We will now see how such a map can be estimated online. Without loss of generality, let us assume that we want to estimate the following non-linear function:

$$y = f(x) \tag{6}$$

Since we have little information about this function, the usual approach consists in approximating $f(x)$ by a set of models that are good local approximations of the original global non-linear function, [1].

In this work, $f(x)$ will be approximated by a mixture of models that are locally linear. Obviously, a single linear approximation would fail to provide the desired degree of accuracy. Each local model has a "confidence" region, the kernel K_j, the mixture of all models yields the approximation:

$$y = f(x) \approx \frac{\sum_{j=1}^{M} K_j B_j^T x}{\sum_{j=1}^{M} K_j}$$

for some regression matrices, B_j to be estimated. The choice of the kernel shapes [2] leads to different properties of the approximating function. We have adopted a Gaussian kernel with mean μ and variance W:

$$K_j = K_{W_j}(\mu_j, x) = \frac{1}{det(W_j)} e^{-(x-\mu_j)^T W_j (x-\mu_j)} \tag{7}$$

Let us assume for the moment that the number and the parameters of each Kernel are known in advance. Each model will be fitted by minimizing the following criteria:

$$\hat{B}_j = \arg\min_{B} \sum_{i=1}^{t} \lambda^{(t-i)} K_j \left\| y_i - B^T x_i \right\|^2 \tag{8}$$

where K_j weights points according to the kernel measure and λ provides a time forgetting factor. The model can be estimated by:

$$\hat{B} = QR^+ \tag{9}$$

with

$$\begin{aligned} Q &= \sum_{i=1}^{t} \lambda^{(t-i)} K_W(\mu, x_i) y_i^T x_i \\ R &= \sum_{i=1}^{t} \lambda^{(t-i)} K_W(\mu, x_i) x_i^T x_i \end{aligned} \tag{10}$$

An advantage of writing these terms in this way is the possibility of defining an online estimator:

$$\begin{aligned} Q_t &= \lambda Q_{t-1} + K_W(\mu, x_t) y_t^T x_t \\ R_t &= \lambda R_{t-1} + K_W(\mu, x_t) x_t^T x_t \end{aligned} \tag{11}$$

Finally, at runtime when an input sample is present, the output will be evaluated as a combination of each model B_i weighted by K_j:

$$\hat{y} = \frac{\sum_{j=1}^{M} K_j \hat{B}_j^T x}{\sum_{j=1}^{M} K_j} \tag{12}$$

If the kernels are C^0 and have an infinite support, this function is guaranteed to be C^0. If the kernels are differentiable, the function will be C^1 .

The final point to discuss is related to the Kernel functions $K_W(\mu, x)$. How many kernels should be used and what should the parameters of each kernel be? The number of kernels can be is iteratively increased during training. When the distance between a new data sample and its nearest kernel exceeds a certain threshold, a new kernel is created with center (μ) in this point. The shape of the kernels (the covariance matrix) can be automatically updated choosing, e.g., a measure of reconstruction quality [22], [23].

Other formulations have already been proposed. The *Locally Weighted Projection Regression* method, proposed in [24], is linear with the number of samples and every new sample can be added easily. As the method is not capable of extrapolating, the work space must be well covered in the training set. Other implementations keep several samples in memory without estimating any explicit models. The prediction is produced online by weighting the points in memory with some kernel functions.

IV. Experimental Results

Several experiments were done with a real robot to assess the quality of the algorithms and the ability to learn the proposed SMM online. The experimental setup was the Baltazar humanoid robot torso [25], consisting of a 4 DOF head, a 6 DOF arm and a 10 DOF under-actuated hand. The image features consist on the image position of the wrist, and we want to position the wrist in the the image. This task requires only two degrees of freedom. The non-redundant DOFs are the shoulder adduction/abduction and flexion/extension. The shoulder axis rotation and elbow flexion/extension are considered as redundant degrees of freedom.

A. Evaluation of the learning method

The first experiment is designed to validate the learning of the Minimum order SMM. The map associates the image position of the robot hand and the DOR to the non-redundant DOFs.

During learning, the head remains in a fixed position and observes the robot hand. The arm is moved to several randomly selected positions. The range of movement of each joint is in the order of $0.55\,rad$. Once, the robot wrist attains one

such position, it remains fixed while different solution for the inverse kinematics are used. This is possible due to the redundancy of this robot's kinematics, when four degrees of freedom are used for a positioning task. Another redundancy exists because, with the use of a single camera, depth information is lost. Hence, for a 2 DOF task we have 4 DOF available.

Fig. 2 shows the evolution of joint angles during this period of auto-observation and learning. It also shows the image position of the robot wrist where, due to elasticity in the robot joints, oscillations occur when the acceleration is high.

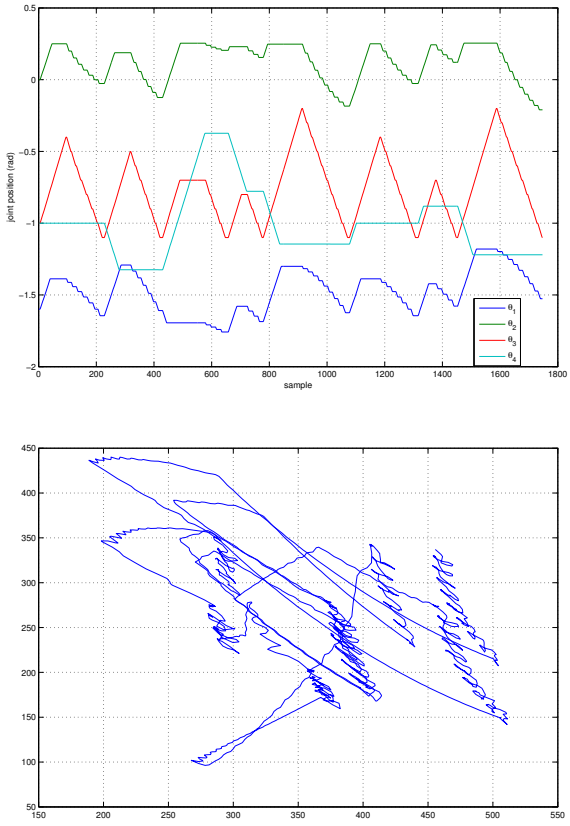

Fig. 2. Dataset for the real robot experiments. The top figure shows the temporal evolution of the joint angles (joint position in radian vs sample number), the bottom presents the trajectories in the image (pixel coordinates), where oscillation is caused by elasticity in the robot joints.

Fig. 3 shows the quality of the SMM estimation, as described in Section III. The top plots show the true and estimated non-redundant joint angles, which are in good agreement. The histogram and cumulative distribution of the error are shown in the bottom plots, for 2000 data points. For both non-redundant joints less than 10% of the points have an error bigger than $0.05\,rad$.

These results show that the online estimation method presented in Section III provides a good approximation to the original Minimum order SMM. The next set of experiments show how to define a secondary task based on an energy minimization criterion, to drive the robot to the desired position, while meeting this secondary goal.

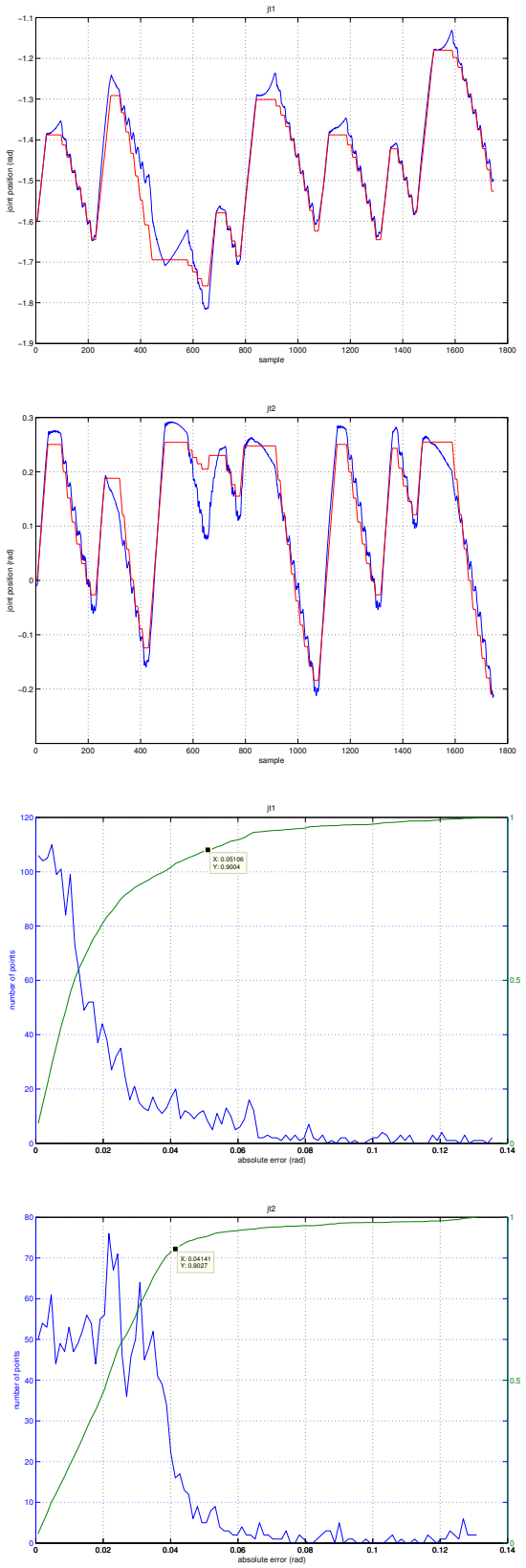

Fig. 3. These figures show the prediction error for (non-redundant) Joint 1 and Joint 2. The absolute error histogram and the cumulative distribution are also shown. Almost 90% of the samples have an error below $0.05\,rad$, see measure in the figures.

B. Sensory-motor coordination for redundant robots

For a given desired image position and an initial position of the redundant degrees of freedom, our goal is to reach a certain image position, while satisfying a secondary criterion (task). This is obtained through the following optimization problem, as defined earlier:

$$\mathcal{L} = \|n - \mu_n\|^2 + \|r - \mu_r\|^2$$

that aims to maximize the distance to joint limits, corresponding to a comfort criterion.

It is worth stressing that the optimization process relies on the estimated Minimum order SMM, as described before. Fig. 4 presents the evolution of the cost function l, for each iteration of the Newton method. It also presents the trajectory of all 4 (redundant and non-redundant) robot joints. We can see that, for this case, the maximum for one joint was $0.5\,rad$.

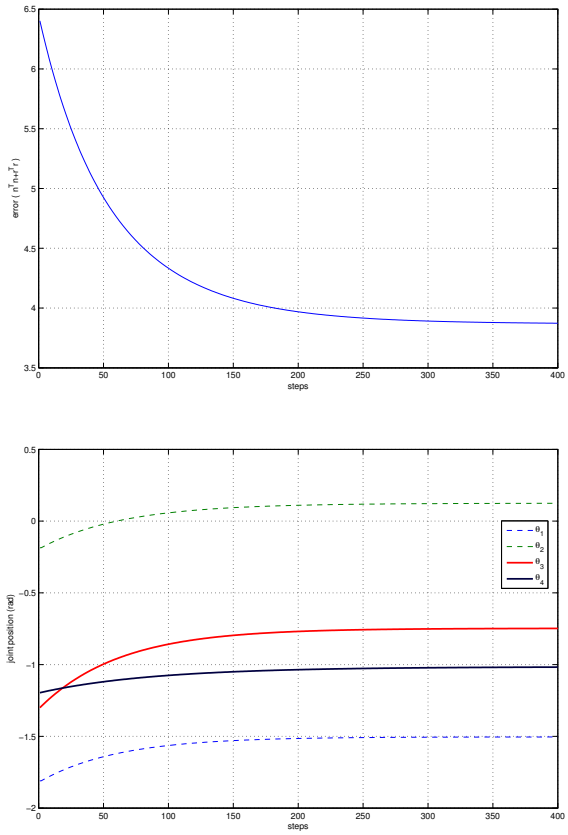

Fig. 4. Convergence rate and evolution of the position for the real robot as a function of the optimization step. It is interesting to see that one joint moved $0.5\,rad$ and the final error in the image corresponds to $0.03\,rad$.

The final error in the image was as small as $0.03\,rad$, and most it is due to elasticity in the robot joints. Fig. 5 shows the robot view of the hand for an intuition for this error (about the size of the target). Due to the redundancy in the arm, it would be possible to fixate the target while changing the arm posture.

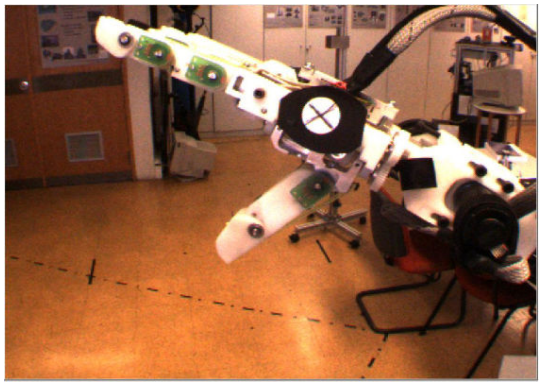

Fig. 5. Robot view. We can see the arm, hand and the target being tracked

V. Conclusions / Future Work

We have addressed the problem of estimating Sensory Motor Maps in redundant systems, which is often the case of humanoid robots. As a consequence of redundancy, the inverse map cannot be estimated since the forward model is not bijective.

For a given task, we started by partitioning the robot degrees of freedom in redundant and non-redundant DOFs. Then, we defined a "Minimum order SMM" that takes as the input general image configurations and redundant degrees of freedom. This partial backward model can be used to determine the configuration for the non-redundant degrees of freedom and can be used for control. Using the "Minimum order SMM", the redundant degrees of freedom are available to meet additional online constraints, arising from secondary tasks or criteria.

A noteworthy observation is that this method is not incremental, in the sense of requiring small steps toward the final goal. It gives directly the goal position so that the robot can be moved directly there. However, the optimization leads to several steps being used for the secondary goal, in this case the posture optimization.

The Minimum Order SMM is learned with a local learning method. Experimental results done in an humanoid torso with 10 degrees of freedom were presented, illustrating both the ability to learn the *Minimum order SMM* and how it can be used for specific tasks.

A large workspace was used of about $40\,degrees$ for each joint, a small reconstruction error was achieved, about $2.5\,degrees$. For the optimization one joint could "travel" $90\,degrees$ to be able to reduce the cost function by 40%, with a corresponding error in the image of only $1.5\,degrees$ (about the same size of the target).

In the future we plan to investigate automatic methods for the division between redundant and non-redundant degrees of freedom. One possible direction of research can go a similar path as the one presented in [18]. The use of more degrees of freedom will be necessary to deal with more complex image features (e.g. position and orientation), a binocular head and changing head positions.

As a final comment, we would like to stress that learning

inverse maps for redundant robots is a frequent need in humanoid robotics, and that the proposed method is simple, computationally efficient and well suited for online learning.

APPENDIX

A. Derivative of Local learning method

If redundant degrees of freedom are to be chosen with some extra criterion, it is important to evaluate the derivative of the prediction function. The prediction of the chosen local learning method is given by:

$$\hat{y} = \frac{\sum_{j=1}^{M} K_j B_j^T x}{\sum_{j=1}^{M} K_j}$$

Now we want to evaluate its derivative as a function of the inputs $\frac{\partial \hat{y}}{\partial x}$:

$$\frac{\partial \hat{y}}{\partial x} = \sum_{j=1}^{M} \left(\frac{\partial K_j}{\partial x} x^T + K_j \right) \frac{B_j}{\tilde{k}} - \frac{1}{\tilde{k}^2} \sum_{l=1}^{M} \frac{\partial K_l}{\partial x} \sum_{j=1}^{M} K_j x^T \beta$$

with $\tilde{k} = \sum_{j=1}^{M} K_j$ and $\frac{dK_j}{dx} = -W_j(x - \mu_j)K_j$

After some computations, we have:

$$\tilde{k} \frac{\partial \hat{y}}{\partial x} = \sum_{j=1}^{M} \frac{\partial K_j}{\partial x} x^T B_j + \sum_{j=1}^{M} B_j K_j - \tilde{dk}\ \hat{y}^T \qquad (13)$$

with $\tilde{dk} = \sum_{j=1}^{M} \frac{\partial K_j}{\partial x}$

ACKNOWLEDGEMENTS

Work partially supported by: EU Proj. IST-2004-004370 , ROBOTCUB, by a FCT personal scholarship and by the FCT Programa Operacional Sociedade de Informação (POSI) in the frame of QCA III.

REFERENCES

[1] Trevor Hastie, Robert Tibshirani, and Jerome Friedman. *The Elements of Statistical Learning*. Springer, 2001.

[2] Chistopher G. Atkeson, Andrew W. Moore, and Stefan Schaal. Locally weighted learning. *Artificial Intelligence Review*, 11(1-5):11–73, 1997.

[3] M. Blackburn and H. Nguyen. Learning in robot vision directed reaching: A comparison of methods. In *ARPA Image Understanding Workshop*, Moterey, CA, 1994.

[4] Aaron D'Souza, Sethu Vijayakumar, and Stephan Schaal. Learning inverse kinematics. In *International Conference on Intelligent Robots and Systems*, Hawaii, USA, 2001.

[5] John J. Craig. *Introduction to Robotics*. Addison-Wesley Pub Co, 1989.

[6] Samuel R. Buss. Introduction to inverse kinematics with jacobian transpose, pseudoinverse and damped least squares methods. Technical report, University of California, San Diego, USA, 2004.

[7] C.W. Wampler. Manipulator inverse kinematics solution based on damped least-squares solutions. *IEEE Trans. Systems, Man and Cybernetics*, 16(1), 1986.

[8] J.B. Rosen. The gradient projection method for nonlinear programmimg, part i, linear constraints. *SIAM Journal of Applied Mathematics*, 8:181–217, 1960.

[9] C. Samson, M. Le Borgne, and B. Espiau. *Robot Control: the Task Function Approach*. Clarendon Press, Oxford, United Kingdom, 1991.

[10] Paolo Baerlocher and Ronan Boulic. An inverse kinematic architecture enforcing an arbitrary number of strict priority levels. *Visual Computer*, 2004.

[11] Nicolas Mansard and François Chaumette. Tasks sequencing for visual servoing. In *IEEE/RSJ Int. Conf. on Intelligent Robots and Systems*, Sendai, Japan, September 2004.

[12] Yoshihiko Nakamura, Katsu Yamane, Ichiro Suzuki, and Yusuke Fujita. Dynamics computation of musculo-skeletal human model based on efficient algorithm for closed kinematic chains. In *2nd International Symposium on Adaptive Motion of Animals and Machines*, Kyoto, Japan, 2003.

[13] Oussama Khatib, Oliver Brock, Kyong-Sok Chang, Diego Ruspini, Luis Sentis, and Sriram Viji. Human-centered robotics and interactive haptic simulation. *International Journal of Robotics Research*, 23(2), 2004.

[14] Koh Hosoda and Minoru Asada. Versatile visual servoing without knowledge of true jacobian. In *International Conference on Intelligent Robots and Systems*, pages 186–193, Munchen, Germany, Sep 1994.

[15] R. Fletcher. *Practical Methods of Optimization*. Chichester, 2nd edition, 1987.

[16] M. Jagersand and R.C. Nelson. On-line estimation of visual-motor models using active vision. In *ARPA Image Understanding Workshop*, pages 677–682, 1996.

[17] Manuel Lopes, Alexandre Bernardino, and José Santos-Victor. A developmental roadmap for task learning by imitation in humanoid robots. In Yannis Demiris, editor, *AISB - Third International Symposium on Imitation in Animals and Artifacts*, Hatfield, Uk, April 2005.

[18] Koh Hosoda and Minory Asada. How does a robot find redundancy by itself? In *Advances in Robot Learning: 8th European Workshop on Learning Robots*, Lausanne, Switzerland, 1999.

[19] A.N. Tikhonov and V.A. Arsenin. *Solution of ill-posed problems*. Washington DC: Winston, 1977.

[20] T. Poggio, V. Torre, and C. Kock. Computational vision and regularization theory. *Nature*, 317:314–319, 1985.

[21] M. Bertero, T. Poggio, and V. Torre. Ill-posed problems in early vision. *Proceedings of the IEEE*, 76(8):869–889, 1988.

[22] S. Schaal and C. G. Atkeson. Constructive incremental learning from only local information. *Neural Computation*, 10(8):2047–2084, 1998.

[23] Trevor Hastie and Clive Loader. Local regression: Automatic kernel carpentry. *Statistical Science*, 8:120–129, 1993.

[24] S. Vijayakumar and S. Schaal. Locally weighted projection regression: An o(n) algorithm for incremental real time learning in high dimensional spaces. In *ICML*, Stanford, USA, 2000.

[25] Manuel Lopes, Ricardo Beira, Miguel Praça, and José Santos-Victor. An anthropomorphic robot torso for imitation: design and experiments. In *IEEE/RSJ - International Conference on Intelligent Robots and Systems*, Sendai, Japan, 2004.